Doping a Mott insulator: Physics of high-temperature superconductivity

Patrick A. Lee

Department of Physics, Massachusetts Institute of Technology, Cambridge, Massachusetts 02139, USA

Naoto Nagaosa

CREST, Department of Applied Physics, The University of Tokyo, 7-3-1 Hongo, Bunkyo-ku, Tokyo 113-8656, Japan and Correlated Electron Research Center, AIST, Tsukuba Central 4, Tsukuba 305-8562, Japan

Xiao-Gang Wen

Department of Physics, Massachusetts Institute of Technology, Cambridge, Massachusetts 02139, USA

This article reviews the physics of high-temperature superconductors from the point of view of the doping of a Mott insulator. The basic electronic structure of cuprates is reviewed, emphasizing the physics of strong correlation and establishing the model of a doped Mott insulator as a starting point. A variety of experiments are discussed, focusing on the region of the phase diagram close to the Mott insulator (the underdoped region) where the behavior is most anomalous. The normal state in this region exhibits pseudogap phenomenon. In contrast, the quasiparticles in the superconducting state are well defined and behave according to theory. This review introduces Anderson's idea of the resonating valence bond and argues that it gives a qualitative account of the data. The importance of phase fluctuations is discussed, leading to a theory of the transition temperature, which is driven by phase fluctuations and the thermal excitation of quasiparticles. However, an argument is made that phase fluctuations can only explain pseudogap phenomenology over a limited temperature range, and some additional physics is needed to explain the onset of singlet formation at very high temperatures. A description of the numerical method of the projected wave function is presented, which turns out to be a very useful technique for implementing the strong correlation constraint and leads to a number of predictions which are in agreement with experiments. The remainder of the paper deals with an analytic treatment of the *t-J* model, with the goal of putting the resonating valence bond idea on a more formal footing. The slave boson is introduced to enforce the constraint against double occupation and it is shown that the implementation of this local constraint leads naturally to gauge theories. This review follows the historical order by first examining the U(1) formulation of the gauge theory. Some inadequacies of this formulation for underdoping are discussed, leading to the SU(2) formulation. Here follows a rather thorough discussion of the role of gauge theory in describing the spin-liquid phase of the undoped Mott insulator. The difference between the high-energy gauge group in the formulation of the problem versus the low-energy gauge group, which is an emergent phenomenon, is emphasized. Several possible routes to deconfinement based on different emergent gauge groups are discussed, which leads to the physics of fractionalization and spin-charge separation. Next the extension of the SU(2) formulation to nonzero doping is described with a focus on a part of the mean-field phase diagram called the staggered flux liquid phase. It will be shown that inclusion of the gauge fluctuation provides a reasonable description of the pseudogap phase. It is emphasized that *d*-wave superconductivity can be considered as evolving from a stable U(1) spin liquid. These ideas are applied to the high-T_c cuprates, and their implications for the vortex structure and the phase diagram are discussed. A possible test of the topological structure of the pseudogap phase is described.

PACS number(s): 74.20.Mn, 74.72.−h, 71.27.+a

CONTENTS

I. INTRODUCTION

The discovery of high-temperature superconductivity in cuprates (Bednorz and Müller, 1986) and the rapid raising of the transition temperature to well above the melting point of nitrogen (Wu *et al.*, 1987) ushered in an era of great excitement for the condensed-matter-physics community. For decades prior to this discovery, the highest T_c had been stuck at 23 K. Not only was the old record T_c shattered, but the fact that high-T_c super-conductivity was discovered in a rather unexpected ma-

terial, a transition-metal oxide, made it clear that some novel mechanism must be at work. The intervening years have seen great strides in high-T_c research. First and foremost, the growth and characterization of cu-prate single crystals and thin films have advanced to the point where sample quality and reproducibility problems which plagued the field in the early days are no longer issues. At the same time, basically all conceivable experimental tools have been applied to cuprates. Indeed, the need for more refined data has spurred the development of experimental techniques such as angle-resolved photoemission spectroscopy (ARPES) and low-temperature scanning tunneling microscopy (STM). Today the cuprate is arguably the best studied material outside of the semiconductor family and a great many facts are known. It is also clear that many of the physical properties are unusual, particularly in the metallic state above the superconductor. Superconductivity is only one aspect of a rich phase diagram which must be understood in its totality.

While there are hundreds of high-T_c compounds, they all share a layered structure made up of one or more copper-oxygen planes. They all fit into a universal phase diagram shown in Fig. 1. We start with the so-called parent compound, in this case La_2CuO_4. There is now general agreement that the parent compound is an insulator, and should be classified as a Mott insulator. The concept of Mott insulation was introduced many years ago (Mott, 1949) to describe a situation where a material should be metallic according to band theory, but is insulating due to strong electron-electron repulsion. In our case, in the copper-oxygen layer there is an odd number of electrons per unit cell. More specifically, the copper ion is doubly ionized and is in a d^9 configuration so that there is a single hole in the d shell per unit cell. According to band theory, the band is half-filled and must be metallic. Nevertheless, there is a strong repulsive energy cost when putting two electrons (or holes) on the same ion, and when this energy (commonly called U) dominates over the hopping energy t, the ground state is an insulator due to strong correlation effects. It also follows that the Mott insulator should be an antiferromagnet
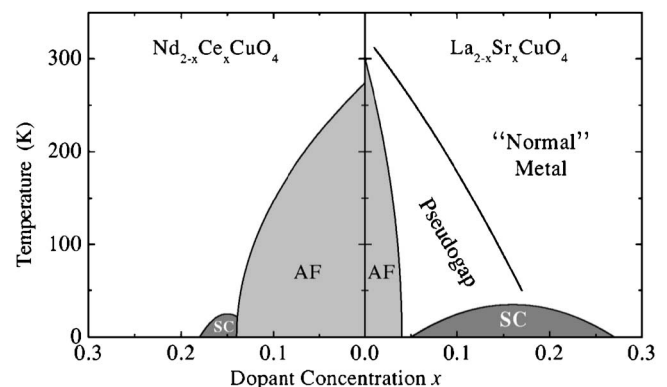

FIG. 1. Schematic phase diagram of high-T_c superconductors showing hole doping (right side) and electron doping (left side). From Damascelli *et al.*, 2003.

because when neighboring spins are oppositely aligned one can gain an energy $4t^2/U$ by virtual hopping. This is called the exchange energy J. The parent compound is indeed an antiferromagnetic insulator. The ordering temperature $T_N \approx 300$ K shown in Fig. 1 is in fact misleadingly low because it is governed by a small interlayer coupling, which is, furthermore, frustrated in La_2CuO_4 (see Kastner *et al.*, 1998). The exchange energy J is in fact extraordinarily high, of order 1500 K, and the parent compound shows strong antiferromagnetic correlation much above T_N.

The parent compound can be doped by substituting some of the trivalent La by divalent Sr. The result is that x holes are added to the Cu-O plane in $La_{2-x}Sr_xCuO_4$, which is called hole doping. In the compound $Nd_{2-x}Ce_xCuO_4$ (Tokura *et al.*, 1989), the reverse happens in that x electrons are added to the Cu-O plane, which is called electron doping. As we can see from Fig. 1, on the hole-doping side the antiferromagnetic order is rapidly suppressed and is gone by a 3–5 % hole concentration. Almost immediately after the suppression of the antiferromagnet, superconductivity appears, ranging from x =6–25 %. The dome-shaped T_c is characteristic of all hole-doped cuprates, even though the maximum T_c varies from about 40 K in the $La_{2-x}Sr_xCuO_4$ (LSCO) family to 93 K and higher in other families such as $YBa_2Cu_3O_{6+y}$ (YBCO) and $Ba_2Sr_2CaCu_2O_{8+y}$ (Bi-2212). On the electron-doped side, the antiferromagnet is more robust and survives up to $x=0.14$, beyond which a region of superconductivity arises. One view is that the carriers are more prone to be localized on the electron-doped side so that electron doping is closer to dilution by nonmagnetic ions, which is less effective in suppressing antiferromagnetic order than itinerant carriers. Another possibility is that the next-neighbor hopping term favors the antiferromagnet on the electron-doped side (Singh and Ghosh, 2002). It is as though a more robust antiferromagnetic region is covering up the more interesting phase diagram revealed on the hole-doped side. In this review we shall focus on the hole-doped materials, even though we shall address the issue of the particle-hole asymmetry of the phase diagram from time to time.

The region in the phase diagram with doping x less than that of the maximum T_c is the underdoped region. The metallic state above T_c has been under intense study and exhibits many unusual properties not encountered before in any other metal. This region of the phase diagram has been called the pseudogap phase. It is not a well-defined phase in that a definite finite-temperature phase boundary has never been found. The line drawn in Fig. 1 should be regarded as a crossover. Since we view the high-T_c problem as synonymous with that of the doping of a Mott insulator, the underdoped region is where the battleground between Mott insulator and superconductivity is drawn and this is what we shall concentrate on in this review.

The region of the normal state above the optimal T_c also exhibits unusual properties. The resistivity is linear in T and the Hall coefficient is temperature dependent (see Chien *et al.*, 1991). These were cited as examples of non-Fermi-liquid behavior since the early days of high T_c. Beyond optimal doping (the overdoped region), sanity gradually returns. The normal state behaves more normally in that the temperature dependence of the resistivity resembles T^2 over a temperature range which increases with further overdoping. The anomalous region above optimal doping is sometimes referred to as the "strange-metal" region. We offer a qualitative description of this region in Sec. IX, but the understanding of the strange metal is even more rudimentary than that of the pseudogap. A popular notion is that the strange metal is characterized by a quantum critical point lying under the superconducting dome (Castellani *et al.*, 1997; Varma, 1997; Tallon and Loram, 2000). In our view, unless the nature of the ordered side of a quantum critical point is classified, the simple statement of quantum criticality does not teach us too much about the behavior in the critical region. For this reason, we prefer to concentrate on the underdoped region and leave the strange-metal phase for future studies.

Contrary to the experimental situation, the development of high-T_c theory follows a rather tortuous path and people often have the impression that the field is highly contentious and without a clear direction or consensus. We do not agree with this assessment and would like to clearly state our point of view from the outset. Our starting point is that the physics of high-T_c superconductivity is the physics of the doping of a Mott insulator. Strong correlation is the driving force behind the phase diagram. We believe that there is a general consensus on this starting point. The simplest model which captures the strong-correlation physics is the Hubbard model and its strong-coupling limit, the *t-J* model. Our view is that one should focus on understanding these simple models before adding various elaborations. For example, further neighbor hopping certainly is significant and, as we shall discuss, plays an important role in understanding the particle-hole asymmetry of the phase diagram. Electron-phonon coupling can generally be expected to be strong in transition-metal oxides, and we shall discuss their role in affecting spectral line shape. However, these discussions must be presented in the context of strong correlation. The logical step is to first understand whether simple models such as the *t-J* model contain enough physics to explain the appearance of superconductivity and pseudogaps in the phase diagram.

The strong-correlation viewpoint was put forward by Anderson (1987), who revived his earlier work on a possible spin-liquid state in a frustrated antiferromagnet. This state, called the resonating valence bond (RVB), has no long-range antiferromagnetic order and is a unique spin-singlet ground state. It has spin-1/2 fermionic excitations which are called spinons. The idea is that when doped with holes, the RVB is a singlet state with coherent mobile carriers and is indistinguishable in terms of symmetry from a singlet BCS superconductor. The process of hole doping was further developed by Kivelson *et al.* (1987), who argued that the combination of the doped hole with the spinon forms a bosonic exci-

tation. This excitation, called the holon, carries charge but no spin whereas the spinon carries spin 1/2 but no charge, and the notion of spin-charge separation was born. Meanwhile, a slave-boson theory was formulated by Baskaran *et al.* (1987). Many authors contributed to the development of the mean-field theory, culminating in the paper by Kotliar and Liu (1988), who found that the superconducting state should have *d* symmetry and that a state with spin-gap properties should exist above the superconducting temperature in the underdoped region. The possibility of *d*-wave superconductivity was discussed in terms of the exchange of spin fluctuations (Emery, 1983, 1986; Miyake *et al.*, 1986; Scalapino *et al.*, 1986, 1987; Monthonx and Pines, 1993). These discussions were either based on phenomenological coupling between spins and fermions or via the random-phase-approximation treatment for the Hubbard model, which is basically a weak-coupling expansion. In contrast, the slave-boson theory was developed in the limit of strong repulsion. Details of the mean-field theory will be discussed in Sec. VIII.

At about the same time, the proposal by Anderson (1987) of using projected mean-field states as trial wave functions was implemented on the computer by Gros (1988, 1989). The idea was to remove by hand on a computer all components of the mean-field wave function with doubly occupied sites and to use this as a variational wave function for the *t-J* model. Gros (1988, 1989) concluded that the projected *d*-wave superconductor was the variational ground state for the *t-J* model over a range of doping. The projected wave-function method remains one of the best numerical tools for tackling the *t-J* or Hubbard model and is reviewed in Sec. VI.

It was soon realized that inclusion of fluctuations about the mean field invariably leads to gauge theory (Baskaran and Anderson, 1988; Ioffe and Larkin, 1989; Nagaosa and Lee, 1990). The gauge-field fluctuations can be treated at a Gaussian level and these early developments together with some of the difficulties are reviewed in Sec. IX.

In hindsight, the slave-boson mean-field theory and the projected wave-function studies contain many of the qualitative aspects of the hole-doped phase diagram. It is indeed quite remarkable that the main tools for treating the *t-J* model, i.e., projected trial wave function, slave-boson mean-field, and gauge theory, were in place a couple of years after the discovery of high T_c. In some ways the theory was ahead of its time because the majority view in the early days was that the pairing symmetry was *s* wave, and the pseudogap phenomenology remained to be discovered. [The first hint came from Knight-shift measurements in 1989 shown in Fig. 4(a).] Some of the early history and recent extensions are reviewed by Anderson *et al.* (2004).

The gauge-theory approach is a difficult one to pursue systematically because it is a strong-coupling problem. One important development is the realization that the original U(1) gauge theory should be extended to SU(2) in order to make a smooth connection to the underdoped limit (Wen and Lee, 1996). This is discussed in Secs. XI and XII. More generally, it was gradually realized that the concepts of confinement and deconfinement, which are central to QCD, also play a key role here except that the presence of fermions and bosons in addition to gauge fields makes this problem even more complex. Since gauge theories are not so familiar to condensed-matter physicists, these concepts are discussed in some detail in Sec. X. One of the notable recent advances is that the notion of the spin liquid and its relation to deconfinement in gauge theory has been greatly clarified and several soluble models and candidates based on numerical exact diagonalization have been proposed (Misguich *et al.*, 1999; LiMing *et al.*, 2000; Misguich and Lhuillier, 2004). It remains true, however, that so far no two-dimensional spin liquid has been convincingly realized experimentally. We would like to mention two promising examples. The first is the organic compound κ_2-(BEDT-TTF)$_2$Cu$_2$(CN)$_3$. This material is a $S=\frac{1}{2}$ system on an approximate triangular lattice just on the insulating side of the Mott transition and shows no spin order down to mK, while the spin susceptibility reaches a finite constant (Shimizu *et al.*, 2003; Kawamoto *et al.*, 2004; Kurosaki *et al.*, 2005). Motrunich (2005) has interpreted this as an example of a spin liquid with a spinon Fermi surface which is stabilized by ring exchange, while Morita *et al.* (2002) and Lee and Lee (2005a) have proposed that the Hubbard model on a triangular lattice may support this spin liquid near the Mott transition. A second example is the nuclear spin of a ^{3}He solid layer adsorbed on graphite surfaces (Masutomo *et al.*, 2004).

Our overall philosophy is that the RVB idea of a spin liquid and its relation to superconductivity contains the essence of the physics and gives a qualitative description of the underdoped phase diagram. The goal of our research is to put these ideas on a more quantitative footing. Given the strong-coupling nature of the problem, the only way progress can be made is for theory to work in consort with experiment. Our aim is to make as many predictions as possible, beyond saying that the pseudogap is a RVB spin liquid, and challenge the experimentalists to perform tests. Ideas along these lines are reviewed in Sec. XII.

High-T_c research is an enormous field and we cannot hope to be complete in our references. Here we refer to a number of excellent review articles on various aspects of the subject. Imada *et al.* (1998) reviewed the general topic of the metal-insulator transition. Orenstein and Millis (2000) and Norman and Pepin (2003) have provided highly readable accounts of experiments and general theoretical approaches. Early numerical work was reviewed by Dagotto (1994). Kastner *et al.* (1998) summarized the earlier optical and magnetic neutron-scattering data mainly on La$_{2-x}$Sr$_x$CuO$_4$. Major reviews of angle-resolved photoemission data (ARPES) have been provided by Campuzano *et al.* (2003) and Damascelli *et al.* (2003). Optics measurements on underdoped materials were reviewed by Timusk and Statt (1999) and Basov and Timusk (2005). The volume edited by Ginzberg (1989) contains excellent reviews of early NMR
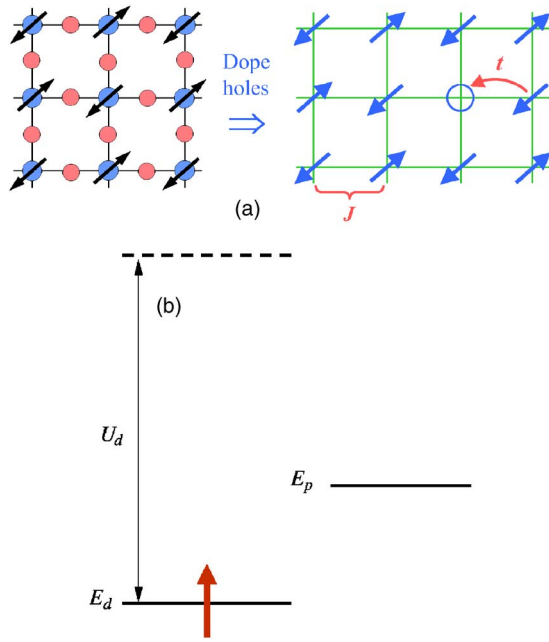
FIG. 2. (Color online) Electronic structure of the cuprates. (a) Two-dimensional copper-oxygen layer (left) simplified to the one-band model (right). (b) The copper d and oxygen p orbitals in the hole picture. A single hole with $S=1/2$ occupies the copper d orbital in the insulator.

work by C. P. Slichter and early transport measurements by N. P. Ong among others. Discussions of stripe physics were recently given by Carlson *et al.* (2003) and Kivelson *et al.* (2003). A discussion of spin-liquid states is given by Sachdev (2003), with an emphasis on dimer order and by Wen (2004), with an emphasis on quantum order. For an account of experiments and early RVB theory, see the book by Anderson (1997).

II. BASIC ELECTRONIC STRUCTURE OF THE CUPRATES

It is generally agreed that the physics of high-T_c superconductivity is that of the copper-oxygen layer, as shown in Fig. 2. In the parent compound such as La$_2$CuO$_4$, the formal valence of Cu is 2+, which means that its electronic state is in the d^9 configuration. The copper is surrounded by six oxygens in an octahedral environment (the apical oxygen lying above and below Cu are not shown in Fig. 2). The distortion from a perfect octahedron due to the shift of the apical oxygens splits the e_g orbitals so that the highest partially occupied d orbital is x^2-y^2. The lobes of this orbital point directly to the p orbital of the neighboring oxygen, forming a strong covalent bond with a large hopping integral t_{pd}. As we shall see, the strength of this covalent bonding is responsible for the unusually high energy scale for the exchange interaction. Thus the electronic state of the cuprates can be described by the so-called three-band model, where in each unit cell we have the Cu $d_{x^2-y^2}$ orbital and two oxygen p orbitals (Emery, 1987; Varma *et al.*, 1987). The Cu orbital is singly occupied while the p orbitals are doubly occupied, but these are admixed by

t_{pd}. In addition, admixtures between the oxygen orbitals may be included. These tight-binding parameters may be obtained by fits to band-structure calculations (Mattheiss, 1987; Yu *et al.*, 1987). However, the largest energy in the problem is the correlation energy for doubly occupying the copper orbital. To describe these correlation energies, it is more convenient to refer to the hole picture. The Cu d^9 configuration is represented by energy level E_d occupied by a single hole with $S=\frac{1}{2}$. The oxygen p orbital is empty of holes and lies at energy E_p, which is higher than E_d. The energy to doubly occupy E_d (leading to a d^8 configuration) is U_d, which is very large and can be considered infinity. The lowest-energy excitation is the charge-transfer excitation in which the hole hops from d to p with amplitude $-t_{pd}$. If E_p-E_d is sufficiently large compared with t_{pd}, the hole will form a local moment on Cu. This is referred to as a charge-transfer insulator in the scheme of Zaanen *et al.* (1985). Essentially, E_p-E_d plays the role of the Hubbard U in the one-band model of the Mott insulator. Experimentally an energy gap of 2.0 eV is observed and interpreted as the charge-transfer excitation (see Kastner *et al.*, 1998).

Just as in the one-band Mott-Hubbard insulator in which virtual hopping to doubly occupied states leads to an exchange interaction $J\mathbf{S}_1\cdot\mathbf{S}_2$, where $J=4t^2/U$, in the charge-transfer insulator the local moments on nearest-neighbor Cu prefer antiferromagnetic alignment because both spins can virtually hop to the E_p orbital. Ignoring the U_p for doubly occupying the p orbital with holes, the exchange integral is given by

$$J = \frac{t_{pd}^4}{(E_p - E_d)^3}. \tag{1}$$

The relatively small size of the charge-transfer gap means that we are not deep in the insulating phase and the exchange term is expected to be large. Indeed experimentally the insulator is found to be in an antiferromagnetic ground state. By fitting Raman scattering to two magnon excitations (Sulewsky *et al.*, 1990), the exchange energy is found to be $J=0.13$ eV. This is one of the largest exchange energies known. (It is even larger in the ladder compounds which involve the same Cu-O bonding.) This value of J is confirmed by fitting the spin-wave energy to theory, in which an additional ring exchange term is found (Coldea *et al.*, 2001).

By substituting divalent Sr for trivalent La, the electron count on the Cu-O layer can be changed in a process called doping. For example, in La$_{2-x}$Sr$_x$CuO$_4$, x holes per Cu are added to the layer. As seen in Fig. 2, due to the large U_d the hole will reside on the oxygen p orbital. The hole can hop via t_{pd}, and due to translational symmetry the holes are mobile and form a metal, unless localization due to disorder or some other phase transition intervenes. The full description of hole hopping in the three-band model is complicated, and a number of theories consider this essential to the understanding of high-T_c superconductivity (Emery, 1987; Varma *et al.*, 1987). On the other hand, there is strong evidence that the low-energy physics (on a scale small compared

with t_{pd} and $E_p - E_d$) can be understood in terms of an effective one-band model, and we shall follow this route. The essential insight is that the doped hole resonates on the four oxygen sites surrounding a Cu and the spin of the doped hole combines with the spin on the Cu to form a spin singlet. This is known as the Zhang-Rice singlet (Zhang and Rice, 1988). This state is split off by an energy of order $t_{pd}^2/(E_p - E_d)$ because the singlet gains energy by virtual hopping. On the other hand, the Zhang-Rice singlet can hop from site to site. Since the hopping is a two-step process, the effective hopping integral t is also of order $t_{pd}^2/(E_p - E_d)$. Since t is the same parametrically as the binding energy of the singlet, the justification of this point of view relies on a large numerical factor for the binding energy, which is obtained by studying small clusters.

By focusing on the low-lying singlet, the hole-doped three-band model simplifies to a one-band tight-binding model on the square lattice, with an effective nearest-neighbor hopping integral t given earlier and with $E_p - E_d$ playing a role analogous to U. In the large $E_p - E_d$ limit this maps onto the t-J model,

$$H = P\left[-\sum_{\langle ij\rangle,\sigma} t_{ij}c_{i\sigma}^\dagger c_{i\sigma} + J\sum_{\langle ij\rangle}\left(\boldsymbol{S}_i \cdot \boldsymbol{S}_j - \tfrac{1}{4}n_i n_j\right)\right]P. \qquad (2)$$

Here the $c_{i\sigma}^\dagger$ is the usual fermion creation operator on site i, $n_i = \Sigma_\sigma c_{i\sigma}^\dagger c_\sigma$ is the number operator, and P is a projection operator restricting the Hilbert space to exclude double occupancy of any site. J is given by $4t^2/U$ and we can see that it is the same functional form as that of the three-band model described earlier. It is also possible to dope with electrons rather than holes. The typical electron-doped system is $Nd_{2-x}Ce_xCuO_{4+\delta}$ (NCCO). The added electron corresponds to the removal of a hole from the copper site in the hole picture (Fig. 2), i.e., the Cu ion is in the d^{10} configuration. This vacancy can hop with a t_{eff} and the mapping to the one-band model is more direct than the hole-doped case. Note that in the full three-band model, the object which is hopping is the Zhang-Rice singlet for hole doping and the Cu d^{10} configuration for electron doping. These have rather different spatial structure and are physically quite distinct. For example, the strength of their coupling to lattice distortions may be quite different. When mapped to the one-band model, the nearest-neighbor hopping t has the same parametric dependence but could have a different numerical constant. As we shall see, the value of t derived from cluster calculations turns out to be surprisingly similar for electron and hole doping. For a bipartite lattice, the t-J model with nearest-neighbor t has particle-hole symmetry because the sign of t can be absorbed by changing the sign of the orbital on one sublattice. Experimentally the phase diagram exhibits strong particle-hole asymmetry. On the electron-doped side, the antiferromagnetic insulator survives up to a much higher doping concentration (up to $x \approx 0.2$) and the superconducting transition temperature is quite low (about 30 K). Many of the properties of the superconductor resemble that of the overdoped region of the

hole-doped side and pseudogap phenomenon, which is prominent in the underdoped region, is not observed with electron doping. It is as though the greater stability of the antiferromagnet has covered up any anomalous regime that might exist otherwise. Precisely why is not clear at the moment. One possibility is that polaron effects may be stronger on the electron-doped side, leading to carrier localization over a broader range of doping. There has been some success in modeling the contrast in the single-hole spectrum by introducing further-neighbor coupling into the one-band model, which breaks the particle-hole symmetry (Shih et al., 2004). This will be discussed further below.

We conclude that the electron correlation is strong enough to produce a Mott insulator at half-filling. Furthermore, the one-band t-J model captures the essence of the low-energy electronic excitations of the cuprates. Particle-hole asymmetry may be accounted for by including further-neighbor hopping t'. This point of view has been tested extensively by Hybertson et al. (1990) who used ab initio local-density-functional theory to generate input parameters for the three-band Hubbard model and then solved the spectra exactly on finite clusters. The results were compared with the low-energy spectra of the one-band Hubbard model and the t-t'-J model. They found an excellent overlap of the low-lying wave functions for both the one-band Hubbard and the t-t'-J model and were able to extract effective parameters. They found J to be 128 ± 5 meV, in excellent agreement with experimental values. Furthermore, they found $t \approx 0.41$ and 0.44 eV for electron and hole doping, respectively. The near particle-hole symmetry in t is surprising because the underlying electronic states are very different in the two cases, as already discussed. Based on their results, the commonly used parameter J/t for the t-J model is $1/3$. They also found a significant next-nearest-neighbor t' term, again almost the same for electron and hole doping.

More recently, Andersen et al. (1996) pointed out that in addition to the three-band model an additional Cu $4s$ orbital has a strong influence on further-neighbor hopping t' and t'', where t' is the hopping across the diagonal and t'' is hopping to the next-nearest neighbor along a straight line. Recently Pavarini et al. (2001) emphasized the importance of the apical oxygen in modulating the energy of the Cu $4s$ orbital and found a sensitive dependence of t'/t on the apical oxygen distance. They also pointed out an empirical correlation between optimal T_c and t'/t. As we shall discuss in Secs. VI.D and VII, t' may play an important role in determining T_c and in explaining the difference between electron and hole doping. However, in view of the fact that on-site repulsion is the largest energy scale in the problem, it would make sense to begin our modeling of the cuprates with the t-J model and ask to what extent the phase diagram can be accounted for. As we shall see, even this is not a simple task and will constitute the major thrust of this review.

III. PHENOMENOLOGY OF THE UNDERDOPED CUPRATES

The essence of the problem of doping into a Mott insulator is readily seen from Fig. 2. When a vacancy is introduced into an antiferromagnetic spin background, it would like to hop with amplitude t to lower its kinetic energy. However, after one hop its neighboring spin finds itself in a ferromagnetic environment, at an energy cost of $\frac{3}{2}J$ if the spins are treated as classical $S=\frac{1}{2}$. It is clear that the holes are very effective in destroying the antiferromagnetic background. This is particularly so at $t \gg J$ when the hole is strongly delocalized. The basic physics is the competition between the exchange energy J and the kinetic energy, which is of order t per hole or xt per unit area. When $xt \gg J$, we expect the kinetic energy to win and the system would be a Fermi-liquid metal with a weak residual antiferromagnetic correlation. When $xt \lesssim J$, however, the outcome is much less clear because the system would like to maintain the antiferromagnetic correlation while allowing the hole to move as freely as possible. Experimentally we know that the Néel order is destroyed with 3% hole doping, after which the d-wave superconducting state emerges as the ground state up to 30% doping. Exactly how and why superconductivity emerges as the best compromise is the centerpiece of the high-T_c puzzle, but we already see that the simple competition between J and xt sets the correct scale $x=J/t=\frac{1}{3}$ for the appearance of nontrivial ground states. We shall focus our attention on the underdoped region where this competition rages most fiercely. Indeed it is known experimentally that the normal state above the superconducting T_c behaves differently from any other metallic state that we have known about up to now. Essentially an energy gap appears in some properties and not others. This region of the phase diagram is referred to as the pseudogap region and is well documented experimentally. Below we review some of the key properties.

A. Pseudogap phenomenon in the normal state

As seen in Fig. 3, the Knight-shift measurement in the YBCO 124 compound shows that while the spin susceptibility χ_s is almost temperature independent between 700 and 300 K, as in an ordinary metal, it decreases below 300 K and by the time the T_c of 80 K is reached, the system has lost 80% of the spin susceptibility (Curro et al., 1997). To emphasize the universality of this phenomenon, we reproduce in Fig. 4 some old data on YBCO and LSCO. Figure 4(a) shows the Knight-shift data from Alloul et al. (1989). We have subtracted the orbital contribution which is generally agreed to be 150 ppm (Takigawa et al., 1993) and drawn in the zero line to highlight the spin contribution to the Knight shift, which is proportional to χ_s. The proportionality constant is known, which allows us to draw in the Knight shift, which corresponds to the two-dimensional square $S=\frac{1}{2}$ Heisenberg antiferromagnet with $J=0.13$ eV (Ding and
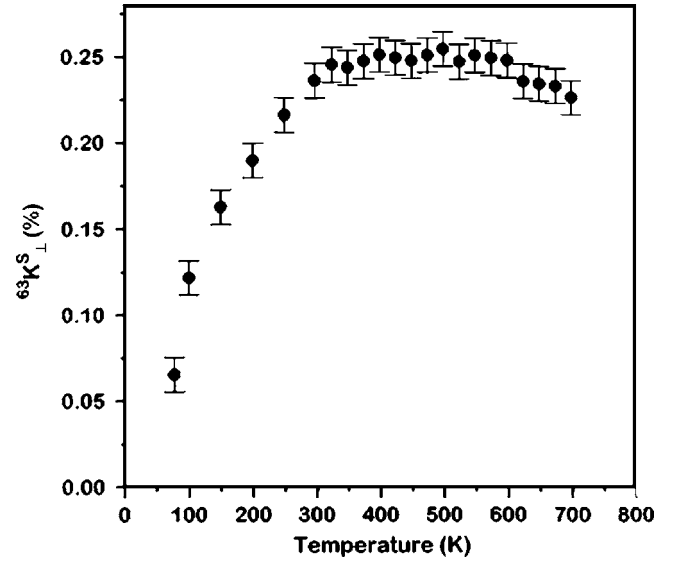
FIG. 3. Knight shift for an underdoped $YB_2Cu_4O_8$ with $T_c=79$ K. From Curro et al., 1997.
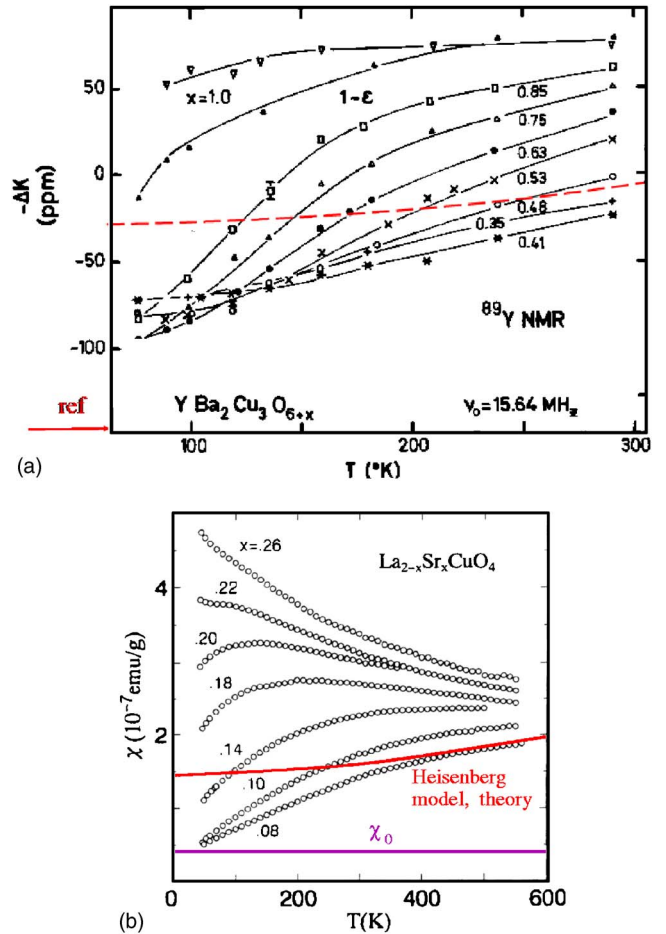
FIG. 4. (Color online) Spin susceptibility data for a variety of doping. (a) Knight-shift data of YBCO (from Alloul et al., 1989). The zero reference level for the spin contribution is indicated by the arrow and the dashed line represents the prediction of the 2D $S=\frac{1}{2}$ Heisenberg model for $J=0.13$ eV. (b) Uniform magnetic susceptibility for LSCO (from Nakano et al., 1994). The orbital contribution χ_0 is shown (see text) and the solid line represents the Heisenberg-model prediction.
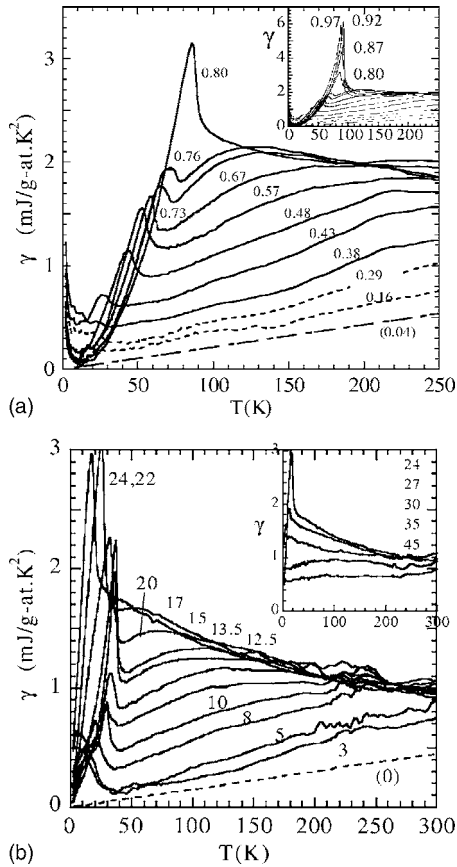
FIG. 5. The specific-heat coefficient γ. (a) $YBa_2Cu_3O_{6+y}$. (b) $La_{2-x}Sr_xCuO_4$. Curves are labeled by the oxygen content y in the top figure and by the hole concentration x in the bottom figure. Optimal and overdoped samples are shown in the inset. The jump in γ indicates the superconducting transition. Note the reduction of the jump size with underdoping. From Loram *et al.*, 1993, 2001.

Makivic, 1991; Sandvik *et al.*, 1997). The point of this exercise is to show that in the underdoped region the spin susceptibility drops below that of the Heisenberg model at low temperatures before the onset of superconductivity. This trend continues even in the severely underdoped limit ($O_{0.53}-O_{0.41}$), showing that the χ_s reduction cannot simply be understood as a fluctuation towards the antiferromagnet. Note that the discrepancy is worse if J were replaced by a smaller J_{eff} due to doping since $\chi_s \sim J_{eff}^{-1}$. The data seen in this light strongly point to singlet formation as the origin of the pseudogap seen in the uniform spin susceptibility.

It is worth noting that the trend shown in Fig. 4(a) is not so apparent if one looks at the measured spin susceptibility directly (Tranquada *et al.*, 1988). This is because the van Vleck part of the spin susceptibility is doping dependent due to the changing chain contribution. This problem does not arise for LSCO, and in Fig. 4(b) we show the uniform susceptibility data (Nakano *et al.*, 1994). The zero of the spin part is determined by comparing susceptibility measurements to O Knight-shift data (Ishida *et al.*, 1991). Nakano *et al.* (1994) found an excellent fit for the $x=0.15$ sample (see Fig. 9 of this
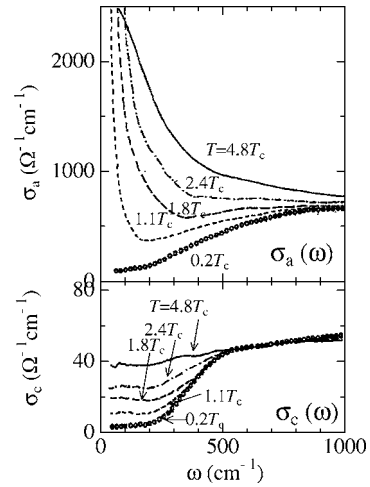
FIG. 6. The frequency-dependent conductivity with electric field parallel to the plane [$\sigma_a(\omega)$, top figure] and perpendicular to the plane [$\sigma_c(\omega)$, bottom figure] in an underdoped YBCO crystal. From Uchida, 1997.

reference) and determined the orbital contribution for this sample to be $\chi_0 \sim 0.4 \times 10^{-7}$ emu/g. This again allows us to plot the theoretical prediction for the Heisenberg model. Just as for YBCO, χ_s for the underdoped samples ($x=0.1$ and 0.08) drops below that of the Heisenberg model. In fact, the behavior of χ_s for the two systems is remarkably similar, especially in the underdoped region.[1]

A second indication of the pseudogap comes from the linear T coefficient of the specific heat, which shows a marked decrease below room temperature (see Fig. 5). Furthermore, the specific-heat jump at T_c is greatly reduced with decreasing doping. It is apparent that the spins are forming into singlets and the spin entropy is gradually lost. On the other hand, as shown in Fig. 6, the frequency-dependent conductivity behaves very differently depending on whether the electric field is in the *ab* plane (σ_{ab}) or perpendicular to it (σ_c).

At low frequencies (below 500 cm^{-1}) σ_{ab} shows a typical Drude-like behavior for a metal with a width which decreases with temperature, but with an area (spectral weight) which is independent of temperature (Santander-Syro *et al.*, 2002). Thus there is no sign of the pseudogap in the spectral weight. This is surprising because in other examples in which an energy gap appears in a metal, such as the onset of charge- or spin-density waves, there is a redistribution of the spectral weight from the Drude part to higher frequencies. An important observation concerning the spectral weight is that the integrated area under the Drude peak is found to be

_____

[1]We note that a comparison of χ_s for YBCO and LSCO was made by Millis and Monien (1993). Their YBCO analysis was similar to ours. However, for LSCO they found a rather different χ_0 by matching the measurement above 600 K to that of the Heisenberg model. Consequently, their χ_s looked different for YBCO and LSCO.

linear in x (Orenstein *et al.*, 1990; Uchida *et al.*, 1991; Cooper *et al.*, 1993; Padilla *et al.*, 2005). In the superconducting state this weight collapses to form the delta-function peak, with the result that the superfluid density n_s/m is also linear in x. It is as though only the doped holes contribute to the charge transport in the plane. In contrast, angle-resolved photoemission spectroscopy shows a Fermi surface at optimal doping very similar to that predicted by band theory, with an area corresponding to $1-x$ electrons [see Fig. 7(d)]. With underdoping, this Fermi surface is partially gapped in an unusual manner, which we shall discuss next.

In contrast to the metallic behavior of σ_{ab}, Homes *et al.* (1993) discovered that below 300 K $\sigma_c(\omega)$ is gradually reduced for frequencies below 500 cm^{-1} and a deep hole is carved out of $\sigma_c(\omega)$ by the time T_c is reached. This is clearly seen in the lower panel of Fig. 6.

Finally, angle-resolved photoemission spectroscopy shows that an energy gap (in the form of a pulling back of the leading edge of the electronic spectrum from the Fermi energy) is observed near momentum $(0,\pi)$. Note that the line shape is extremely broad and completely incoherent. The onset of superconductivity is marked by the appearance of a small coherent peak at this gap edge (Fig. 7). The size of the pullback of the leading edge is the same as the energy gap of the superconducting state as measured by the location of the coherence peak. As shown in Fig. 7, this gap energy increases with decreasing doping while the superconducting T_c decreases. This trend is also seen in tunneling data.

It is possible to map out the Fermi surface by tracking the momentum of the minimum excitation energy in the superconducting state for each momentum direction. Along the Fermi surface the energy gap does exactly what is expected for a d-wave superconductor. It is maximal near $(0,\pi)$ and vanishes along the line connection $(0,0)$ and (π,π), where the excitation is often referred to as nodal quasiparticles. Above T_c the gapless region expands to cover a finite region near the nodal point, beyond which the pseudogap gradually opens as one moves towards $(0,\pi)$. This unusual behavior is sometimes referred to as the Fermi arc (Ding *et al.*, 1996; Loeser *et al.*, 1996; Marshall *et al.*, 1996). It is worth noting that unlike the antinodal direction [near $(0,\pi)$], the line shape is relatively sharp along the nodal direction even above T_c. From the width in momentum space, a lifetime which is linear in temperature has been extracted for a sample near optimal doping (Valla *et al.*, 1999). A narrow line shape in the nodal direction has also been observed in LSCO (Yoshida *et al.*, 2003) and in Na-doped $Ca_2CuO_2Cl_2$ (Ronning *et al.*, 2003). So the notion of relatively well-defined nodal excitations in the normal state is most likely a universal feature.

As mentioned earlier, the onset of superconductivity is marked by the appearance of a sharp coherence peak near $(0,\pi)$. The spectral weight of this peak is small and gets even smaller with decreasing doping, as shown in Fig. 8(b). Note that this behavior is totally different from conventional superconductors. There the quasiparticles
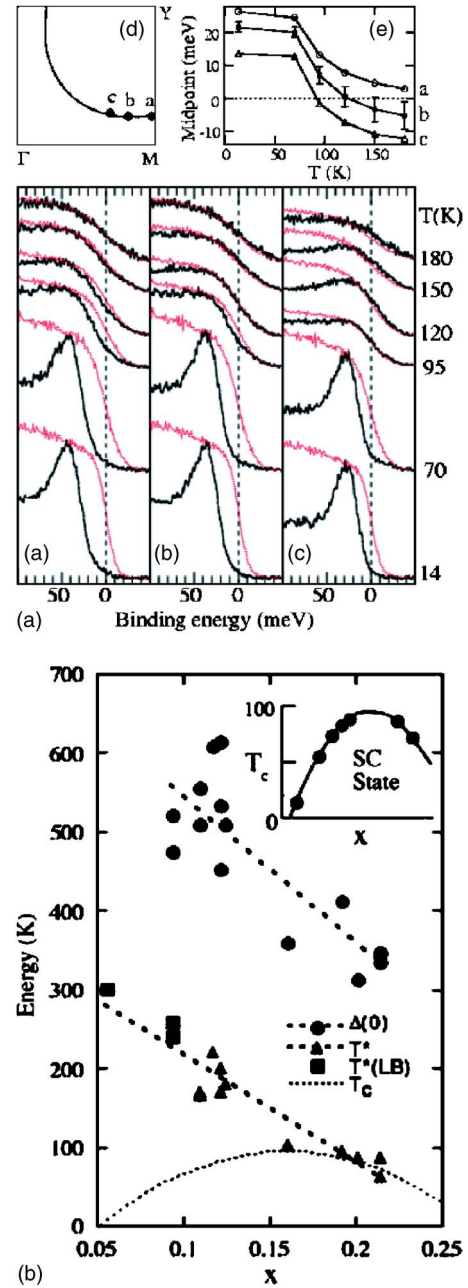
FIG. 7. (Color online) Angle-resolved photoemission data for underdoped cuprates. (a)–(c) Spectra from underdoped Bi-2212 ($T_c=85$ K) taken at different k points along the Fermi surface shown in (d). Note the pullback of the spectrum from the Fermi surface as determined by the Pt reference shown by grey lines (red online) for $T>T_c$. (e) Temperature dependence of the leading-edge midpoints (from Norman *et al.*, 1998). The temperature T^* where the pseudogap determined from the leading edge first appears plotted as a function of doping for Bi-2212 samples (bottom). Triangles are determined from data such as shown in (a) and squares are lower-bound estimates. Circles show the energy gap Δ measured at $(0,\pi)$ at low temperatures. From Campuzano *et al.*, 2003.

are well defined in the normal state and according to BCS theory the sharp peak pulls back from the Fermi energy and opens an energy gap in the superconducting state.
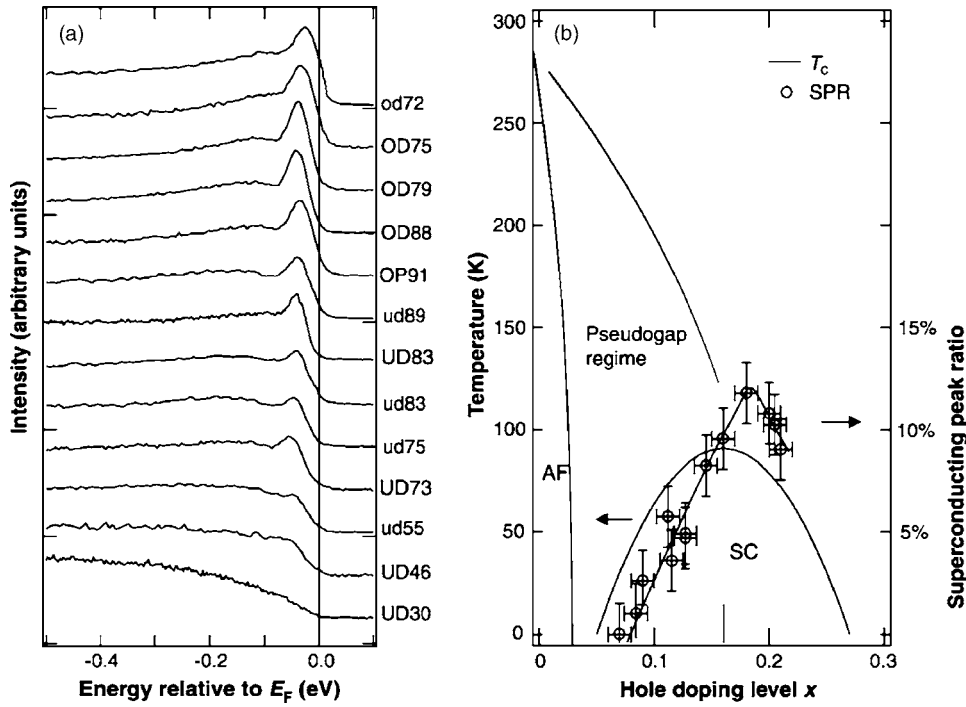
FIG. 8. Photoemission spectra and spectral weight. (a) Doping dependence of the ARPES spectra at $(0, \pi)$ at $T \ll T_c$ for overdoped (OD), optimally doped (OP), and underdoped (UD) materials labeled by their T_c's. (b) The spectral weight of the coherent peak in (a) normalized to the background is plotted vs doping x. From Feng et al., 2000.

Yet another indication that the superconducting transition is different from BCS theory comes from the measurement of the change in kinetic energy through the transition. In conventional BCS theory, pairing between quasiparticles leads to a gain in the attractive potential energy at the expense of increasing the kinetic energy since the Fermi distribution is smeared by the creation of the energy gap. By carefully monitoring the optical spectral weight above and below T_c, it was found that while optimally doped samples behave as expected for BCS superconductors, underdoped samples exhibit the opposite behavior in that the kinetic energy is lowered by the onset of superconductivity (Molegraaf et al., 2002; Santander-Syro et al., 2002; Boris et al., 2004; Kuzmenko et al., 2005; Santander-Syro and Bontemps, 2005).

In the past few years, low-temperature STM data have become available, mainly on Bi-2212 samples. STM provides a measurement of the local density of states $\rho(E, r)$ with atomic resolution. It is complementary to ARPES in that it provides real-space information but no direct momentum-space information. One important outcome is that STM reveals the spatial inhomogeneity of Bi-2212 on roughly a 50–100-Å length scale, which becomes more significant with underdoping. As shown in Fig. 9(f), spectra with different energy gaps are associated with different patches and with progressively more underdoping; patches with large gaps become more predominant. Since ARPES is measuring the same surface, it becomes necessary to reinterpret the ARPES data with inhomogeneity in mind. In particular, the decrease of the weight of the coherent peak shown in Fig. 8(b) may simply be due to a reduction of the fraction of the sample which has sharp coherent peaks. However, we should note that there are concerns as to whether the surface inhomogeneity may behave differently depending on the temperature at which the crystals are cleaved since the

STM experiments shown here are cleaved at low temperatures, whereas ARPES and other STM experiments (Maggio-Aprile et al., 1995) are typically cleaved at higher temperatures.

A second remarkable observation by STM is that the low-lying density of states $[\rho(E, r)$ for $E \lesssim 10–15$ meV] is remarkably homogeneous. This is clearly seen in Fig. 9(f). It is reasonable to associate this low-energy excitation with quasiparticles near the nodes. Indeed, low-lying quasiparticles exhibit interference effects due to scattering by impurities, which is direct evidence for their spatial coherence over long distances. Then the combined STM and ARPES data suggest a kind of phase separation in momentum space, i.e., the spectra in the antinodal region (near $0, \pi$) is highly inhomogeneous in space, whereas the quasiparticles near the nodal region are homogeneous and coherent. The nodal quasiparticles must be extended and capable of averaging over the spatial homogeneity, while the antinodal quasiparticles appear more localized. In this picture the pseudogap phenomenon mainly has to do with the antinodal region.

McElroy et al. (2005) have argued that there is a limiting spectrum [the broadest curve in Fig. 9(f)] which characterizes the extreme underdoped region at zero temperature. It has no coherent peak at all, but shows a reduction of spectral weight up to a very high energy of 100–200 meV. Very recently, Hanaguri et al. (2004) have provided support for this point of view in their study of Na-doped $Ca_2CuO_2Cl_2$. In this material the apical oxygen in the CuO_4 cage is replaced by Cl and the crystal cleaves easily. For Na doping ranging from $x = 0.08$ to 0.12, a tunneling spectrum very similar to the limiting spectrum for Bi-2212 is observed. This material appears free of the inhomogeneity which plagues the Bi-2212
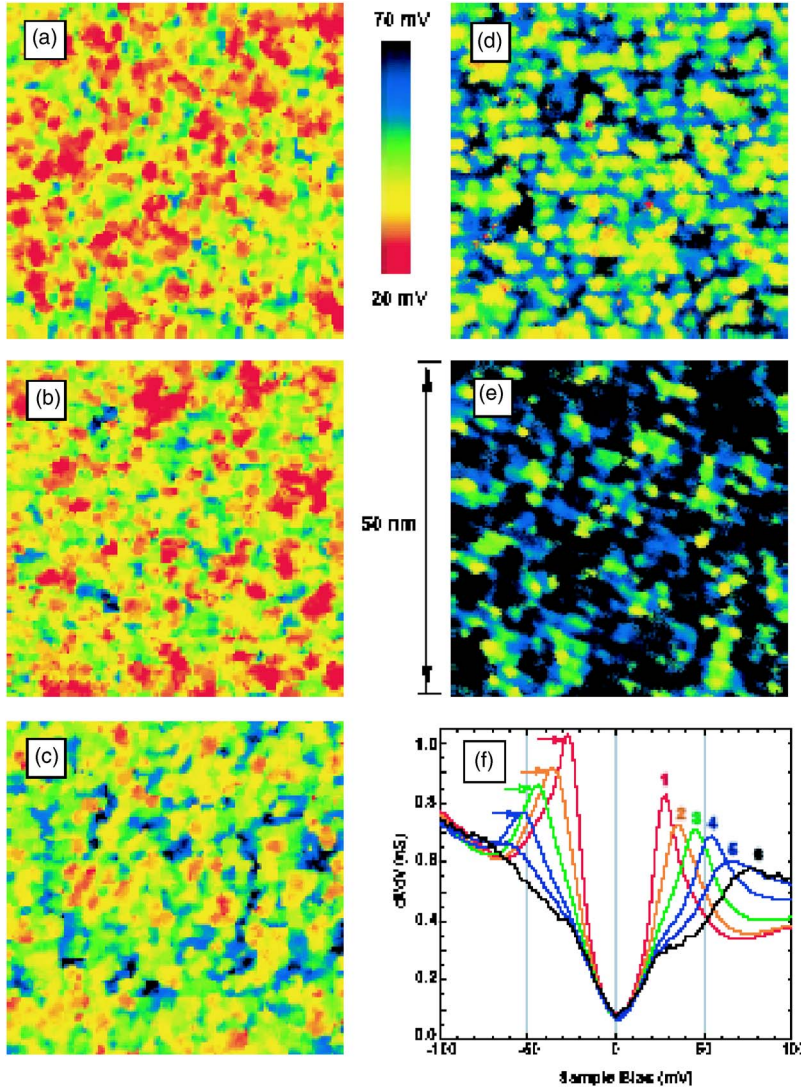
FIG. 9. (Color online) STM images showing the spatial distribution of energy gaps for a variety of samples which are progressively more underdoped from (a) to (e). (f) The average spectrum for a given energy gap. From McElroy *et al.*, 2005.

surface. ARPES experiments on these crystals are becoming available (Ronning *et al.*, 2003) and the combination of STM and ARPES should yield much information on the real- and momentum-space dependence of the electron spectrum. There is much excitement concerning the discovery of a static 4×4 pattern in this material and its relation to the incommensurate pattern seen in the vortex core of Bi-2212 (Hoffman *et al.*, 2002) and also reported in the absence of a magnetic field, albeit in a much weaker form (Howland *et al.*, 2003; Vershinin *et al.*, 2004). How this spatial modulation is related to the pseudogap spectrum is a topic of current debate.

In the literature, pseudogap behavior is often associated with the anomalous behavior of the nuclear-spin relaxation rate $1/T_1$. In normal metals the nuclear spin relaxes by producing low-energy particle-hole excitations, leading to Koringa behavior, i.e., $1/T_1 T$ is temperature independent. In high-T_c materials, it is instead $1/T_1$ which is temperature independent, and the enhanced relaxation (relative to Koringa) as the temperature is reduced as ascribed to antiferromagnetic spin fluctuations. It was found that in underdoped YBCO,

the nuclear-spin relaxation rate at the copper site reaches a peak at a temperature of T_1^* and decreases rapidly below this temperature (Warren *et al.*, 1989; Yasuoka *et al.*, 1989; Takigawa *et al.*, 1991). The resistivity also shows a decrease below T_1^*. In some work in the literature T_1^* is referred to as the pseudogap scale. However, we note that T_1^* is lower than the energy scale we have been discussing so far, especially compared with that for the uniform spin susceptibility and the *c*-axis conductivity. Furthermore, the gap in $1/T_1$ is not universally observed in cuprates, e.g., it is not seen in LSCO. In $YBa_2Cu_4O_8$, which is naturally underdoped, the gap in $1/T_1 T$ is wiped out by 1% Zn doping, while the Knight shift remains unaffected (Zheng *et al.*, 2003). It is known from neutron scattering that low-lying spin excitations near (π, π) are sensitive to disorder. Since $1/T_1$ at the copper site is dominated by these fluctuations, it is reasonable that $1/T_1$ is sensitive as well. In contrast, the gaplike behavior we have described thus far in a variety of physical properties is universally observed across different families of cuprates (wherever data exist) and are

FIG. 10. (Color online) Plot of the incommensurability δ vs hole concentration x. From Matsuda *et al.*, 2000. In the superconducting state, the open circles denote the position of the fluctuating spin-density wave observed by neutron scattering. Data from Yamada *et al.*, 1998. In the i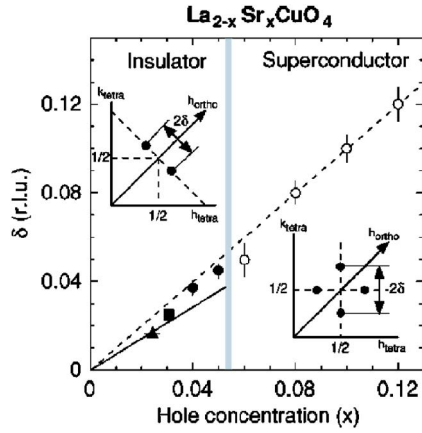nsulator the spin-density wave becomes static at low temperatures and its orientation is rotated by 45°. The dashed line ($\delta=x$) is the prediction of the stripe model, which assumes a fixed density of holes along the stripe.

robust. Thus we prefer not to consider T_1^* as the pseudogap temperature scale.

B. Neutron scattering, resonance, and stripes

Neutron scattering provides a direct measure of the spin-excitation spectrum. Early work (see Kastner *et al.*, 1998) showed that with doping, the long-range Néel order gives way to short-range order with a progressively shorter correlation length so that at optimal doping the static spin-correlation length is no more than two or three lattice spacings. Much of the early work was focused on the $La_{2-x}Sr_xCuO_4$ family because of the availability of large single crystals. It was found that there is enhanced spin scattering at low energies, centered around the incommensurate positions $q_0=(\pm\pi/2,\pm\delta)$ (Cheong *et al.*, 1991). Yamada *et al.* (1998) found that δ increases systematically with doping, as shown in Fig. 10. Meanwhile it was noted that in the La_2CuO_4 family there is a marked suppression of T_c near $x=\frac{1}{8}$. This suppression is particularly strong with Ba doping, and T_c is completely destroyed if some Nd is substituted for La, as in $La_{1.6-x}Nd_{0.4}Sr_xCuO_4$ for $x=\frac{1}{8}$. Tranquada *et al.* (1995) discovered static spin-density-wave and charge-density-wave order in this system, which appears below about 50 K. The period of the spin- and charge-density waves are eight and four lattice constants, respectively. The static order is modeled by a stripe picture in which holes are concentrated in period-4 charge stripes separated by spin-ordered regions with antiphase domain walls. Recently, the same kind of stripe order was observed in $La_{1.875}Ba_{0.125}CuO_4$ (Fujita *et al.*, 2004). Note that in this model there is one hole per two sites along the charge stripe. It is tempting to interpret the low-energy spin-density wave observed in LSCO as a slowly fluctuating

form of stripe order, even though the associated charge order (presumably dynamical also) has not yet been seen. The most convincing argument for this interpretation comes from the observation that over a range of doping $x=0.06$ to $x=0.125$ the observed incommensurability δ is given precisely by the stripe picture, i.e., $\delta=x$, while δ saturates at approximately $\frac{1}{8}$ for $x\gtrsim 0.125$ (see Fig. 10). However, it must be noted that with this interpretation the charge stripe must be incompressible, i.e., it behaves as a charge insulator. Upon changing x, it is energetically more favorable to add or remove stripes and change the average stripe spacing, rather than to change the hole density on each stripe, which is pinned at $\frac{1}{4}$ filling. It is difficult to reconcile this picture with the fact that LSCO is metallic and superconducting in the same doping range. An alternative interpretation of the incommensurate spin scattering is that it is due to Fermi-surface nesting (Littlewood *et al.*, 1993; Si *et al.*, 1993; Tanamoto *et al.*, 1993). However, in this case the x dependence of δ requires some fine-tuning. Regardless of interpretation, it is clear that in the LSCO family there are low-lying spin-density-wave fluctuations which are almost ready to condense. At low temperatures, static spin-density-wave order is stabilized by Zn doping (Kimura *et al.*, 1999) near $x=\frac{1}{8}$ (Wakimoto *et al.*, 1999) and in oxygen-doped systems (Lee *et al.*, 1999). However, in the latter case there is evidence from muon spin rotation (Savici *et al.*, 2002) that there may be microscopic phase separations in this material (not too surprising in view of the STM data on Bi-2202). It was also found that spin-density-wave order is stabilized in the vicinity of vortex cores (Kitano *et al.*, 2000; Lake *et al.*, 2001; Khaykovich *et al.*, 2002).

The key question then is whether the fluctuating stripe picture is special to the LSCO family or plays a significant role in all the cuprates. Outside of the LSCO family, the spin response is dominated by a narrow resonance at (π,π). The resonance was first discovered at 41 meV for optimally doped YBCO (Rossat-Mignod *et al.*, 1991; Mook *et al.*, 1993). Careful subtraction of an accidentally degenerate phonon line reveals that the resonance appears only below T_c at optimal doping (Fong *et al.*, 1995). Now it is known that with underdoping the resonance moves down in energy and survives into the pseudogap regime above T_c. The resonance moves smoothly to almost zero energy at the edge of the transition to Néel order in $YBa_2Cu_3O_{6.35}$ (Stock *et al.*, 2005a) and clearly plays the role of a soft mode at that transition.

The resonance was interpreted as a spin-triplet exciton bound below $2\Delta_0$ (Fong *et al.*, 1995). This idea was elaborated upon by a number of random-phase-approximation calculations (Liu *et al.*, 1995; Bulut and Scalapino, 1996; Brinckmann and Lee, 1999, 2002; Kao *et al.*, 2000; Norman, 2000, 2001; Abanov *et al.*, 2002; Onufrieva and Pfeuty, 2002). An alternative picture was proposed which made use of the particle-particle channel (Demler and Zhang, 1995). However, as explained by Tchernyshyov *et al.* (2001) and by Norman and Pepin
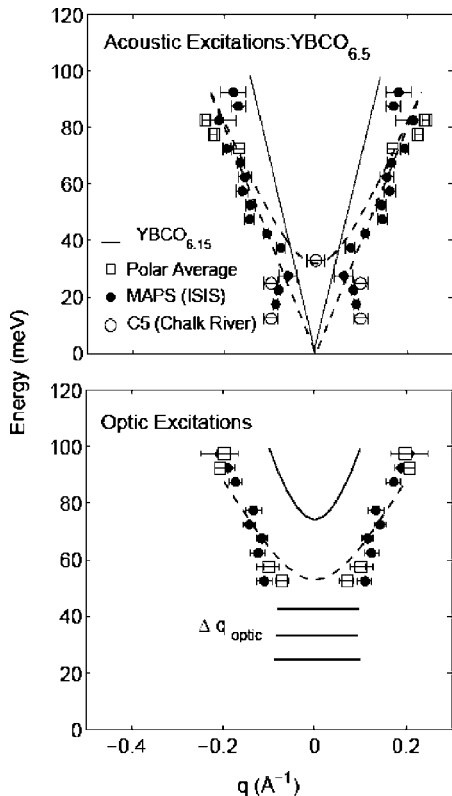
FIG. 11. Neutron scattering from YBCO$_{6.5}$. This sample has $T_c = 59$ K and the experiment was performed at 6 K (from Stock et al., 2005). Top panel refers to in-phase fluctuations between the bilayer which shows a resonance located at (π, π) $(q=0)$ and at energy 33 meV. Incommensurate peaks disperse down from the resonance. Broad peaks also disperse upward from the resonance forming the hourglass pattern. The solid line is the spin-wave spectrum of the insulating parent compound. Bottom panel denotes out-of-phase fluctuations between the bilayers.

(2003), this theory predicts an antibound resonance above the two-particle continuum, which is not in accord with experiments.

Further support of the triplet exciton idea comes from the observation that incommensurate branches extend below the resonance energy (Bourges et al., 2000). This behavior is predicted by random-phase-approximation-type theories (Kao et al., 2000; Norman, 2000; Brinckmann and Lee, 2002; Li and Gong, 2002; Onufrieva and Pfeuty, 2002) in that the gap in the particle-hole continuum extends over a region near (π, π), where the resonance can be formed. With further underdoping this incommensurate branch extends to lower energies (see Fig. 11). Now it becomes clear that the low-energy incommensurate scattering previously reported for underdoped YBCO (Mook et al., 2000) is part of this downward dispersing branch (Pailhes et al., 2004; Stock et al., 2004).

It should be noted that while the resonance is prominent due to its sharpness, its spectral weight is actually quite small, of order 2% of the total spin moment sum rule for optimal doping and increasing somewhat with

underdoping. There is thus considerable controversy over its significance in terms of its contribution to the electron self-energy and towards pairing (see Norman and Pepin, 2003). The transfer of this spectral weight from above to below T_c has been studied in detail by Stock et al. (2004). These authors have emphasized that in the pseudogap state above T_c in YBa$_2$Cu$_3$O$_{6.5}$ the scattering below the resonance is gapless and in fact increases in strength with decreasing temperature. This is in contrast to the sharp drop seen in $1/T_1T$ below 150 K. Either a gap opens up at very low energy (below 4 meV) or the (π, π) spins fluctuating seen by neutrons are not the dominant contribution to the nuclear-spin relaxation, i.e., the latter may be due to excitations which are smeared out in momentum space and undetected by neutrons. We note that a similar discrepancy between the neutron-scattering spectral weight and $1/T_1T$ was noted for LSCO (Aeppli et al., 1995). This reinforces our view that the decrease in $1/T_1T$ should not be considered a signature of the pseudogap. We also note that an enhanced (π, π) scattering together with singlet formation is just what is predicted by the SU(2) theory in Sec. XI.D.

Recently, neutron scattering has been extended to energies much above the resonance. It is found that very broad features disperse upward from the resonance, resulting in the "hourglass" structure shown in Fig. 11, which was first proposed by Bourges et al. (2000) (Hayden et al., 2004; Stock et al., 2004). Interestingly, there has also been a significant evolution of the understanding of neutron scattering in the LSCO family. For a long time it was thought that the LSCO family does not exhibit the resonance which shows up prominently below T_c in YBCO and other compounds. However, neutron scattering does show a broad peak around 50 meV, which is temperature independent. Tranquada et al. (2004) have studied La$_{1.875}$Ba$_{0.125}$CuO$_4$, which exhibits static charge and spin stripes below 50 K and a greatly suppressed T_c. Their data also exhibit an hourglass-type dispersion, remarkably similar to that of underdoped YBCO. In particular, the incommensurate scattering which was previously believed to be dispersionless now exhibits downward dispersion (Fujita et al., 2004). The same phenomenon is also seen in optimally doped La$_{2-x}$Sr$_x$CuO$_4$ (Christensen et al., 2004). It is remarkable that in these materials known to have static or dynamic stripes the incommensurate low-energy excitations are not spin waves emanating from $(\pi/2 \pm \delta)$ as one might have expected, but instead are connected to the peak at (π, π) in the hourglass fashion. Tranquada et al. (2004) fit the $\boldsymbol{k}$-integrated intensity to a model of a two-leg ladder. It is not clear how unique this fit is because one may expect high-energy excitations to be relatively insensitive to details of the model. What is emerging though is a picture of a universal hourglass-shaped spectrum, which is common to LSCO and YBCO families. The high-energy excitations appear common while the major difference seems to be in the rearrangement of spectral weight at low energy. In La$_{1.875}$Ba$_{0.125}$CuO$_4$ significant
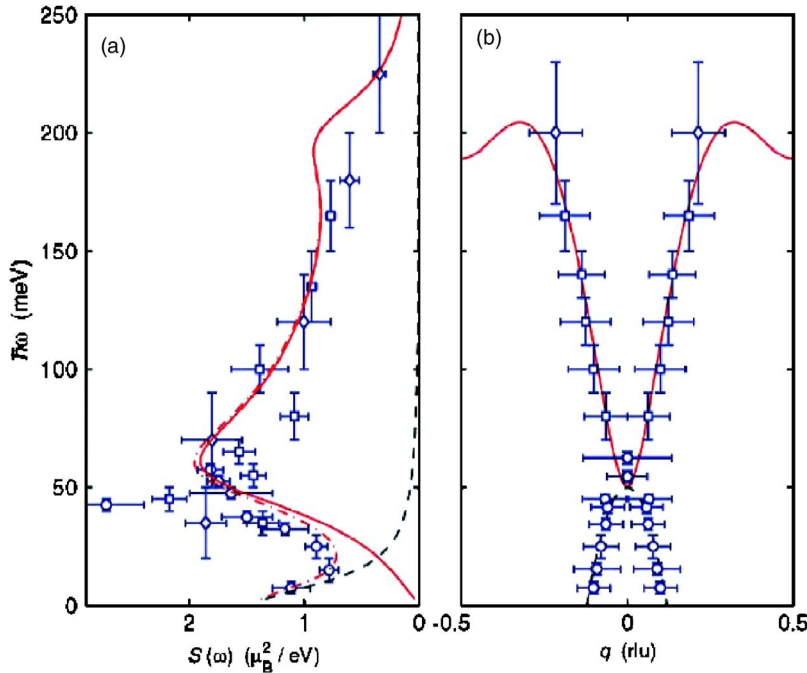
FIG. 12. (Color online) Neutron scattering from $La_{1.875}Ba_{0.125}CuO_4$ at 12 K ($>T_c$) (from Tranquada *et al.*, 2004). (b) The hourglass pattern of the excitation spectrum (cf. Fig. 11). The solid line is a fit to a two-leg-ladder spin model. (a) The momentum-integrated scattering intensity. The dashed line is a Lorenztian fit to the rising intensity at the incommensurate positions. The sharp peak at 40 meV could be a phonon.

weight has been transferred to the low-energy incommensurate scattering, as shown in Fig. 12, and is associated with stripes. In our view the universality supports the picture that all the cuprates share the same short-distance and high-energy physics, which includes the pseudogap behavior. Stripe formation is a competing state which becomes prominent in the LSCO family, especially near $x=\frac{1}{8}$, and may dominate the low-energy and low-temperature (below 50 K) physics. There is a school of thought which holds the opposite view (see Carlson *et al.*, 2003), that fluctuating stripes are responsible for the pseudogap behavior and the appearance of superconductivity. From this point of view the same data have been interpreted as an indication that stripe fluctuations are also important in the YBCO family (Tranquada *et al.*, 2004). Clearly, this is a topic of much current debate.

C. Quasiparticles in the superconducting state

In contrast with the anomalous properties of the normal state, the low-temperature properties of the superconductor seem relatively normal. There are two major differences with conventional BCS superconductors, however. First, due to the proximity to the Mott insulator, the superfluid density of the superconductor is small and vanishes with decreasing hole concentration. Second, because the pairing is d wave, the gap vanishes on four points on the Fermi surface (called gap nodes) so that the quasiparticle excitations are gapless and affect the physical properties even at the lowest temperatures. We shall focus on these nodal quasiparticles in this subsection.

The nodal quasiparticles clearly contribute to the thermal dynamical quantities such as the specific heat. Because their density of states vanish linearly in energy,

they give rise to a T^2 term, which dominates the low-temperature specific heat. In practice, disorder rounds off the linear density of states, giving instead an $\alpha T + \beta T^3$ behavior. An interesting effect in the presence of a magnetic field was proposed by Volovik (1993). He argued that in the presence of a vector potential A or superfluid flow, the quasiparticle dispersion $E(k) = \sqrt{(\epsilon_k-\mu)^2+\Delta_k^2}$ is shifted by

$$E_A(k) = E(k) + \left(\frac{1}{2e}\boldsymbol{\nabla}\,\theta - A\right)\cdot j_k, \qquad (3)$$

where j_k is the current carried by normal-state quasiparticles with momentum k and is usually taken to be $-e\partial_{\epsilon_k}/\partial k$. Note that since the BCS quasiparticle is a superposition of a particle and a hole, the charge is not a good quantum number. However, the particle component with momentum k and the hole component with momentum $-k$ each carry the same electrical current $j_k=-e(\partial_{\epsilon_k}/\partial k)$ and it makes sense to consider this to be the current carried by the quasiparticle. Note that j_k/e is very different from the group velocity $\partial E(k)/\partial k$.

In a magnetic field which exceeds H_{c1}, vortices enter the sample. The superfluid flow $\boldsymbol{\nabla}\theta\sim 2\pi/r$, where r is the distance to the vortex core. On average, $\frac{1}{2}|\boldsymbol{\nabla}\theta|\approx\pi/R$, where $R=(\phi_0/H)^{1/2}$ is the average spacing between vortices and $\phi_0=hc/2e$ is the flux quantum. Volovik then predicted a shift of the quasiparticle spectra by $\approx ev_F(H/\phi_0)^{1/2}$, which in turn gives a contribution to the specific heat proportional to $\sqrt{H}$. This contribution was observed experimentally (Moler *et al.*, 1994). Very recently Wen *et al.* (2005) have used this effect to extract v_Δ, the velocity of the nodal quasiparticle in the direction of the maximum gap Δ_0. The result is consistent with that shown in Fig. 13, which will be discussed later.
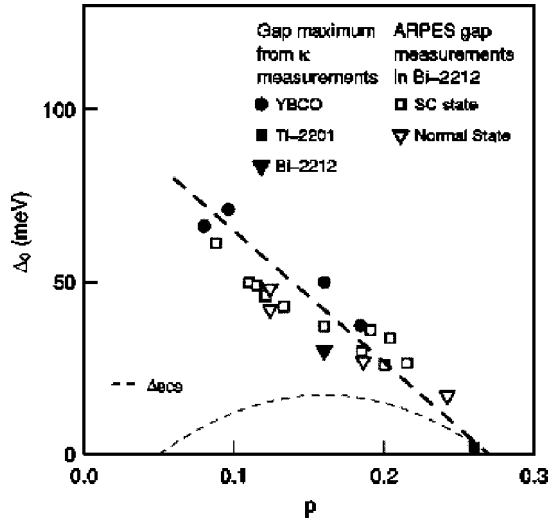
FIG. 13. Doping dependence of the superconducting gap Δ_0 obtained from the quasiparticle velocity v_Δ using Eq. (4) (filled symbols). Here we assume $\Delta = \Delta_0 \cos 2\phi$ so that $\Delta_0 = \hbar k_F v_\Delta / 2$, and plot data for YBCO alongside Bi-2212 (Chiao *et al.*, 2000) and Tl-2201 (Proust *et al.*, 2002). For comparison, a BCS gap of the form $\Delta_{BCS} = 2.14 k_B T_c$ is also plotted. The value of the energy gap in Bi-2212, as determined by ARPES, is shown as measured in the superconducting state (Campuzano *et al.*, 1999) and the normal state (Norman *et al.*, 1998) (open symbols). The thick dashed line is a guide to the eye. From Sutherland *et al.*, 2003.

The quasiparticles contribute to the low-temperature transport properties as well. Lee (1993) considered the frequency-dependent conductivity $\sigma(\omega)$ due to quasiparticle excitations. In the low-temperature limit, he found that the low-frequency limit of the conductivity is universal in the sense that it does not depend on impurity strength, but only on the ratio v_F/v_Δ, i.e., $\sigma(\omega \to 0) = e^2 \pi v_F / h v_\Delta$ if $v_F \gg v_\Delta$. This result was derived within the self-consistent t-matrix approximation and can easily be understood as follows. In the presence of impurity scattering, the density of states at zero energy becomes finite. At the same time, the scattering rate is proportional to the self-consistent density of states. Since conductivity is proportional to the density of states and inversely to the scattering rate, the impurity dependence cancels.

The frequency-dependent $\sigma(\omega)$ is difficult to measure and it was realized that the thermal conductivity κ may provide a better test of the theory because according to the Wiedemann-Franz law, κ/T is proportional to the conductivity and should be universal. Unlike $\sigma(\omega)$, thermal conductivity does not have a superfluid contribution and can be measured at dc. More detailed considerations by Durst and Lee (2000) showed that $\sigma(\omega)$ has two nonuniversal corrections: one due to backscattering effects, which distinguishes the transport rate from the impurity rate which enters the density of state, and a second one due to Fermi-liquid corrections. On the other hand, these corrections do not exist for thermal conductivity. Consequently, the Wiedemann-Franz law is

violated but the thermal conductivity per layer is truly universal and is given by

$$\frac{\kappa}{T} = \frac{k_B^2}{3\hbar c}\left(\frac{v_F}{v_\Delta} + \frac{v_\Delta}{v_F}\right). \tag{4}$$

We note that this result is obtained within the self-consistent t-matrix approximation, which is expected to break down if the impurity scattering is strong, leading to localization effects. The localization of nodal quasiparticles is a complex subject. Due to particle-hole mixing in the superconductor, zero energy is a special point and quasiparticle localization belongs to a different universality class (Senthil and Fisher, 1999) than the standard ones. Senthil and Fisher also pointed out that since quasiparticles carry well-defined spin, the Wiedemann-Franz law for spin conductivity should hold and spin conductivity should be universal. We note that Durst and Lee (2000) argued that Fermi-liquid corrections enter the spin conductivity, but we now believe their argument on this point is faulty.

Thermal conductivity has been measured to mK temperatures in a variety of YBCO and Bi-2212 samples. The universal nature of κ/T has been demonstrated by studying samples with different Zn doping and showing that κ/T extrapolates to the same constant at low temperatures (Taillefer *et al.*, 1997). A magnetic-field dependence analogous to the Volovik effect for the specific heat has also been observed (Chiao *et al.*, 2000). Using Eq. (4), the experimental data can be used to extract the ratio v_F/v_Δ. In the case of Bi-2212 for which photoemission data for v_F and the energy gap are available, the extracted ratio v_F/v_Δ is in excellent agreement with ARPES results assuming a simple d-wave extrapolation of the energy gap from the node to the maximum gap Δ_0. In particular, the trend that Δ_0 increases with decreasing doping x is directly observed as a decrease of v_F/v_Δ extracted from κ/T. A summary of the data is shown in Fig. 13 (Sutherland *et al.*, 2003). The results of such systematic studies strongly support the notion that in clean samples nodal quasiparticles behave exactly as one expects for well-defined quasiparticles in a d-wave superconductor. We should add that in LSCO the ratio v_F/v_Δ extracted from κ/T seems anomalously small, suggesting that strong disorder may be playing a role here to invalidate Eq. (4).

Lee and Wen (1997) pointed out that nodal quasiparticles also manifest themselves in the linear T dependence of the superfluid density. They showed that by treating them as well-defined quasiparticles in the sense of Landau, a general expression of the linear T coefficient can be written down, independent of the microscopic origin of the superconductivity. We have

$$\frac{n_s(T)}{m} = \frac{n_s(0)}{m} - \frac{2\ln 2}{\pi}\alpha^2\left(\frac{v_F}{v_\Delta}\right)T. \tag{5}$$

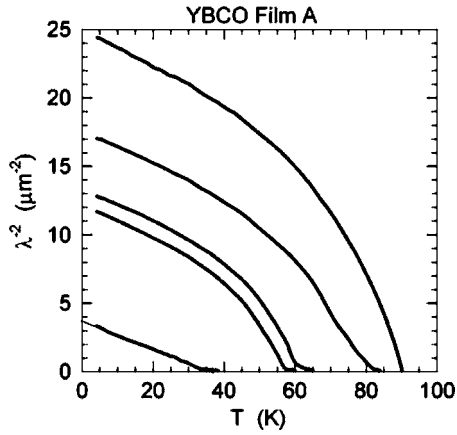The only assumption made is that the quasiparticles carry an electric current,

FIG. 14. The London penetration depth measured in a series of YBCO films with different oxygen concentrations and T_c's. The plot shows λ^{-2} plotted vs temperature. Data provided by T. R. Lemberger and published in Boyce *et al.*, 2000.

$$\boldsymbol{j}(\boldsymbol{k}) = -e\alpha\boldsymbol{v}_F, \tag{6}$$

where α is a phenomenological Landau parameter, which was left out in the original Lee-Wen paper but added in by Millis *et al.* (1998). While the linear T dependence is well known in the conventional BCS theory of a d-wave superconductor, the same theory gives n_s/m of order unity. It is therefore useful to write n_s in this phenomenological way, and choose $n_s(T=0)$ to be of order x as discussed in Sec. III.A. The key question raised by Eq. (6) is whether α depends on x or not. There is experimental evidence that the linear T coefficient of $n_s(T)/m$, which is directly related to London penetration depth measurements, is almost independent of x for x less than optimal doping. Figure 14 shows data obtained for a series of thin films of YBCO (Boyce *et al.*, 2000; Stajis *et al.*, 2003). The thin-film data are in full agreement with earlier but less extensive data on bulk crystals (Bonn *et al.*, 1996). However, we note that very recent data on a severely underdoped YBCO crystal (T_c <22 K and x estimated to be less than 0.064) show that $d(n_s/m)/dT$ decreases with decreasing T_c and extrapolates to zero as T_c goes to zero (Broun *et al.*, 2005; Liang *et al.*, 2005).

Since v_F/v_Δ is known to go to a constant for small x (and, indeed, decreases with decreasing x), the independence of the linear T term in n_s/m on x means that α is almost independent on x. By combining with v_F/v_Δ extrapolated from the thermal conductivity, α^2 has been estimated to be 0.5 [see Ioffe and Millis (2002a) for an excellent summary]. This is an important result because it states that despite the proximity to the Mott insulator nodal quasiparticles carry a current which is similar to that of the tight-binding Fermi-liquid band. We note that the simplest microscopic theory, which correctly gives $n_s(T=0)$ to be proportional to x, is the slave-boson mean-field theory discussed in Sec. IX.B. That theory predicts α to be proportional to x and the resulting x^2T term is in strong disagreement with experiment. Re-

cently α has been calculated numerically based on a projected trial wave function of the quasiparticle state (Nave *et al.*, 2005). It has a value of ≈ 0.7 near optimal doping and more or less saturates for higher doping. For low doping it decreases to zero rather sharply as $x \to 0$. This improves the agreement with experiment, particularly with the recent data on highly underdoped samples, but still does not explain why α appears to be independent of x over a wide range of intermediate doping in the thin film data shown in Fig. 14. More extensive simple crystal data will be highly desirable. We mention that a recent study which improves on the slave-boson mean-field theory by including binding between bosons and fermions yields an enhanced α proportional to x^γ, with $\gamma < 1/2$ (Ng, 2005).

The unusual combination of a small n_s ($T=0$) and a large linear T reduction due to quasiparticles has a number of immediate consequences. Simply by extrapolating the linear T dependence, we can conclude that n_s vanishes at the temperature scale proportional to x and T_c must be bound by it. Furthermore, at T_c the number of quasiparticles which are thermally excited is still small and not sufficient to close the gap as in standard BCS theory. Thus the transition must not be thought of as a gap-closing transition, and the effect of an energy gap must persist considerably above T_c. This can potentially explain at least part of the pseudogap phenomenon. As we shall see in the next section, when combined with phase fluctuations, the quasiparticle excitations explain the magnitude of T_c in the underdoped cuprates and account for a wide phase-fluctuation region above T_c, but not the full pseudogap phenomenon.

The disconnect between the gap energy Δ_0 and kT_c introduces two length scales, $\xi_0 = \hbar v_F/\Delta_0$ and $R_2 = \hbar v_F/kT_c$, where kT_c is proportional to x. Around a vortex, the supercurrent induces a population of quasiparticles with the Volovik effect, and in analogy to Eq. (5) causes a reduction in n_s. Lee and Wen (1997) showed that at a radius of R_2 the circulating supercurrent exceeds the critical current and inside that radius the superconductor loses its phase stiffness. They suggested that the system becomes normal once the large core radius R_2 overlaps and $H_{c2} \approx \phi_0/2\pi R_2^2$, in contrast with $H_{c2}^* \approx \phi_0/2\pi\xi_0^2$ as in conventional BCS theory. Note that H_{c2} decreases while H_{c2}^* increases with underdoping. Experimentally the resistive transition to the normal state indeed takes place at an H_{c2} which decreases with decreasing T_c. However, there are signs that vortices survive above this magnetic field up to H_{c2}^*, as will be discussed in Sec. V.B.

Finally, we comment on suggestions in the literature that classical fluctuations of the superconducting phase can lead to a linear reduction of n_s at low temperatures (Carlson *et al.*, 1999). Just as in the case of lattice displacements, such fluctuations must be treated quantum mechanically at low temperatures (as phonons in that case) to avoid the $3k_B$ low-temperature limit for the specific heat. In the case of phonons, the characteristic temperature scale is the phonon frequency. In the case of

the superconductor, the phase mode is pushed up to the plasma frequency by a long-range Coulomb interaction. Nevertheless, due to the coupling to low-lying particle-hole excitations, the crossover from classical to quantum fluctuations must be treated with some care. Paramekanti *et al.* (2000), Benfatto *et al.* (2001), and Paramekanti (2002) calculated that the crossover happens at quite a high-temperature scale and we believe the low-temperature linear reduction of n_s is entirely due to thermal excitations of quasiparticles.

IV. INTRODUCTION TO THE RESONATING VALENCE BOND AND A SIMPLE EXPLANATION OF THE PSEUDOGAP

We have explained in the last section that the Néel spin order is incompatible with hole hopping. The question is whether there is another arrangement of the spin which achieves a better compromise between the exchange energy and the kinetic energy of the hole. For $S = \frac{1}{2}$ spins it appears possible to take advantage of the special stability of the singlet state. The ground state of two spins S coupled with an antiferromagnetic Heisenberg exchange is a spin singlet with energy $-S(S+1)J$. Compared with the classical large spin limit, we see that quantum mechanics provides additional stability in the term unity in $S+1$ and this contribution is strongest for $S = \frac{1}{2}$. Let us consider a one-dimensional spin chain. A Néel ground state with $S_z = \pm \frac{1}{2}$ gives an energy of $-\frac{1}{4}J$ per site. On the other hand, a simple trial wave function of singlet dimers already gives a lower energy of $-\frac{3}{8}J$ per site. This trial wave function breaks translational symmetry and the exact ground state can be considered to be a linear superposition of singlet pairs, which are not limited to nearest neighbors, resulting in a ground-state energy of 0.443 J. In a square and cubic lattice the Néel energy is $-\frac{1}{2}J$ and $-\frac{3}{4}J$ per site, respectively, while the dimer variational energy stays at $-\frac{3}{8}J$. It is clear that in a 3D cubic lattice the Néel state is a far superior starting point, and in two dimensions the singlet state may present serious competition. Historically, the notion of a linear superposition of spin-singlet pairs spanning different ranges, called the *resonating valence bond* (RVB), was introduced by Anderson (1973) and Fazekas and Anderson (1974) as a possible ground state for the $S = \frac{1}{2}$ antiferromagnetic Heisenberg model on a triangular lattice. The triangular lattice is of special interest because an Ising-like ordering of the spins is frustrated. Subsequently it was decided that the ground state forms a $\sqrt{3} \times \sqrt{3}$ superlattice in which the moments lie on the same plane and form 120° angles between neighboring sites (Huse and Elser, 1988). Up to now there is no known spin Hamiltonian with full SU(2) spin-rotational symmetry outside of one dimension which is known to have a RVB ground state. However, there have been suggestions that ring exchange or proximity to the Mott insulator may stabilize such a state (Morita *et al.*, 2002; Misguich and Lhuillier, 2004; Lee and Lee, 2005a; Motrunich, 2005). We also refer the reader to Sec. X.H

for examples either which violate spin rotation or which permit charge fluctuations.

The Néel state has long-range order of the staggered magnetization and an infinite degeneracy of ground states leading to Goldstone modes, which are magnons. In contrast, the RVB state is a unique singlet ground state with either a short-range or power-law decay of antiferromagnetic order. This state of affairs is sometimes referred to as a spin liquid. However, the term spin liquid is often used more generally to denote any kind of short-range or power-law decay, i.e., the absence of long-range order even when the unit cell is doubled, either spontaneously or explicitly. For example, the ladder system has two states per unit cell and in the limit of strong coupling across the rung the ground state is naturally a spin singlet with short-range antiferromagnetic order. Another example is the spontaneously dimerized ground state for the frustrated spin chains when the next-nearest-neighbors exchange energy J' is sufficiently large. This kind of ground state is more properly called a valence-band solid and is smoothly connected to spin-singlet ground states often observed for systems with an even number of electrons per unit cell, the extreme example being Si. Thus we think it is better to reserve the term spin liquid to cases in which there is an odd number of electrons per unit cell.

Soon after the discovery of high-T_c superconductors, Anderson (1987) revived the RVB idea and proposed that with the introduction of holes the Néel state is destroyed and the spins form a superposition of singlets. The vacancy can hop in the background of what he envisioned as a liquid of singlets and a better compromise between the hole kinetic energy and the spin exchange energy may be achieved. Many elaborations of this idea followed, but here we argue that the basic physical picture described above gives a simple account of the pseudogap phenomenon. Singlet formation explains the decrease of the uniform spin susceptibility and the reduction of the specific heat γ. The vacancies are responsible for transport in the plane. The conductivity spectral weight in the *ab* plane is given by the hole concentration x and is unaffected by singlet formation. On the other hand, for *c*-axis conductivity an electron is transported between planes. Since an electron carries spin $\frac{1}{2}$, it is necessary to break a singlet. This explains the gap formation in $\sigma_c(\omega)$ and the energy scale of this gap should be correlated with that of uniform susceptibility. In photoemission, an electron leaves the solid and reaches the detector. The pullback of the leading edge simply reflects the energy cost to break a singlet. The lowering of the kinetic energy below the onset of superconductivity may also be explained qualitatively in this picture because superconductivity is driven by the phase coherence of holes, which lowers the kinetic energy, while the cost of smearing out the Fermi surface by the creation of the gap has already been paid for by the creation of the spin gap at higher temperatures.

A second concept associated with the RVB idea is the notion of spinons and holons and spin-charge separa-
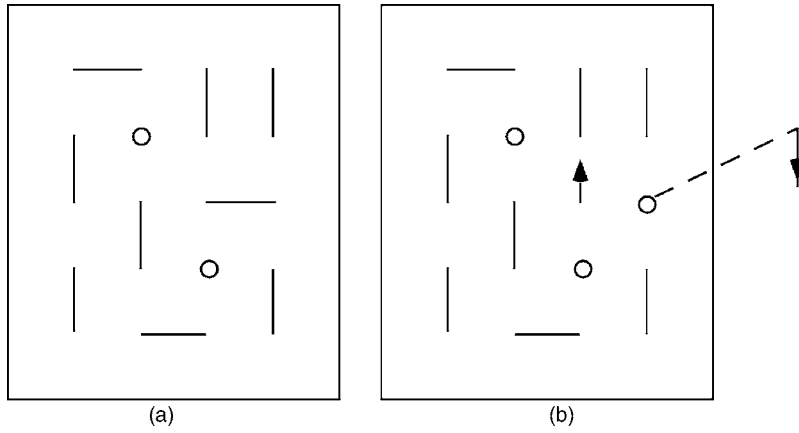
FIG. 15. (a) A cartoon representation of the resonating valence bond (RVB) liquid or singlets. The solid bond represents a spin-singlet configuration and the circles represents a vacancy. (b) An electron is removed from the plane in photoemission or a c-axis conductivity experiment. This necessitates the breaking of a singlet.

tions. Anderson postulated that spin excitations in a RVB state are $S=\frac{1}{2}$ fermions, which he called spinons. This is in contrast with excitations in a Néel state which are $S=1$ magnons or $S=0$ gapped singlet excitations.

It was initially suggested that the spinons form a Fermi surface, with the Fermi volume equal to that of $1-x$ fermions. Later it was proposed that the Fermi surface is gapped to form a d-wave-type structure, with the maximum gap near $(0,\pi)$. This $\boldsymbol{k}$ dependence of the energy gap is needed to explain the momentum dependence observed in photoemission.

The concept of spinons is a familiar one in one-dimensional spin chains where they are well understood to be domain walls. In two dimensions the concept is a novel one which does not involve domain walls. Instead, a rough physical picture is as follows. If we assume a background of short-range singlet bonds forming the so-called short-range RVB state, a cartoon of the spinon is shown in Fig. 15. If the singlet bonds are "liquid," two $S=\frac{1}{2}$ spins formed by breaking a single bond can drift apart, with the liquid of singlet bonds filling in the space between them. They behave as free particles and are called spinons. The concept of holons follows naturally (Kivelson *et al.*, 1987) as the vacancy left over by removing a spinon. A holon carries charge e but no spin.

V. PHASE FLUCTUATION VERSUS COMPETING ORDER

One of the hallmarks of doping a Mott insulator is that the spectral weight of the frequency-dependent conductivity $\sigma(\omega)$ should go to zero in the limit of small doping. Indeed, $\sigma(\omega)$ shows a Drude-like peak at low frequencies and its area was shown to be proportional to the hole concentration (Orenstein *et al.*, 1990; Uchida *et al.*, 1991; Cooper *et al.*, 1993; Padilla *et al.*, 2005). Results from an exact diagonalization of small samples are consistent with a Drude weight of order xt (Dagotto *et al.*, 1992). When the metal becomes superconducting, all the spectral weight collapses into a δ function if the sample is in the clean limit. The London penetration depth for field penetration perpendicular to the ab plane is given by

$$\lambda_\perp^{-2} = \frac{4\pi n_s^{3d} e^2}{m^* c^2},\tag{7}$$

where n_s^{3d}/m^* is the spectral weight and n_s^{3d} is the $3d$ superfluid charge density. As an example, if we take $\lambda_\perp = 1600$ Å for $YBa_2Cu_3O_{6.9}$ and take n_s^{3d} to be the hole density, we find from Eq. (7) $m^* \approx 2m_e$, which corresponds to an effective hopping $t^* = \frac{1}{3}t$. The notion that $\lambda_\perp^{-2}$ is proportional to xt is also predicted by slave-boson theory, as discussed in Sec. IX.B.

Uemura *et al.* (1989) discovered empirically a linear relation between $\lambda_\perp^{-2}$ measured by muon spin rotation and the superconducting T_c. They interpreted this relation as indicative of the Bose condensation of holes since in two dimensions the Bose-Einstein condensation temperature is proportional to the areal density. Since $\lambda_\perp^{-2}$ is proportional to the $3d$ density, in principle, some adjustment for the layer spacing should be made. Furthermore, $\lambda_\perp^{-2}$ is highly sensitive to disorder, and it is now known that in many systems not all the spectral weight collapses to the δ function, i.e., some residual normal conductivity is left, presumably due to inhomogeneity (Basov *et al.*, 1994; Corson *et al.*, 2000). Thus the Uemura *et al.* plot should be viewed as providing a qualitative trend, rather than a quantitative relation. Nevertheless, it is important in that it draws a relationship between T_c and carrier density.

A. A theory of T_c

The next important step was taken by Emery and Kivelson (1995), who noted that it is the superfluid density which controls the phase stiffness of the superconducting order parameter $\Delta = |\Delta| e^\theta$, i.e., the energy density cost of a phase twist is

$$H = \frac{1}{2} K_s^0 (\nabla \theta)^2.\tag{8}$$

Here the superscript on K_s^0 denotes the bare stiffness on a short distance scale. For two-dimensional layers the stiffness $K_s = \hbar^2 (n_s/2)/2m^*$, i.e., the kinetic energy of Cooper pairs. The spectral weight n_s/m^* and the stiffness are given by

$$K_s = \frac{1}{4}\frac{\hbar^2 n_s}{m^*} = \frac{1}{4}\frac{\hbar^2 n_s^{3d} c_0}{m^*}, \qquad (9)$$

where c_0 is the spacing between the layers and using Eqs. (7) and (9) can be directly measured in terms of $\lambda_\perp$. If K_s^0 is small due to the proximity to the Mott insulator, then phase fluctuation is strong and the T_c in the underdoped cuprates may be governed by phase fluctuations. The theory of phase fluctuations in two dimensions is well understood due to the work of Berezinskii (1971) and Kosterlitz and Thouless (1973). The Berezinskii-Kosterlitz-Thouless transition is described by the thermal unbinding of vortex-antivortex pairs. The energy of a single vortex is given by

$$E_{\mathrm{vortex}} = E_c + 2\pi K_s^0 \ln(L/\xi_0), \qquad (10)$$

where L is the sample size, ξ_0 is the BCS coherence length which serves as a short-distance cutoff, and E_c is the core energy. For vortex-antivortex pairs, the sample size L is replaced by the separation of the pairs. The vortex unbinding transition is driven by the balance between this energy and the entropy, which also scales logarithmically with the vortex separation. At T_c, K_s is predicted to jump between zero and a finite value $K_s(T_c)$ given by a universal relation

$$kT_c = (\pi/2)K_s(T_c) = \frac{\pi}{8}\frac{\hbar^2 n_s}{m^*} \qquad (11)$$

(Nelson and Kosterlitz, 1977). The precise value of T_c depends on $K_s(T=0)$ and weakly on the core energy. In the limit of very large core energy, $kT_c = 1.5K_s^0$, whereas for an XY model on a square lattice E_c is basically zero if ξ_0 in Eq. (10) is replaced by the lattice constant and $T_c = 0.95K_s^0$. Thus K_s^0 should give a reasonable guide to T_c in the phase-fluctuation scenario. Emery and Kivelson estimated K_s^0 from $\lambda_\perp$ data for a variety of materials and concluded that K_s^0 is indeed on the scale of T_c. However, they assumed that each layer is fluctuating independently, even for systems with strongly Josephson-coupled bilayers. Subsequent work using microwave conductivity confirmed the Berezinskii-Kosterlitz-Thouless nature of the phase transition but concluded that in Bi-2212 it is the bilayer which should be considered as a unit, i.e., the superconducting phase is strongly correlated between the two layers of a bilayer (Corson *et al.*, 1999). This increases the K_s^0 estimate by a factor of 2. For example, for $\lambda_\perp = 1600$ Å, Emery and Kivelson noted K_s^0 to be 145 K for YBCO. This should really be replaced by 290 K, a factor of 3 higher than T_c.

We can get around this difficulty by realizing that K_s is reduced by thermal excitation of quasiparticles and the bare K_s^0 in the Berezinskii-Kosterlitz-Thouless theory should include this effect. In Sec. III.B we have shown empirical evidence that the linear T coefficient of $n_s(T)$ is relatively independent of x. The bare K_s^0 was measured as the high-frequency limit in a microwave experiment (Corson *et al.*, 1999). As seen in Fig. 16, the bare phase stiffness $T_\theta^0 \equiv \hbar^2 n_s^0 / m^*$ continues to decrease lin-
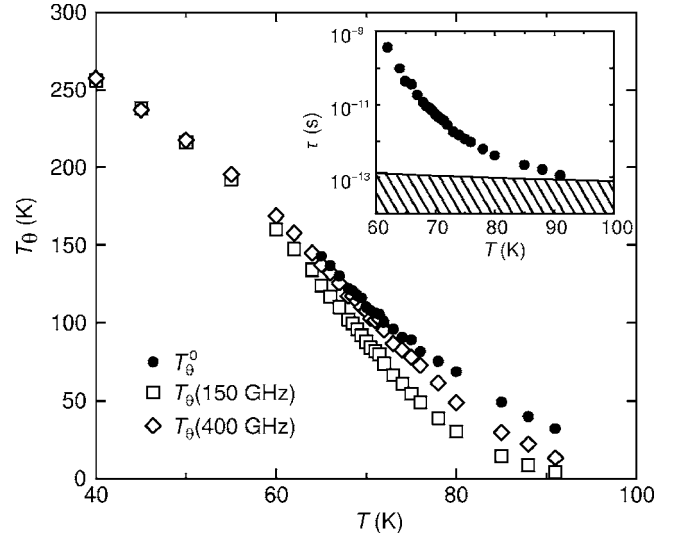
FIG. 16. The phase stiffness T_θ measured at different frequencies ($T_\theta = \hbar^2 n_s / m^*$). The solid dots give the bare stiffness obtained by extrapolation to infinite frequency. T_c of this sample is 74 K. This is where the phase stiffness measured at low frequency would vanish according to Berezinskii-Kosterlitz-Thouless (BKT) theory. Note the linear decrease of the bare stiffness with T which extends considerably above T_c. This decrease is due to thermal excitations of nodal quasiparticles. Inset: The time scale of the phase fluctuation. The hatched region denotes $\hbar/\tau = kT_c$. From Corson *et al.*, 1999.

early with T above $T_c = 74$ K. Given the universal relation (11), an estimate of T_c can be obtained by the interception of the straight line $T_\theta = (8/\pi)kT$ with the bare stiffness. This yields an estimate of the Berezinskii-Kosterlitz-Thouless transition temperature of ≈ 60 K. The somewhat higher actual T_c of 74 K is due to three-dimensional ordering effects between bilayers. Now we can extend this procedure to a multilayer superconductor. In Fig. 17 we show schematically a $T_\theta^0 = \hbar^2 n_s^0 / m^*$ plot of single-layer, bilayer, and trilayer systems ($N = 1, 2, 3$) assuming that the layers are identical. We expect $n_s^0(T=0)$, which is the areal density per N layers, to scale linearly with N. On the other hand, the linear T slope also scales with N because the number of thermally excited quasiparticles per area scale with N. The extrapolated T_c's are therefore the same. Now we may
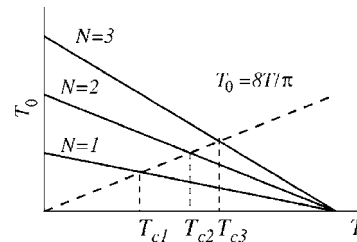
FIG. 17. Schematic plot of the phase stiffness $T_\theta = \hbar^2 n_s / m^*$ for superconductors with N-coupled layers. The linear decrease with temperature is due to the thermal excitation of quasiparticles. The transition temperatures T_{cN}, $N = 1, 2, 3$, are estimated by the interception with the BKT line $T_\theta = 8T/\pi$.

estimate $T_c(N)$ from the interception of the line $T_\theta^0 = (8/\pi)kT$. We see that T_c increases monotonically with N, but much slower than linearly. This trend is in agreement with what is seen experimentally, notably in the Tl and Hg compounds. As N increases further, the assumption that the layers are identical breaks down as the charge density of each layer begins to differ. We therefore conclude that the combination of phase fluctuations and the thermal excitation of d-wave quasiparticles can account for T_c in underdoped cuprates, including the qualitative trend as a function of the number of layers within a unit cell.

This theory of T_c receives confirmation from the measurement of the oxygen isotope effect of T_c and on the penetration depth. It is found that there is a substantial isotope effect on the n_s/m^* for both underdoped and optimally doped YBCO films. On the other hand, there is a significant isotope effect on T_c in underdoped YBCO (Khasanov et $al.$, 2003) but no effect on optimally doped samples (Khasanov et $al.$, 2004). Setting aside the origin of the isotope effect on n/m^*, the remarkable doping dependence of the isotope effect on T_c is readily explained in our theory since T_c is controlled by n_s/m^* in the underdoped but not in the overdoped region. In fact, a more detailed examination of the data for two underdoped samples shows that $n_s(T)/m^*$ appears to be shifted down by a constant when ^{16}O is replaced by ^{18}O. This suggests that there is no isotope effect on the temperature-dependent term in Eq. (5), which depends on v_F. This is consistent with direct ARPES measurements (Gweon et $al.$, 2004). Thus the data are consistent with an isotope effect only on the zero-temperature spectral weight $n_s(0)/m^*$. The latter is a complicated many-body property of the ground state, which is not simply related to the effective mass of the quasiparticles in the naive manner.

B. Cheap vortices and the Nernst effect

Emery and Kivelson (1995) also suggested that the notion of strong phase fluctuations may provide an explanation of the pseudogap phenomenon. They proposed that the pairing amplitude is formed at a temperature T_{MF}, which is much higher than T_c, and that the region between T_{MF} and T_c is characterized by a robust pairing amplitude and energy gap.

This leaves open the microscopic origin of the robust pairing amplitude and high T_{MF} but we shall argue that even as phenomenology, phase fluctuations alone cannot be the full explanation of the pseudogap. Since T_c is driven by the unbinding of vortices, let us examine the vortex energy more carefully. As an extreme example, let us suppose T_{MF} is described by standard BCS theory. The vortex core energy in BCS theory is estimated as $E_c \approx (\Delta_0^2/E_F a^2)\xi_0^2$, where Δ_0 is the energy gap, $\Delta_0^2/E_F a^2$ is the condensation energy per area, ξ_0^2 is the core size, and a is the lattice constant. Using $\xi_0 = v_F/\Delta_0$, we conclude that $E_c \approx E_F$ in BCS theory, an enormous energy compared with T_c. Even if we assume E_c to be of order of

the exchange energy J or the mean-field energy T_{MF}, it is still much larger than T_c. We already note that in Berezinskii-Kosterlitz-Thouless theory, T_c is relatively insensitive to the core energy. Now we emphasize that despite the insensitivity of T_c to E_c, the physical properties above T_c are very sensitive to the core energy. This is because the Berezinskii-Kosterlitz-Thouless theory is an asymptotic long-distance theory which becomes simple in the limit of dilute vortex or large E_c. The typical vortex spacing is $n_v^{-1/2}$ when the vortex density n_v goes as $e^{-E_c/kT}$. Vortex unbinding happens on a renormalized length scale, i.e., the typical spacing between free vortices, which is much larger than $n_v^{-1/2}$. As a result, the physics of the system above T_c is very sensitive to E_c. If $E_c \gg kT_c$, vortices are dilute, the system will behave as a superconductor for all measurements performed on a reasonable spatial or temporal scale. However, except for the close vicinity of T_c, the pseudogap region is not characterized by strong superconducting fluctuations, but rather behaves as a metal. Thus a large vortex core energy can be ruled out. The core energy must be small, of the order T_c, i.e., it is comparable to the second term in Eq. (10). The notion of "cheap" vortices has two important consequences. First, it is clear that the amplitude fluctuation and the phase fluctuation are controlled by the same energy scale, kT_c. This is because the vortex core is a region where the pairing amplitude vanishes and in addition the phase θ winds by 2π. If we do away with the phase winding and retain the amplitude fluctuation, this should cost even less energy. Thus the temperature scale where vortices proliferate is also the scale where amplitude fluctuation proliferates. Then the notion of strong phase fluctuations is applicable only on a temperature scale of say $2T_c$ and this scale must become small as x becomes small. Thus phase fluctuations cannot explain a pseudogap phenomenon which extends to finite T in the small x limit.

Second, the notion of a cheap vortex means that there is a nonsuperconducting state which is very close in energy. In an ordinary superconductor, the core can be thought of as a patch of normal metals with a finite density of states at the Fermi level. The reason the core energy is large is because the energy gained by opening up an energy gap is lost. In underdoped and in slightly overdoped cuprates there is experimental evidence from STM tunneling into the core that the energy gap is retained inside the core (Maggio-Aprile et $al.$, 1995; Pan et $al.$, 2000). The large peak in the density state predicted for d-wave BCS theory (Wang and MacDonald, 1995) is simply not there. The nature of the state in the core, which one can think of as a competing state to the superconductor, is highly nontrivial and is a topic of current debate.

The above discussion is summarized with a schematic phase diagram shown in Fig. 18. A temperature scale of about $2T_c$ in the underdoped region marks the range of phase fluctuations. This is the region where the picture envisioned by Emery and Kivelson (1995) may be valid. Here the phase is locally well defined and vortices are
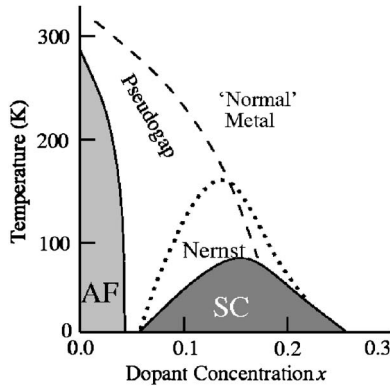
FIG. 18. Schematic phase diagram showing the phase-fluctuation regime where the Nernst effect is large. Note that this regime is a small part of the pseudogap region for small doping.

identifiable objects. Indeed, this is the region where a large Nernst effect has been measured (Wang *et al.*, 2001, 2002, 2003). The *Nernst effect* is the voltage transverse to a thermal gradient in the presence of a magnetic field perpendicular to the plane. It is exquisitely sensitive to the presence of vortices because vortices drift along the thermal gradient and produce the phase winding, which supports a transverse voltage by the Josephson effect. A large Nernst signal has been taken to provide evidence for the presence of well-defined vortices above T_c (Wang *et al.*, 2001, 2002, 2003). At higher temperatures, vortices overlap and the Nernst signal smoothly crosses over to that describable by Gaussian fluctuations of the superconducting amplitude and phase (Ussishkin *et al.*, 2002). Very recently, the identification of the Nernst region with fluctuating superconductivity was confirmed by the observation of diamagnetic fluctuations, which persist up to the same temperature as the onset of the Nernst signal (Wang *et al.*, 2005).

It remains necessary to explain why the resistivity looks metalliclike in this temperature range and does not show the strong magnetic-field dependence one ordinarily expects for flux-flow resistivity in the presence of thermally excited vortices. The explanation may lie in the breakdown of the standard Bardeen-Stephen model of flux-flow resistivity. Here the vortices have anomalously low dissipation because in contrast to BCS superconductors, there are no states inside the core to dissipate. Ioffe and Millis (2002b) have proposed that the vortices are fast and yield a large flux-flow resistivity. In the two-fluid model, the conductivity is the sum of the flux-flow conductivity (the superfluid part) and the quasiparticle conductivity (the normal part). The small flux-flow conductivity is quickly shorted out by nodal quasiparticle contributions, and the system behaves as a metal but with carriers only in the nodal region. This is also reminiscent of the Fermi arc picture. Unfortunately, a more detailed modeling requires an understanding of the state inside the large core radius R_2 introduced in Sec. III.C, which is not available yet.

Instead of generating vortices thermally, one can also generate them by applying a magnetic field. Wang *et al.* (2003) have applied fields up to 45 T and found evidence that the Nernst signal remains large beyond the underdoped samples. They estimate that the field needed to suppress the Nernst signal to be of order $H_{c2}^* \approx \phi_0/2\pi\xi_0^2$, where $\xi_0 \approx \hbar v_F/\Delta_0$. This is the core size consistent with what is reported by STM tunneling experiments. At the same time, the field needed for a resistive transition is much lower. Recently Sutherland *et al.* (2005) have shown that in YBCO$_{6.35}$ superconductivity is destroyed by annealing or by applying a modest magnetic field. Beyond this point the material is a thermal metal with a thermal conductivity which is unchanged from the superconducting side, where it is presumably due to nodal quasiparticles and described by Eq. (4). As a result the field-induced metal may coexist with a pairing amplitude and may be a very interesting new metallic state.

What is the nature of the gapped state inside the vortex core as revealed by STM tunneling and how is it related to the pseudogap region? A popular notion is that the vortex core state is characterized by a competing order. A variety of competing orders has been proposed in the literature. An early suggestion was that the core has antiferromagnetic order and an explicit model was constructed based on the SU(5) model of Zhang (1997) (Arovas *et al.*, 1997). However, this particular version has been criticized for its failure to take into account the strong Coulomb repulsion and the proximity to the Mott insulator (Greiter, 1997; Baskaran and Anderson, 1998). Recently, more phenomenological versions based on Landau theory have been proposed (Demler *et al.*, 2001; Chen *et al.*, 2004) in which antiferromagnetism may be incommensurate.

As the temperature is raised in the pseudogap regime, vortices proliferate and their cores overlap and according to this view the pseudogap is characterized by fluctuating competing order. The dynamic stripe picture (Carlson *et al.*, 2003) is an example of this point of view. Another proposal for competing order is orbital currents (Varma, 1997; Chakravarty, Laughlin, *et al.*, 2002). In this case the competing order is proposed as persisting in the pseudogap region but is "hidden" from detection because of the difficulties of coupling to the order. Finally, as discussed earlier, the recent observation of checkerboard patterns in the vortex core and in some underdoped cuprates has inspired various proposals of charge-density ordering.

Most of the proposals for competing order are phenomenological in nature. For example, the proximity of *d*-wave superconductivity to antiferromagnetism is simply assumed as an experimental fact. However, from a microscopic point of view the surprise is that *d*-wave superconductivity turns out to be the winner of this competition. Our goal is a microscopic explanation of both the superconducting and pseudogap states. We give a detailed proposal for the vortex core in Sec. XII.C. Here we mention that while our proposal also calls for slowly varying orbital currents in the core, this fluctuating order is simply one manifestation of a quantum state. For ex-

ample, an enhanced antiferromagnetic fluctuation is another manifestation. As discussed in Sec. VI.C, this picture is fundamentally different from competing states described by Landau theory. In the pseudogap phase, vortices proliferate and overlap and all orders become very short range. Apart from characterizing this state as a spin liquid (or RVB), the only possibility of order is a subtle one, called topological or quantum order. These concepts are described in Sec. X and a possible experimental consequence is described in Sec. XII.E.

C. Two kinds of pseudogaps

Since the pseudogap is fundamentally a crossover phenomenon, there is a lot of confusion about the size of the pseudogap and the temperature scale where it is observed. Upon surveying the experimental literature, it seems to us that we should distinguish between two kinds of pseudogaps. The first is clearly due to superconducting fluctuations. The energy scale of the pseudogap is the same as the low-temperature superconducting gap and it extends over a surprisingly large range of temperatures above T_c. This is what we called the Nernst region in the last section. This kind of pseudogap has been observed in STM tunneling in which it has been found that a reduction of the density of states persists above T_c even in overdoped samples (Kugler et al., 2001). We believe the pullback of the leading edge observed in ARPES shown in Fig. 7(a) should be understood along these lines. There is another kind of pseudogap which is associated with singlet formation. A clear signature of this phenomenon is the downturn in uniform spin susceptibility shown in Figs. 3 and 4. The temperature scale of the onset is high and increases up to 300–400 K with underdoping. The energy scale associated with this pseudogap is also very large and can extend up to 100 meV or beyond. For example, the onset of the reduction of the c-axis conductivity (which one may interpret as twice the gap) has been reported to exceed 1000 cm^{-1}. This is also the energy scale one associates with the limiting STM tunneling spectrum observed in highly underdoped Bi-2212 [Fig. 9(f)] and in Na-doped $Ca_2CuO_2Cl_2$ (Hanaguri et al., 2004). The gap in these spectra is very broad and ill defined. In the ARPES literature it is described as the "high-energy pseudogap" (see Damascelli et al., 2003) or the "hump" energy. These spectra evolve smoothly into that of the insulating parent, as emphasized by Laughlin (1997). This is most clearly demonstrated in Na-doped $Ca_2CuO_2Cl_2$ and the ARPES spectrum near the antinodal point looks remarkably similar to that seen by STM (Ronning et al., 2003). Examples of this kind of a spectrum can be seen in the samples UD46 and UD30 shown in Fig. 8(a). In contrast to the low-energy pseudogap, a coherent quasiparticle peak is never seen at these very high energies when the system enters the superconducting state. Instead, weak peaks may appear at lower energies, but judging from the STM data these may be associated with inhomogeneity. In this connec-

tion, we point out that the often quoted T^* line shown in Fig. 7 is actually a combination of the two kinds of pseudogaps. The solid triangles marking the onset of the leading edge refer to the fluctuating superconductor gap, while the solid squares are lower bounds based on the observation of the hump. Another example of this difference is that in LSCO the superconducting gap is believed to be much smaller and the pullback of the leading edge is not seen by ARPES. On the other hand, the singlet formation is clearly seen in Fig. 3 and the broad humplike spectra is also seen by ARPES (Zhou et al., 2004).

We note that in contrast to superconducting fluctuations, which extend across the entire doping range but are substantially reduced for overdoped samples, the onset of singlet formation seems to end rather abruptly near optimal doping. The Knight shift is basically temperature independent just above T_c in optimally doped and certainly in slightly overdoped samples (Horvatic et al., 1993; Takigawa et al., 1993). For this reason, we propose that the pseudogap line and the Nernst line may cross in the vicinity of optimal doping, as sketched in Fig. 18. In this connection it is interesting to note that the pseudogap has also been seen inside the vortex core (Maggio-Aprile et al., 1995; Pan et al., 2000). By definition, this is where the superconducting amplitude is suppressed to zero and the gap is surely not associated with the pairing amplitude. We have argued that the gap offers a glimpse of the state which lies behind the pseudogap associated with singlet formation. It is interesting to note that the gap in the vortex core has been reported in a somewhat overdoped sample (Hoogenboom et al., 2001). It is as though at zero temperature the state with a gap in the core is energetically favorable compared with the normal metallic state up to quite high doping. It will be interesting to extend these measurements to even more highly overdoped samples to see when the gap in the vortex core finally fills in. At the same time, it will be interesting to extend the tunneling into the vortex core in overdoped samples to higher temperatures to see if the gap will fill in at some temperature below T_c.

VI. PROJECTED TRIAL WAVE FUNCTIONS AND OTHER NUMERICAL RESULTS

In the original RVB article, Anderson (1987) proposed a projected trial wave function as a description of the RVB state,

$$\Psi = P_G|\psi_0\rangle, \tag{12}$$

where $P_G = \Pi_i(1 - n_{i\uparrow}n_{i\downarrow})$, the Gutzwiller projection operator, has the effect of suppressing all amplitudes in $|\psi_0\rangle$ with double occupation and thereby enforcing the constraint of the t-J model exactly. The unprojected wave function contains variational parameters and its choice is guided by mean-field theory (see Sec. XIII). The full motivation for the choice of $|\psi_0\rangle$ becomes clear only after the discussion of mean-field theory, but we discuss the projected wave function first because the results are

concrete and the concepts are simple. The projection operator is too complicated to be treated analytically, but properties of the trial wave function can be evaluated using Monte Carlo sampling.

A. The half-filled case

We first discuss the half-filled case in which the problem reduces to the Heisenberg model. While the original proposal was for $|\psi_0\rangle$ to be the s-wave BCS wave function, it was soon found that the d-wave BCS state is a better trial wave function, i.e., consider

$$H_d = - \sum_{\langle ij\rangle,\sigma} (\chi_{ij}f_{i\sigma}^\dagger f_{j\sigma} + \text{c.c.}) - \sum_{i,\sigma} \mu f_{i\sigma}^\dagger f_{i\sigma}$$
$$+ \sum_{\langle ij\rangle} [\Delta_{ij}(f_{i\uparrow}^\dagger f_{j\downarrow}^\dagger - f_{i\downarrow}^\dagger f_{j\uparrow}^\dagger) + \text{c.c.}], \tag{13}$$

where $\chi_{ij} = \chi_0$ for nearest neighbors, and $\Delta_{ij} = \Delta_0$ for $j = i + \hat{x}$ and $-\Delta_0$ for $j = i + \hat{y}$. The eigenvalues are the well-known BCS spectrum

$$E_k = \sqrt{(\epsilon_k - \mu)^2 + \Delta_k^2}, \tag{14}$$

where

$$\epsilon_k = - 2\chi_0(\cos k_x + \cos k_y), \tag{15}$$

$$\Delta_k = 2\Delta_0(\cos k_x - \cos k_y). \tag{16}$$

At half-filling, $\mu = 0$ and $|\psi_0\rangle$ is the usual BCS wave function $|\psi_0\rangle = \Pi_k(u_k + v_k f_{k\uparrow}^\dagger f_{-k\downarrow}^\dagger)|0\rangle$.

A variety of mean-field wave functions were soon discovered which give identical energy and dispersion. Notable among these is the staggered flux state (Affleck and Marston, 1988). In this state the hopping χ_{ij} is complex, $\chi_{ij} = \chi_0 \exp[i(-1)^{i_x+j_y}\Phi_0]$, and the phase is arranged in such a way that it describes free fermion hopping on a lattice with a fictitious flux $\pm 4\Phi_0$ threading alternative plaquettes. Remarkably, the eigenvalues of this problem are identical to those of the d-wave superconductor given by Eq. (14), with

$$\tan \Phi_0 = \frac{\Delta_0}{\chi_0}. \tag{17}$$

The case $\Phi_0 = \pi/4$, called the π-flux phase, is special in that it does not break the lattice translational symmetry. As we can see from Eq. (17), the corresponding d-wave problem has a very large energy gap and its dispersion is shown in Fig. 19. The key feature is that the energy gap vanishes at the nodal points located at $(\pm\pi/2, \pm\pi/2)$. Around the nodal points the dispersion rises linearly forming a cone which resembles the massless Dirac spectrum. For the π-flux state the dispersion around the node is isotropic. For Φ_0 less than $\pi/4$, the gap is smaller and the Dirac cone becomes progressively anisotropic. The anisotropy can be characterized by two velocities, v_F in the direction towards (π,π) and v_Δ in the direction towards the maximum gap at $(0,\pi)$.

The reason various mean-field theories have the same energy was explained by Affleck et al. (1988) and Dag-
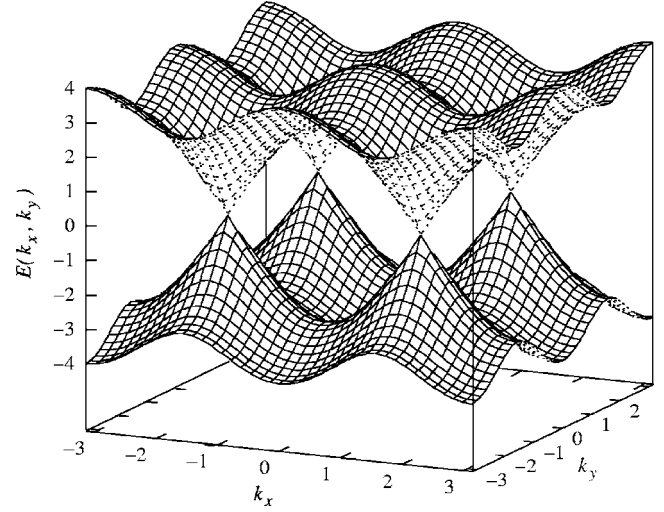
FIG. 19. The energy dispersion of the π-flux phase. Note the massless Dirac spectrum at the nodal points at $(\pm\pi/2, \pm\pi/2)$.

otto et al. (1988) due to a certain SU(2) symmetry. We defer a full discussion of the SU(2) symmetry to Sec. X but mention here that it corresponds to the following particle-hole transformation:

$$f_{i\uparrow}^\dagger \rightarrow \alpha_i f_{i\uparrow}^\dagger + \beta_i f_{i\downarrow},$$
$$f_{i\downarrow} \rightarrow - \beta_i^* f_{i\uparrow}^\dagger + \alpha_i^* f_{i\downarrow}. \tag{18}$$

Note that the spin quantum number is conserved. It describes the physical idea that adding a spin-up fermion or removing a spin-down fermion are the same state after projection to the subspace of singly occupied fermions. It is then not a surprise to learn that the Gutzwiller projection of the d-wave superconductor and that of the staggered flux state give the same trial wave function, up to a trivial overall phase factor, provided $\mu = 0$ and Eq. (17) is satisfied. A simple proof of this is given by Zhang et al. (1988). The energy of this state is quite good. The best estimate for the ground-state energy of the square-lattice Heisenberg antiferromagnet, which is a Néel ordered state, is $\langle S_i \cdot S_j \rangle = -0.3346\ J$ (Trivedi and Ceperley, 1989; Runge, 1992). The projected π-flux state (Gros, 1988; Yokoyama and Ogata, 1996) gives $-0.319\ J$, which is in excellent agreement considering that there is no variational parameter.

We note that the projected d-wave state has a power-law decay for the spin-spin correlation function. The equal-time spin-spin correlator decays as $r^{-\alpha}$, where α has been estimated to be 1.5 (Ivanov, 2000; Paramekanti et al., 2005). This projection has considerably enhanced the spin correlation compared with the exponent of 4 for the unprojected state. One might expect a better trial wave function by introducing a sublattice magnetization in the mean-field Hamiltonian. A projection of this state gives an energy which is marginally better than the projected flux state, $-0.3206\ J$. It also has a sublattice magnetization of 84%, which is too classical. The best trial wave function is one which combines staggered flux and sublattice magnetization before projection (Gros, 1988,

FIG. 20. Energy of projected wave functions. (a) Comparison of the energy of various projected trial wave functions. From Ivanov, 2004. (b) The condensation energy estimated from the difference of the projected d-wave superconductor and the projected staggered flux state. From Ivanov and Lee, 2003.

1989; Lee and Feng, 1988). It gives an energy of −0.332 J and a sublattice magnetization of about 70%, both in excellent agreement with the best estimates.

B. The doped case

In the presence of a hole, the projected wave function (12) has been studied for a variety of mean-field states ψ_0. Here P_G stands for a double projection: the amplitudes with double occupied sites are projected out and only amplitudes with the desired number of holes are kept. The ratios Δ_0/χ_0, μ/χ_0, and h_s/χ_0, where h_s is the field conjugate to the sublattice magnetization, are variational parameters. It was found that the best state is a projected d-wave superconductor and the sublattice magnetization is nonzero for $x<x_c$, where $x_c=0.11$ for $t/J=3$ (Yokoyama and Ogata, 1996). The energetics of various states are shown in Fig. 20(a). It is interesting to note that the projected staggered flux state always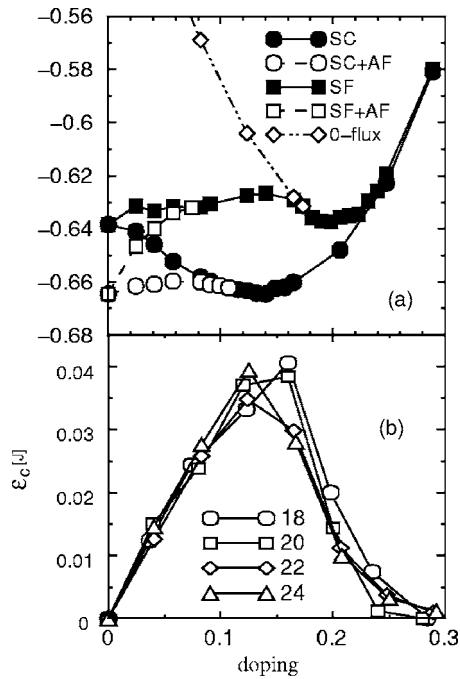 lies above the projected d-wave superconductor, but the energy difference is small and vanishes as x goes to zero, as expected. The staggered flux state also prefers antiferromagnetic order for small x, and the critical x_c^{SF} is now 0.08, considerably less than that for the projected d-wave superconductor. The energy difference between the projected flux state and projected d superconductor (with antiferromagnetic order) is shown in Fig. 20(b). As we can see from Fig. 20(a), the inclusion of an antiferromagnet will only give a small enhancement of the energy difference for small $x \lesssim 0.05$. The projected staggered flux state is the lowest-energy nonsuperconducting state

that has been constructed so far. For $x>0.18$, the flux Φ_0 vanishes and this state connects smoothly to the projected Fermi sea, which one ordinarily thinks of as the normal state. It is then tempting to think of the projected staggered flux state as the "normal" state in the underdoped region ($x<0.18$) and interpret the energy difference shown in Fig. 20(b) as the condensation energy. Such a state may serve as the competing state that we have argued must live inside the vortex core. The fact that the energy difference vanishes at $x=0$ guarantees that it is small for small x.

Ivanov (2004) has pointed out that the concave nature of the energy curves shown in Fig. 20(a) for small x indicates that the system is prone to phase separation. Such a phase separation may be suppressed by the long-range Coulomb interaction and the energy curves are indeed sensitive to nearest-neighbor repulsion. Thus we believe that Fig. 20(a) still provides a useful comparison of different trial wave functions.

C. Properties of projected wave functions

It is interesting to put aside the question of energetics and study the nature of the projected d-wave superconductor. A thorough study by Paramekanti *et al.* (2001, 2004) shows that it correctly captures many of the cuprate superconductors properties. For example, the superfluid density vanishes linearly in x for small x. This is to be expected since the projection operator is designed to yield an insulator at half-filling. The momentum distribution exhibits a jump near the noninteracting Fermi surface. The size of the jump is interpreted as the quasiparticle weight z according to Fermi-liquid theory and again goes to zero smoothly as $x\to0$. Using the sum rule and assuming Ferm-liquid behavior for nodal quasiparticles, the Fermi velocity is estimated and found to be insensitive to doping, in agreement with photoemission experiments.

A distinctive feature of the projected staggered flux state is that it breaks translational symmetry and orbital currents circulate the plaquettes in a staggered fashion as soon as $x\neq0$. Motivated by the SU(2) symmetry, which predicts a close relationship between the projected d-wave superconductor and the projected staggered flux states, Ivanov *et al.* (2000) examined whether there were signs of the orbital current in the projected d-wave superconductor. Since this state does not break translational or time-reversal symmetry, there is no static current. However, the current-current correlation

$$G_j = \langle j(\alpha)j(\beta)\rangle, \qquad (19)$$

where $j(\alpha)$ is the current on the α bond, shows a power-law-type decay and its magnitude is much larger than the naive expectation that it should scale as x^2. Note that before projection the d-wave superconductor shows no hint of the staggered current correlation. The correlation that emerges is entirely a consequence of the projection. We believe the emergence of orbital current fluctuations provides strong support for the importance

of SU(2) symmetry near half-filling. Orbital current fluctuations of similar magnitude were found in the exact ground-state wave function of the *t-J* model on a small lattice; two holes on 32 sites. Leung (2000) and Lee and Sha (2003) showed that the orbital current correlation has the same power-law decay as the hole-chirality correlation,

$$G_{\chi_h} = \langle \chi_h(i)\chi_h(j) \rangle,$$

where χ_h is defined on a plaquette i as $n_h(4)\boldsymbol{S}_1 \cdot (\boldsymbol{S}_2 \times \boldsymbol{S}_3)$, where 1–4 labels the sites around the plaquette and $n_h(\boldsymbol{i}) = 1 - c_{i\sigma}^\dagger c_{i\sigma}$ is the hole density operator. This is in agreement with the notion that a hole moving around the plaque experiences a Berry's phase due to the non-collinearity of the spin quantization axis of the instantaneous spin configurations. For $S = \frac{1}{2}$ spins the Berry's phase is given by $\frac{1}{2}\phi$, where ϕ is the solid angle subtended by the instantaneous spin orientations $\boldsymbol{S}_1$, $\boldsymbol{S}_2$, and $\boldsymbol{S}_3$ (Wen *et al.*, 1989; Fradkin, 1991). This solid angle is related to the spin chirality $\boldsymbol{S}_1 \cdot (\boldsymbol{S}_2 \times \boldsymbol{S}_3)$. This phase drives the hole in a clockwise or anticlockwise direction depending on its sign, just as a magnetic flux through the center of the plaquette would. Thus the flux Φ_0 of the staggered flux state has its physical origin in the coupling between the hole kinetic energy and the spin chirality.

It is important to emphasize that the projected *d*-wave state possesses long-range superconducting pairing order, while at the same time exhibiting a power-law correlation in antiferromagnetic order and staggered orbital current. On the other hand, the projection of a staggered flux phase at finite doping will possess long-range orbital current order, but short-range pairing and antiferromagnetic order. Different versions of projected states shown in Fig. 20(a) all have the same kinds of fluctuations; it is just that one kind of order may dominate over the others. Then it is easy to imagine that the system may shift from one state to another. For instance, in Sec. XII.C we argue that the pairing state will switch to a projected staggered flux state inside the vortex core. Note that this is a different picture from the traditional Landau picture of competing states as advocated by Chakravarty, Laughlin, *et al.* (2002), for instance. These authors have suggested on phenomenological grounds that the pseudogap region is characterized by staggered orbital current order, which they call *d*-density waves. The symmetry of this order is indistinguishable from the doped staggered flux phase (Hsu *et al.*, 1991; Lee, 2002). According to Landau theory, the competition between *d*-density waves and superconducting order will result in either a first-order transition or a region of coexisting phases at low temperatures. This view of competing order is very different from the one proposed here, where a single quantum state possesses a variety of fluctuating orders.

D. Improvement of projected wave functions, effect of *t′*, and the Gutzwiller approximation

The projected wave function is the starting point for various schemes to further improve the trial wave function. Indeed, the variational energy can be lowered and Sorella *et al.* (2002) have provided strong evidence that a *d*-wave superconducting state may be the ground state of the *t-J* model. On the other hand, others (Heeb and Rice, 1993; Shih *et al.*, 1998) have found that the superconducting tendency decreases with improvement of the trial wave functions. Studies based on other methods such as density-matrix renormalization group (White and Scalapino, 1999) found that next-nearest-neighbor hopping $t′$ with $t′/t > 0$ is needed to stabilize the *d*-wave superconductor; otherwise the holes are segregated into striplike structures. All these computational schemes suffer from some form of approximation and cannot give definitive answers. What is clear is that the *d*-wave superconductor is a highly competitive candidate for the ground state of the *t-J* model.

Recently Shih *et al.* (2004) have examined the pairing correlation in projected wave functions, including the effect of $t′$. They find that for moderate doping ($x \gtrsim 0.1$), $t′/t$ with a negative sign greatly enhances the pairing correlation. The effect increases with increasing $t′$ and is maximal around $t′/t \approx -0.4$. Their result contradicts expectations based on earlier density-matrix renormalization-group work (White and Scalapino, 1999), which found a suppression of superconductivity with negative $t′/t$. However, Shih *et al.* pointed out that the earlier work was limited to very low doping and is not in disagreement with their finding for $x \gtrsim 0.1$. This result should be confirmed by improving the wave function but the pair correlation with $t′$ is so robust that the controversy surrounding the $t′ = 0$ case may well be avoided. It should be noted that a negative $t′$ is what band theory predicts. Furthermore, Pavarini *et al.* (2001) have noted a correlation of T_c with $|t′|$ and have shown that the Hg and Tl compounds which have the highest T_c have $t′/t$ in the range -0.3 to -0.4. Thus the role of $t′$ may well explain the variation of T_c among different families of cuprates.

The Gutzwiller projection is rather cumbersome to implement and a simple approximate scheme was proposed, called the Gutzwiller approximation (Zhang *et al.*, 1988; Hsu, 1990). The essential step is to construct an effective Hamiltonian

$$H_{\text{eff}} = -g_t t \sum_{\langle ij \rangle \sigma} c_{i\sigma}^\dagger c_{i\sigma} + g_J J \sum_{\langle ij \rangle} \boldsymbol{S}_i \cdot \boldsymbol{S}_j \qquad (20)$$

and treat this in the Hartree-Fock-BCS approximation. The projection operator in the original *t-J* model is eliminated in favor of the reduction factors $g_t = 2x/(1+x)$ and $g_J = 4/(1+x)^2$, which are estimated by assuming statistical independence of the population of the sites (Vollhardt, 1984). The important point is that $g_t = 2x/(1+x)$ reduces the kinetic energy to zero in the $x \to 0$ limit in an attempt to capture the physics of the approach to

the Mott insulator. The Gutzwiller approximation bears a strong resemblance to the slave-boson mean-field theory and is just as easy to handle analytically. It has the advantage that the energetics compare well with the Monte Carlo projection results. The Gutzwiller approximation has been applied to more complicated problems such as impurity and vortex structure (Tsuchiura *et al.*, 2000, 2003) with good results.

VII. THE SINGLE-HOLE PROBLEM

The motion of a single hole doped into the antiferromagnet is a fundamental issue to start with. The *t-J*–type model is again the canonical Hamiltonian for studying this problem. The key physics of the problem is the competition between the antiferromagnetic correlation–long-range ordering and the kinetic energy of the hole. The motion of the single hole distorts the antiferromagnetic ordering when it hops between different sublattices. Shraiman and Siggia (1988) have studied this distortion in a semiclassical way and found the new coupling between the spin current of the hole and the magnetization current of the background. This coupling leads to the long-range dipolar distortion of the staggered magnetization and the minimum of the hole dispersion at $k=(\pi/2,\pi/2)$. This position of the energy minimum is interpreted as follows. Even if we start with the pure *t-J* model, the direct hopping between nearest-neighbor sites is suppressed, while the second-order processes in *t* lead to the effective hopping between the sites belonging to the same sublattice. This effective t' and t'' have a negative sign and hence lower the energy of $k=(\pi/2,\pi/2)$ compared with $k=(\pi,0),(0,\pi)$.

The dynamics of the single hole, i.e., the spectral function of the Green's function, was also studied with an analytic method. Kane *et al.* (1989) have studied the motion of the hole in an antiferromagnetic background as well as a RVB background. They concluded that in both cases the spectrum consists of a coherent part with a bandwidth proportional to *J* and a broad incoherent part spread out over an energy proportional to *t*. The weight of the coherent part is $\sim J/t$. In the case of the antiferromagnetic background, when the spin excitation is approximated by the magnon (spin wave), the Hamiltonian for the single hole is given by

$$H = \frac{t}{N}\sum_{\boldsymbol{k},\boldsymbol{q}} M_{\boldsymbol{k},\boldsymbol{q}}[h_{\boldsymbol{k}}^{\dagger}h_{\boldsymbol{k}-\boldsymbol{q}}\alpha_{\boldsymbol{q}} + \text{H.c.}] + \sum_{\boldsymbol{q}} \Omega_{\boldsymbol{q}}\alpha_{\boldsymbol{q}}^{\dagger}\alpha_{\boldsymbol{q}}, \quad (21)$$

where

$$\Omega_{\boldsymbol{q}} = 2J\sqrt{1-\gamma_{\boldsymbol{q}}^2}, \quad (22)$$

with $\gamma_{\boldsymbol{q}}=(\cos q_x+\cos q_y)/2$ and

$$M(\boldsymbol{k},\boldsymbol{q}) = 4(u_{\boldsymbol{q}}\gamma_{\boldsymbol{k}-\boldsymbol{q}} + v_{\boldsymbol{q}}\gamma_{\boldsymbol{k}}), \quad (23)$$

$u_{\boldsymbol{k}}=\sqrt{(1+\eta_{\boldsymbol{k}})/(2\eta_{\boldsymbol{k}})}$, $v_{\boldsymbol{k}}=-\text{sgn}(\gamma_{\boldsymbol{k}})\sqrt{(1-\eta_{\boldsymbol{k}})/(2\eta_{\boldsymbol{k}})}$, and $\eta_{\boldsymbol{k}}=\sqrt{1-\gamma_{\boldsymbol{k}}^2}$. This Hamiltonian dictates that the magnon is emitted or absorbed every time the hole hops. The most widely accepted method for studying this model is the

self-consistent Born approximation in which the Feynman diagrams with the crossing magnon propagators are neglected (Schmitt-Rink *et al.*, 1988; Kane *et al.*, 1989). This leads to the self-consistent equation for the hole propagator:

$$G(\boldsymbol{k},\omega) = \left(\omega - \sum_{\boldsymbol{q}} g(\boldsymbol{k},\boldsymbol{q})^2 G(\boldsymbol{k}-\boldsymbol{q},\omega-\Omega_{\boldsymbol{q}})\right)^{-1}. \quad (24)$$

The result is that there are two components of the spectral function $A(\boldsymbol{k},\omega)=-(1/\pi)\text{Im}\,G^R(\boldsymbol{k},\omega)$; one is the coherent sharp peak corresponding to the quasiparticle and the other is the incoherent background. The former has the lowest energy at $k=(\pi/2,\pi/2)$ at energy $\sim -t$ and disperses of the order of *J*, while the latter does not depend on the momentum *k* so much and extends over the energy of the order of *t*. Intuitively the hole has to wait for the spins to flip in order to hop, which takes a time of the order of J^{-1}. Therefore the bandwidth is reduced from $\sim t$ to $\sim J$. This mass enhancement leads to the reduced weight $z \sim J/t$ for the quasiparticle peak. Later, more detailed studies were done with the self-consistent Born approximation (Marsiglio *et al.*, 1991; Martinez and Horsch, 1991; Liu and Manousakis, 1992). The conclusions obtained are as follows: (i) At $k=(\pi/2,\pi/2)$, two peaks appear at $E_{2,3}$ in addition to the ground-state delta-function peak at E_1.

These energies are given for $J/t<0.4$ by

$$E_n/t = -b + a_n(J/t)^{2/3}, \quad (25)$$

where $a_1=2.16$, $a_2=5.46$, $a_3=7.81$, and $b=3.28$. (ii) The spectral weight *z* at $k=(\pi/2,\pi/2)$ scales as $z=0.65(J/t)^{2/3}$. These can be understood as the "string" excitation of the hole moving in the linear confining potential due to the antiferromagnetic background. It has also been interpretted in terms of the confining interaction between spinon and holon (Laughlin, 1997). Exact diagonalization studies have reached consistent results with the self-consistent Born approximation.

Experimentally, angle-resolved photoemission spectroscopy (ARPES) (Wells *et al.*, 1995; Ronning *et al.*, 1998) in undoped cuprates has revealed the spectral function of the single doped hole. The band minimum is indeed at $(\pi/2,\pi/2)$ but there is considerable dispersion towards $(0,\pi)$. The cone-shaped dispersion around $(\pi/2,\pi/2)$ looks like that of the π-flux state shifted by the Mott gap to low energy (Laughlin, 1997). However, in real materials the second (t') and third (t'') nearest-neighbor hoppings are important. The calculated energy dispersion is found to be sensitive to t' and t''. For $t'=t''=0$, the dispersion is flat between $(\pi/2,\pi/2)$ and $(0,\pi)$ and does not agree with the data. It turns out that the data are well fitted by $J/t=0.3$, $t'/t=-0.3$, and $t''/t=0.2$. On the other hand, ARPES in slightly electron-doped $Nd_{2-x}Ce_xCuO_4$ showed that the electron is doped at the point $k=(\pi,0)$ and $(0,\pi)$ (Armitage *et al.*, 2001). This difference will be discussed below.

The variational wave-function approach to the antiferromagnet and single-hole problem has been pursued by

several authors (Lee, Ho, *et al.*, 2003; Lee, Lee, *et al.*, 2003). A good ground-state variational wave function at half-filling is

$$|\Psi_0\rangle = P_G\left[\sum_{\boldsymbol{k}}(A_{\boldsymbol{k}}a^\dagger_{\boldsymbol{k}\uparrow}a^\dagger_{-\boldsymbol{k}\downarrow} + B_{\boldsymbol{k}}b^\dagger_{\boldsymbol{k}\uparrow}b^\dagger_{-\boldsymbol{k}\downarrow})\right]^{N/2}|0\rangle, \quad (26)$$

with N the number of atoms. The operators $a^\dagger_{\boldsymbol{k}\sigma}, b^\dagger_{\boldsymbol{k}\sigma}$ are those for the upper and lower bands split by the spin-density wave with the energy $\pm\xi_{\boldsymbol{k}}$, respectively, and $A_{\boldsymbol{k}} = (E_{\boldsymbol{k}}+\xi_{\boldsymbol{k}})/\Delta_{\boldsymbol{k}}$, $B_{\boldsymbol{k}} = (-E_{\boldsymbol{k}}+\xi_{\boldsymbol{k}})/\Delta_{\boldsymbol{k}}$ with $E_{\boldsymbol{k}} = \sqrt{\xi^2_{\boldsymbol{k}}+\Delta^2_{\boldsymbol{k}}}$ and $\Delta_{\boldsymbol{k}} = (3/8)J\Delta(\cos k_x - \cos k_y)$. The picture here is that in addition to the spin-density wave, the RVB singlet formation represented by Δ is taken into account. As mentioned in the last section, this variational wave function gives much better energy compared to that of $\Delta = 0$. Hence the ground state is far from the classical Néel state and includes strong quantum fluctuations. Next the variational wave function in the case of a single doped hole with momentum q and $S^z = 1/2$ is

$$|\Psi_q\rangle = P_G c^\dagger_{q\uparrow}\left[\sum_{\boldsymbol{k}(\neq q)}(A_{\boldsymbol{k}}a^\dagger_{\boldsymbol{k}\uparrow}a^\dagger_{-\boldsymbol{k}\downarrow} + B_{\boldsymbol{k}}b^\dagger_{\boldsymbol{k}\uparrow}b^\dagger_{-\boldsymbol{k}\downarrow})\right]^{N/2-1}|0\rangle.$$
$$(27)$$

This variational wave function does not contain the information of t', t'' except the very small dependence of $A_{\boldsymbol{k}}$ and $B_{\boldsymbol{k}}$. The robustness of this variational wave function is the consequence of the large quantum fluctuations already present in the half-filled case, so that the hole motion is possible even without disturbing the spin-liquid-like state. Although the variational wave function does not depend on the parameters t', t'', the energy dispersion $E(\boldsymbol{k})$ is given by the expectation value as

$$E(\boldsymbol{k}) = \langle\Psi_{\boldsymbol{k}}|H_{t-J} + H_{t'-t''}|\Psi_{\boldsymbol{k}}\rangle \quad (28)$$

and depends on these parameters. This expression gives a reasonable agreement with the experiments in both undoped- (Ronning *et al.*, 1998) and electron-doped materials (Armitage *et al.*, 2001). Here an important question is the relation between the hole- and electron-doped cases. There is a particle-hole-symmetry operation which relates the t-t'-t''-J model for a hole to that for an electron. The conclusion is that the sign change of t' and t'' together with the shift in the momentum by (π,π) gives the mapping between the two cases. Using this transformation, one can explain the difference between hole- and electron-doped cases in terms of the common variational wave function (27). The former has a minimum at $k = (\pi/2,\pi/2)$ while the latter at $k = (\pi,0),(0,\pi)$.

An exact diagonalization study (Tohyama *et al.*, 2000) showed that the electronic state is very different between $k = (\pi/2,\pi/2)$ and $k = (\pi,0)$ for the appropriate values of t' and t'' for the hole-doped case. The spectral weight becomes very small at $(\pi,0)$ and the hole is surrounded by antiparallel spins sitting on the same sublattice. Both these features are captured by a trial wave function which differs from Eq. (27) in that the momentum $\boldsymbol{q}$ of the broken pair is different from the momentum of the inserted electron. This can also be interpreted as the decay of the quasiparticle state via the emission of a spin wave (Lee, Lee, *et al.*, 2003). There are thus two types of wave functions with qualitatively different natures, i.e., one which describes the quasiparticle state and another which is highly incoherent and may be realized as a spin-charge separated state.

One important discrepancy between experiment and theory is the line shape of the spectral function. Namely, the experiments show a broad peak with the width of the order of ~0.3 eV in contrast to the delta-function peak expected for the ground state at $k = (\pi/2,\pi/2)$. One may attribute this large width to the disorder effect in the sample. However, ARPES in the overdoped region shows an even sharper peak at the Fermi energy even though the doping introduces further disorder. Therefore the disorder effect is unlikely to explain this discrepancy. Recently electron-phonon coupling to the single hole in the *t-J* model has been studied using a quantum Monte Carlo simulation (Mishchenko and Nagaosa, 2004). It was found that the small polaron formation in the presence of strong correlation reduced the dispersion and the weight of the zero-phonon line, while the center of mass of the spectral weight for the originally "quasiparticle" peak remained the same as the pure *t-J* model, even though the shape was broadened. Therefore the polaron effect is a promising scenario for explaining the spectral shape.

Recently, Shen *et al.* (2004) have pointed out that the polaron picture also explains a long-standing puzzle regarding the location of the chemical potential with doping. The naive expectation based on doping a Hubbard model predicts that the chemical potential should lie at the top of the valence band, whereas experimentally in Na-doped $Ca_2CuO_2Cl_2$ it was found that the chemical potential appears to lie somewhere in the midgap. For example, with a small but finite density of holes, the chemical potential is several tenths of eV higher than the energy of the peak position of the one-hole spectrum. This is naturally explained if the one-hole spectrum has been shifted down by polaron effects so that the top of the valence band should be at the zero-phonon line, rather than the center of mass of the one-hole spectrum.

VIII. SLAVE-BOSON FORMULATION OF THE *t-J* MODEL AND MEAN-FIELD THEORY

As discussed in Sec. II, it is widely believed that the low-energy physics of high-T_c cuprates is described in terms of the *t-J*–type model, which is given by (Lee and Nagaosa, 1992)

$$H = \sum_{\langle ij\rangle}J\left(\boldsymbol{S}_i\cdot\boldsymbol{S}_j - \frac{1}{4}n_in_j\right) - \sum_{ij,\sigma}t_{ij}(c^\dagger_{i\sigma}c_{j\sigma} + \text{H.c.}), \quad (29)$$

where $t_{ij} = t, t', t''$ for the nearest-, second-nearest-, and third-nearest-neighbor pairs, respectively. The effect of the strong Coulomb repulsion is represented by the fact that the electron operators $c^\dagger_{i\sigma}$ and $c_{i\sigma}$ are the projected

ones in which double occupation is forbidden. This is written as the inequality

$$\sum_\sigma c_{i\sigma}^\dagger c_{i\sigma} \le 1, \qquad (30)$$

which is very difficult to handle. A powerful method for treating this constraint is the slave-boson method (Barnes, 1976; Coleman, 1984). In the most general form the electron operator is represented as

$$c_{i\sigma}^\dagger = f_{i\sigma}^\dagger b_i + \epsilon_{\sigma\sigma'} f_{i\sigma'} d_i^\dagger, \qquad (31)$$

where $\epsilon_{\uparrow\downarrow} = -\epsilon_{\downarrow\uparrow} = 1$ is the antisymmetric tensor. $f_{i\sigma}^\dagger, f_{i\sigma}$ are the fermion operators, while $b_i, d_i^\dagger$ are the slave-boson operators. This representation together with the constraint

$$f_{i\uparrow}^\dagger f_{i\uparrow} + f_{i\downarrow}^\dagger f_{i\downarrow} + b_i^\dagger b_i + d_i^\dagger d_i = 1 \qquad (32)$$

reproduces all the algebra of the electron (fermion) operators. From Eqs. (31) and (32), the physical meaning of these operators is clear. Namely, there are four states per site and $b^\dagger, b$ corresponds to the vacant state, $d^\dagger, d$ to double occupancy, and $f_\sigma^\dagger, f_\sigma$ to the single electron with spin σ. With this formalism it is easy to exclude double occupancy just by deleting $d^\dagger, d$ from Eqs. (31) and (32). Then the projected electron operator is written as

$$c_{i\sigma}^\dagger = f_{i\sigma}^\dagger b_i, \qquad (33)$$

with the condition

$$f_{i\uparrow}^\dagger f_{i\uparrow} + f_{i\downarrow}^\dagger f_{i\downarrow} + b_i^\dagger b_i = 1. \qquad (34)$$

This constraint can be enforced with a Lagrange multiplier λ_i. Note that unlike Eq. (31), Eq. (33) is not an operator identity and the right-hand side does not satisfy the fermion commutation relation. Rather, the requirement is that both sides have the correct matrix elements in the reduced Hilbert space with no doubly occupied states. For example, the Heisenberg exchange term is written in terms of $f_{i\sigma}^\dagger, f_{i\sigma}$ only (Baskaran *et al.*, 1987),

$$\mathbf{S}_i \cdot \mathbf{S}_j = -\frac{1}{4} f_{i\alpha}^\dagger f_{j\alpha} f_{j\beta}^\dagger f_{i\beta} - \frac{1}{4}(f_{i\uparrow}^\dagger f_{j\downarrow}^\dagger - f_{i\downarrow}^\dagger f_{j\uparrow}^\dagger)(f_{j\downarrow} f_{i\uparrow} - f_{j\uparrow} f_{i\downarrow})$$
$$+ \frac{1}{4}(f_{i\alpha}^\dagger f_{i\alpha}). \qquad (35)$$

We write

$$n_i n_j = (1 - b_i^\dagger b_i)(1 - b_j^\dagger b_j). \qquad (36)$$

Then $\mathbf{S}_i \cdot \mathbf{S}_j - \frac{1}{4} n_i n_j$ can be written in terms of the first two terms of Eq. (35) plus quadratic terms, provided we ignore the nearest-neighbor hole-hole interaction $\frac{1}{4} b_i^\dagger b_i b_j^\dagger b_j$. We then decouple the exchange term in both the particle-hole and particle-particle channels via the Hubbard-Stratonovich transformation.

Then the partition function is written in the form

$$Z = \int Df Df^\dagger Db Db^* D\lambda D\chi D\Delta \exp\left(-\int_0^\beta d\tau L_1\right), \qquad (37)$$

where

$$L_1 = \tilde{J} \sum_{\langle ij \rangle} (|\chi_{ij}|^2 + |\Delta_{ij}|^2) + \sum_{i\sigma} f_{i\sigma}^\dagger (\partial_\tau - i\lambda_i) f_{i\sigma}$$
$$- \tilde{J}\left[\sum_{\langle ij \rangle} \chi_{ij}^* \left(\sum_\sigma f_{i\sigma}^\dagger f_{j\sigma}\right) + \text{c.c.}\right]$$
$$+ \tilde{J}\left[\sum_{\langle ij \rangle} \Delta_{ij}(f_{i\uparrow}^\dagger f_{j\downarrow}^\dagger - f_{i\downarrow}^\dagger f_{j\uparrow}^\dagger) + \text{c.c.}\right]$$
$$+ \sum_i b_i^*(\partial_\tau - i\lambda_i + \mu_B) b_i - \sum_{ij} t_{ij} b_i b_j^* f_{i\sigma}^\dagger f_{j\sigma}, \qquad (38)$$

with χ_{ij} representing fermion hopping and Δ_{ij} representing fermion pairing corresponding to the two ways of representing the exchange interaction in terms of the fermion operators. From Eqs. (35) and (38) one can conclude that $\tilde{J} = J/4$, but in practice the choice of $\tilde{J}_{ij}$ is not so trivial. Namely, one would like to study the saddle-point approximation and the Gaussian fluctuation around it, and it requires the saddle-point approximation to reproduce the mean-field theory. The latter requirement is satisfied when only one Hubbard-Stratonovich variable is relevant, but not for the multicomponent Hubbard-Stratonovich variables (Negele and Orland, 1987; Ubbens and Lee, 1992). In the latter case, it is better to choose the parameters in the Lagrangian to reproduce the mean-field theory. In the present case, $\tilde{J} = 3J/8$ reproduces the mean-field self-consistent equation, which is obtained with the Feynman variational principle (Brinckmann and Lee, 2001).

We note that L_1 in Eq. (38) is invariant under a local U(1) transformation,

$$f_{i\sigma} \to e^{i\theta_i} f_{i\sigma}, \quad b_i \to e^{i\theta_i} b_i,$$
$$\chi_{ij} \to e^{-i\theta_i} \chi_{ij} e^{i\theta_j}, \quad \Delta_{ij} \to e^{i\theta_i} \Delta_{ij} e^{i\theta_j}, \quad \lambda_i \to \lambda_i + \partial_\tau \theta_i, \qquad (39)$$

which is called a U(1) gauge transformation. Due to this U(1) gauge invariance, the fluctuations of λ_i and the phase of χ_{ij} have the dynamics of a U(1) gauge field (see Sec. IX).

Now we describe the various mean-field theories corresponding to the saddle-point solution to the functional integral. The mean-field conditions are

$$\chi_{ij} = \sum_\sigma \langle f_{i\sigma}^\dagger f_{j\sigma} \rangle, \qquad (40)$$

$$\Delta_{ij} = \langle f_{i\uparrow} f_{j\downarrow} - f_{i\downarrow} f_{j\uparrow} \rangle. \qquad (41)$$

Let us first consider the *t-J* model in the undoped case, i.e., the half-filled case. There are no bosons in this case, and the theory is purely that of fermions. The

original mean-field solution, i.e., the uniform RVB state proposed by Baskaran, Zou, and Anderson (Baskaran *et al.*, 1987), is given by

$$\chi_{ij} = \chi = \text{real} \tag{42}$$

for all bonds and $\Delta_{ij}=0$. The fermion spectrum is that of the tight-binding model

$$H_{\text{uRVB}} = -\sum_{k\sigma} 2\tilde{J}\chi(\cos k_x + \cos k_y) f_{k\sigma}^\dagger f_{k\sigma}, \tag{43}$$

with the saddle-point value of the Lagrange multiplier $\lambda_i=0$. The "spinon Fermi surface" is large, i.e., it is given by the condition $k_x \pm k_y = \pm\pi$ with a diverging density of states (van Hove singularity) at the Fermi energy. Soon after, many authors found lower-energy states than the uniform RVB state. One can easily understand that lower-energy states exist because the Fermi surface is perfectly nested with the nesting wave vector $\vec{Q}=(\pi,\pi)$ and the various instabilities with $\vec{Q}$ are expected. Of particular importance are the d-wave state [see Eq. (13)] and the staggered flux state [see Eq. (17)], which give identical energy dispersion. This was explained as being due to a local SU(2) symmetry when the spin problem is formulated in terms of fermions (Affleck *et al.*, 1988; Dagotto *et al.*, 1988). We write

$$\Phi_{i\uparrow} = \begin{pmatrix} f_{i\uparrow} \\ f_{i\downarrow}^* \end{pmatrix}, \quad \Phi_{i\downarrow} = \begin{pmatrix} f_{i\downarrow} \\ -f_{i\uparrow}^* \end{pmatrix}. \tag{44}$$

Then Eq. (38) can be written in the more compact form,

$$L_1 = \frac{\tilde{J}}{2}\sum_{\langle ij \rangle} \text{Tr}[U_{ij}^\dagger U_{ij}] + \frac{\tilde{J}}{2}\sum_{\langle ij \rangle,\sigma} (\Phi_{i\sigma}^\dagger U_{ij}\Phi_{j\sigma} + \text{c.c.})$$
$$+ \sum_{i\sigma} f_{i\sigma}^*(\partial_\tau - i\lambda_i)f_{i\sigma} + \sum_i b_i^*(\partial_\tau - i\lambda_i + \mu_B)b_i$$
$$- \sum_{ij,\sigma} t_{ij} b_i b_j^* f_{i\sigma}^* f_{j\sigma}, \tag{45}$$

where

$$U_{ij} = \begin{pmatrix} -\chi_{ij}^* & \Delta_{ij} \\ \Delta_{ij}^* & \chi_{ij} \end{pmatrix}. \tag{46}$$

At half-filling $b=\mu_B=0$ and the mean-field solution corresponds to $\lambda_i=0$. The Lagrangian is invariant under

$$\Phi_{i\sigma} \to W_i \Phi_{i\sigma}, \tag{47}$$

$$U_{ij} \to W_i U_{ij} W_j^\dagger, \tag{48}$$

where W_i is a SU(2) matrix [see Eq. (18)]. We reserve a fuller discussion of the SU(2) gauge symmetry to Sec. X, and here we give a simple example. In terms of the link variable U_{ij}, the π-flux and d-RVB states are represented as

$$U_{ij}^{\pi\text{-flux}} = -\chi[\tau^3 - i(-1)^{i_x+j_y}] \tag{49}$$

and

$$U_{i,i+\mu}^d = -\chi(\tau^3 + \eta_\mu \tau^1), \tag{50}$$

respectively, where τ^i are the Pauli matrices and $\eta_x = -\eta_y = 1$. These two are related by

$$U_{ij}^{SF} = W_i^\dagger U_{ij}^d W_j, \tag{51}$$

where

$$W_j = \exp\left[i(-1)^{j_x+j_y}\frac{\pi}{4}\tau^1\right]. \tag{52}$$

Therefore the SU(2) transformation of the fermion variable

$$\Phi_i' = W_i \Phi_i \tag{53}$$

relates the π-flux and d-RVB states. Some remarks are in order. First, it should be noted that at half-filling we are discussing the Mott insulating state and its spin dynamics. The charge transport is completely suppressed by the constraint (34). Implementation of the constraint is discussed in Secs. IX and X where the mean-field theory is elaborated into gauge theory. Second, it is now established that the ground state of the two-dimensional antiferromagnetic Heisenberg model shows antiferromagnetic long-range ordering. This corresponds to the third (and most naive) way of decoupling the exchange interaction, i.e.,

$$\mathbf{S}_i \cdot \mathbf{S}_j = \frac{1}{4} f_{i\alpha}^\dagger \sigma_{\alpha\beta}^\mu f_{i\beta} f_{j\gamma}^\dagger \sigma_{\gamma\delta}^\mu f_{j\delta}. \tag{54}$$

However, even with the antiferromagnetic long-range ordering, the singlet formation represented by χ_{ij} and Δ_{ij} dominates and antiferromagnetic long-range ordering occurs on top of it. This view was stressed by Hsu and co-workers (Hsu, 1990; Hsu *et al.*, 1991) generalizing the π-flux state to include antiferromagnetic long-range ordering and is in accord with the energetics of the projected wave functions, as discussed in Sec. VI.A. An alternative route to reaching the antiferromagnetic ground state is to start with the π-flux mean-field state and include gauge fluctuations. The phenomenon of confinement in lattice gauge theory will also lead to antiferromagnetic order, as discussed in Secs. IX.D and X.

Now we turn to the doped case, i.e., $x \neq 0$. Then the behavior of the bosons is crucial for charge dynamics. Within mean-field theory, bosons are free and condensed at T_{BE}. In a three-dimensional system, T_{BE} is finite while $T_{BE}=0$ for a purely two-dimensional system. These theories assume weak three-dimensional hopping between layers and obtain the finite T_{BE} roughly proportional to the boson density x (Kotliar and Liu, 1988; Suzumura *et al.*, 1988). This makes concrete the original idea by Anderson (1987) that spin-singlet formation (RVB) turns into real superconductivity via the Bose condensation of holons. Kotliar and Liu (1988) and Suzumura *et al.* (1988) found d-wave superconductivity in the slave-boson mean-field theory presented above, and the schematic phase diagram is given in Fig. 21. There are five phases classified by the order parameters χ, Δ, and $b=\langle b_i \rangle$ for Bose condensation. In the incoherent
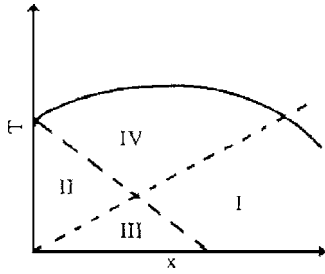
FIG. 21. Schematic phase diagram of the U(1) mean-field theory. The solid line denotes the onset of the uniform RVB state ($\chi \neq 0$). The dashed line denotes the onset of fermion pairing ($\Delta \neq 0$) and the dotted line denotes mean-field Bose condensation ($b \neq 0$). The four regions are (I) Fermi liquid $\chi \neq 0$, $b \neq 0$; (II) spin gap $\chi \neq 0$, $\Delta \neq 0$; (III) d-wave superconductor $\chi \neq 0$, $\Delta \neq 0$, $b \neq 0$; and (IV) strange metal $\chi \neq 0$. From Lee and Nagaosa, 1992.

state at high temperature, the order parameters are zero. In the uniform RVB state (IV in Fig. 21), only χ is finite. In the spin-gap state (II), Δ and χ are nonzero while $b=0$. This corresponds to spin-singlet superconductivity with incoherent charge motion and can be viewed as the precursor phase of superconductivity. This state has been interpreted as the pseudogap phase (Fukuyama, 1992). We note that at the mean-field level, the SU(2) symmetry is broken by the nonzero μ_B in Eq. (45) and the d-wave pairing state is chosen because it has lower energy than the staggered flux state. We shall return to this point in Sec. X. In the Fermi-liquid state (I), both χ and b are nonzero while $\Delta=0$. This state is similar to the slave-boson description of the heavy fermion state. Last, when all the order parameters are nonzero, we obtain the d-wave superconducting state (III). This mean-field theory, in spite of its simplicity, captures rather well the experimental features as described in Secs. III and IV.

Before closing this section, we mention the slave-fermion method and its mean-field theory (Arovas and Auerbach, 1988; Yoshioka, 1989; Chakraborty *et al.*, 1990). One can exchange the statistics of fermions and bosons in Eqs. (31) and (32). Then the boson has the spin index, i.e., $b_{i\sigma}$, while the fermion becomes spinless, i.e., f_i. This boson is called the Schwinger boson and is suitable for describing the antiferromagnetically long-range ordered state. The large-N limit of Schwinger boson theory gives the antiferromagnetically long-range ordered state for $S=1/2$ spins. The holes are represented by the spinless fermion forming a small hole pocket around $k=(\pi/2, \pi/2)$. The size of the hole pocket is twice as large as the usual doped spin-density wave state due to the absence of the spin index. Therefore the slave-fermion method violates the Luttinger theorem. Finally, we mention that by introducing a phase string in the slave-fermion approach one obtains a phase-string formulation of high-T_c superconductivity (Weng *et al.*, 2000; Weng, 2003). In such an approach both spin-1/2 neutral particles and spin-0 charged particles are bosons with nontrivial mutual statistics between them.

IX. U(1) GAUGE THEORY OF THE UNIFORM RVB STATE

The mean-field theory only enforces the constraint of no double occupancy on average. Furthermore, fermions and bosons introduce redundancy in representing the original electron, which results in an extra gauge degree of freedom. To include these effects we need to consider fluctuations around the mean-field saddle points, which immediately become gauge theories, as first pointed out by Baskaran and Anderson (1988). Here we review the early work on the U(1) gauge theory, which treats gauge fluctuations on the Gaussian level (Ioffe and Larkin, 1989; Ioffe and Kotliar, 1990; Nagaosa and Lee, 1990; Lee and Nagaosa, 1992). The theory can be worked out in some detail, leading to a nontrivial method for obtaining physical response functions in terms of the fermion and boson ones, called the Ioffe-Larkin composition rule. It highlights the importance of calculating gauge-invariant quantities and the fact that the fermion and bosons only enter as useful intermediate steps. The Gaussian U(1) gauge theory was mainly designed for the high-temperature region of the optimally doped cuprate, i.e., the so-called strange-metal phase (IV) in Fig. 21. We shall describe its failure in the underdoped region, which leads to the SU(2) formulation of the next two sections. The Gaussian theory also misses the confinement physics, which is important for the ground state.

A. Effective gauge action and non-Fermi-liquid behavior

As discussed in Sec. III, the phenomenology of the optimally doped Mott insulator is required in order to describe the two seemingly contradictory features, i.e., the doped insulator with small hole carrier concentration and electrons forming the large Fermi surface. The former is supported by various transport and optical properties, such as the Drude weight proportional to x, while the latter is supported by the angle-resolved photoemission spectroscopy spectra in the normal state of optimally doped samples. In the conventional single-particle picture, the reduction of the first Brillouin zone due to the antiferromagnetically long-range ordered distinguishes these two. Namely, small hole pockets with area x are formed in the reduced first Brillouin zone in the antiferromagnetically long-range ordered state, while the large metallic Fermi surface of area $1-x$ appears otherwise. The challenge for the theory of the optimally doped case is that aspects of the doped insulator appear in some experiments even with the large Fermi surface. Also it is noted that ARPES shows that there is no sharp peak corresponding to the quasiparticle in the normal state, especially at the antinodal region near $\boldsymbol{k} = (\pi, 0)$. The Fermi surface is defined by a rather broad peak dispersing near the Fermi energy. These strongly suggest that the normal state of high-temperature superconductors is not described in terms of the usual Landau–Fermi-liquid picture.

A promising theoretical framework for resolving this dilemma is the slave-boson formalism introduced above.

It has the two species of particles, i.e., fermions and bosons. Due to strong correlation, the electron is "fractionalized" into these two particles. However, one must be mindful that fermions and bosons are not gauge invariant and they are strongly coupled to the gauge field. This arises from the fact that the conservation of the gauge charge $Q_i = \Sigma_\sigma f_{i\sigma}^\dagger f_{i\sigma} + b_i^\dagger b_i$ can be derived by the Noether theorem starting from the local U(1) gauge transformation,

$$f_{i\sigma} \to e^{i\varphi_i} f_{i\sigma}, \quad b_i \to e^{i\varphi_i} b_i. \tag{55}$$

Therefore the constraint (34) is equivalent to a local gauge symmetry. The Green's functions for fermions and bosons $G_F(\boldsymbol{i},\boldsymbol{j};\tau) = -\langle T_\tau f_{i\sigma}(\tau) f_{j\sigma}^\dagger \rangle$ and $G_B(\boldsymbol{i},\boldsymbol{j};\tau) = -\langle T_\tau b_i(\tau) b_j^\dagger \rangle$ transform as

$$G_F(\boldsymbol{i},\boldsymbol{j};\tau) \to e^{i(\varphi_i - \varphi_j)} G_F(\boldsymbol{i},\boldsymbol{j};\tau),$$

$$G_B(\boldsymbol{i},\boldsymbol{j};\tau) \to e^{i(\varphi_i - \varphi_j)} G_B(\boldsymbol{i},\boldsymbol{j};\tau). \tag{56}$$

Therefore these fermions and bosons are not gauge invariant and should be regarded only as the particles which are useful in the intermediate step of the theory to calculate the physical (gauge-invariant) quantities, as will be done in the next section.

The question is often asked whether the fermions and bosons are real particles. Strictly speaking, the physical electron operator is also not gauge invariant under the electromagnetic-field gauge transformation. Yet, due to the small size of the coupling constant e, we can mentally turn off the coupling for the electromagnetic field and have no trouble thinking of the electron as real. In our case, for the fermion and boson to emerge as useful concepts, we require that on some short-distance scale (or finite temperature) the confinement effects due to the compactness of the gauge fields are not important and the problem can be treated as noncompact, as done below. We find that fermions and bosons are not close to being free particles, but are coupled to the gauge field with a coupling constant of order unity. (This coupling has been reduced from infinity to unity by screening.) Thus in the following we regard fermions and bosons as intermediate steps in the theory and focus on the calculation of physical (gauge-invariant) quantities. The notion of spinons as emergent low-energy excitations will be discussed further in Sec. X.

At the mean-field level, the constraint was replaced by the averaged one $\langle Q_i \rangle = 1$. This average is controlled by the saddle-point value of the Lagrange multiplier field $\langle \lambda_i \rangle = \lambda$. Originally λ_i is the functional integral variable and is a function of (imaginary) time. When this integration is done exactly, the constraint is imposed. Therefore we have to go beyond the mean-field theory and take into account the fluctuation around it. In other words, the local gauge symmetry is restored by the gauge fields which transform as

$$a_{ij} \to a_{ij} + \varphi_i - \varphi_j,$$

$$a_0(\boldsymbol{i}) \to a_0(\boldsymbol{i}) + \frac{\partial \varphi_i(\tau)}{\partial \tau}, \tag{57}$$

corresponding to Eq. (55). The fields satisfying this condition are already in the Lagrangian (38). Namely, the phase of the Hubbard-Stratonovich variable χ_{ij} and the fluctuation part of the Lagrange multiplier λ_i are a_{ij} and $a_0(\boldsymbol{i})$, respectively.

Let us study this U(1) gauge theory for the uniform RVB (uRVB) state in the phase diagram of Fig. 21. This state is expected to describe the normal state of the optimally doped cuprates in which the SU(2) particle-hole symmetry described by Eqs. (47) and (48) is not important. Here we neglect the Δ field and consider the χ and λ fields. There are amplitude and phase fluctuations of the χ field, but the amplitude fluctuations are massive and do not play an important role in the low-energy limit. Therefore the relevant Lagrangian to start with is

$$L_1 = \sum_{i,\sigma} f_{i\sigma}^* \left(\frac{\partial}{\partial \tau} - \mu_F + ia_0(\boldsymbol{r}_i) \right) f_{i\sigma}$$

$$+ \sum_i b_i^* \left(\frac{\partial}{\partial \tau} - \mu_B + ia_0(\boldsymbol{r}_i) \right) b_i$$

$$- \tilde{J}\chi \sum_{\langle ij \rangle, \sigma} (e^{ia_{ij}} f_{i\sigma}^* f_{j\sigma} + \text{H.c.}) - t\eta \sum_{\langle ij \rangle} (e^{ia_{ij}} b_i^* b_j + \text{H.c.}),$$

$$\tag{58}$$

where η is the saddle-point value of a Hubbard-Stratonovich variable needed to decouple the hopping term. We take $\eta = \chi$ using Eq. (40). Equation (58) takes the form of a lattice gauge theory. The spatial component of the gauge fields are a_{ij} defined on the $(\boldsymbol{ij})$ link while the time component $a_0(\boldsymbol{r}_i)$ is defined on the lattice site $\boldsymbol{r}_i$. Note that the a_{ij} appears as a phase variable, i.e., the Lagrangian is invariant under the transformation $a_{ij} \to a_{ij} + 2\pi$, which identifies this theory as a compact U(1) gauge theory. The gauge fields are coupled to fermions and bosons hopping on the lattice. The fermions and bosons are referred to as matter fields in the field-theory literature. We also note that the usual Maxwell term $(1/g)f_{\mu\nu}^2$, where $f_{\mu\nu} = \partial_\mu a_\nu - \partial_\nu a_\mu$ familiar in electrodynamics, which controls the gauge fluctuations and describes their dynamics, is absent in Eq. (58). In other words, the coupling constant g is infinite. This is because the gauge field represents the constraint; by integrating over the gauge field we obtain the original problem with the constraint.

In the mean-field theory the gauge fluctuations are completely ignored. One consequence is that the entropy is grossly overestimated since extra degrees of freedom have been introduced. This was shown explicitly by Hlubina et al. (1992), who compared the entropy of the mean-field theory with the high-temperature expansion and found that it is too large by a factor of 2. They also found that by including gauge fluctuations in the random-phase approximation, the agreement is im-

proved considerably. In the random-phase approximation, we exchange the order of the integration between the gauge field (a_{ij}, a_0) and matter fields (fermions and bosons). Namely, the matter fields are integrated over first, and we obtain the effective action for the gauge field,

$$e^{-S_{\text{eff}}(a)} = \int Df^* Df Db^* Db\, e^{-\int_0^\beta L_1}. \tag{59}$$

However, this integration cannot be done exactly, and an approximation is introduced here. The most standard one is the Gaussian approximation or random-phase approximation in which the effective action is obtained using perturbation theory up to the quadratic order in a. For this purpose we introduce here the continuum approximation to the Lagrangian L_1 in Eq. (58),

$$L = \int d^2\boldsymbol{r}\left[\sum_\sigma f_\sigma^*(\boldsymbol{r})\left(\frac{\partial}{\partial\tau} - \mu_F + ia_0(\boldsymbol{r})\right)f_\sigma(\boldsymbol{r})\right.$$
$$+ b^*(\boldsymbol{r})\left(\frac{\partial}{\partial\tau} - \mu_B + ia_0(\boldsymbol{r})\right)b(\boldsymbol{r}) - \frac{1}{2m_F}\sum_{\sigma, j=x,y} f_\sigma^*(\boldsymbol{r})$$
$$\times\left(\frac{\partial}{\partial x_j} + ia_j\right)^2 f_\sigma(\boldsymbol{r}) - \frac{1}{2m_B}\sum_{j=x,y} b^*(\boldsymbol{r})\left(\frac{\partial}{\partial x_j} + ia_j\right)^2 b(\boldsymbol{r})\left.\right], \tag{60}$$

where the vector field $\boldsymbol{a}$ is introduced by $a_{ij} = (\boldsymbol{r}_i - \boldsymbol{r}_j)\cdot\boldsymbol{a}[(\boldsymbol{r}_i + \boldsymbol{r}_j)/2]$. Note that $1/m_F \approx J$ and $1/m_B \approx t$. The coupling between the matter fields and gauge field is given by

$$L_{\text{int}} = \int d^2\boldsymbol{r}(j_\mu^F + j_\mu^B)a_\mu, \tag{61}$$

where j_μ^F is the fermion current density and j_μ^B is the boson current density.

Note that integration over a_0 recovers the constraint (34) and integration over the vector potential $\boldsymbol{a}$ yields the constraint

$$\boldsymbol{j}_F + \boldsymbol{j}_B = \boldsymbol{0}, \tag{62}$$

i.e., the fermion and boson can move only by exchanging places. Thus the Gaussian approximation apparently enforces the local constraint exactly (Lee, 2000). We must caution that this is true only in the continuum limit, and an important lattice effect related to the 2π periodicity of the phase variable, i.e., the compactness of the gauge field, has been ignored. These latter effects lead to instantons and confinement, as discussed in Sec. IX.D. Thus it is not surprising that the "exact" treatment of Lee (2000) yields the same Ioffe-Larkin composition rule which is derived based on the Gaussian theory (see Sec. IX.B).

We now proceed to reverse the order of integration. We integrate out the fermion and boson fields to obtain an effective action for a_μ. We then consider the coupling of the fermions and bosons to the gauge fluctuations, which are controlled by the effective action. To avoid double counting, it may be useful to consider this procedure in the renormalization-group sense, i.e., we integrate out the high-energy fermion and boson fields to produce an effective action of the gauge field, which in turn modifies the low-energy matter field. This way we convert the initial problem of infinite coupling to one of finite coupling. The coupling is of order unity but may be formally organized as a $1/N$ expansion by artificially introducing N species of fermions. Alternatively, we can think of this as a random-phase approximation, i.e., a sum of fermion and boson bubbles. The effective action for a_μ is given by

$$S_{\text{eff}}^{\text{RPA}}(a) = [\Pi_{\mu\nu}^F(q) + \Pi_{\mu\nu}^B(q)]a_\mu(q)a_\nu(-q), \tag{63}$$

where $q = (\boldsymbol{q}, \omega_n)$ is a three-dimensional vector. The current-current correlation function $\Pi_{\mu\nu}^F(q)$ $[\Pi_{\mu\nu}^B(q)]$ of the fermions (bosons) is given by

$$\Pi_{\mu\nu}^\alpha(q) = \langle j_\mu^\alpha(q)j_\nu^\alpha(-q)\rangle, \tag{64}$$

with $\alpha = F, B$. Taking the transverse gauge by imposing the gauge-fixing condition

$$\nabla\cdot\boldsymbol{a} = 0, \tag{65}$$

the scalar $(\mu = 0)$ and vector parts of the gauge-field dynamics are decoupled. The scalar part $\Pi_{00}^\alpha(q)$ corresponds to the density-density response function and does not show any singular behavior in the low-energy–momentum limit. On the other hand, the transverse current-current response function shows singular behavior for small $\boldsymbol{q}$ and ω. Explicitly the fermion correlation function is given by

$$\Pi_T^F(q) = i\omega\sigma_{F1}^T(\boldsymbol{q},\omega) - \chi_F\boldsymbol{q}^2, \tag{66}$$

where $\chi_F = 1/24\pi m_F$ is the fermion Landau diamagnetic susceptibililty. The first term describes the dissipation, and the static limit of σ_{F1}^T (real part of the fermion conductivity) for $\omega < \gamma_{\boldsymbol{q}}$ is $\sigma_{F1}^T(\boldsymbol{q},\omega) = \rho_F/m_F\gamma_{\boldsymbol{q}}$, where ρ_F is the fermion density and

$$\gamma_{\boldsymbol{q}} = \begin{cases} \tau_{\text{tr}}^{-1} & \text{for } |\boldsymbol{q}| < (v_F\tau_{\text{tr}})^{-1} \\ v_F|\boldsymbol{q}|/2 & \text{for } |\boldsymbol{q}| > (v_F\tau_{\text{tr}})^{-1}, \end{cases} \tag{67}$$

where τ_{tr} is the transport lifetime due to the scatterings by the disorder and/or the gauge field and v_F is the Fermi velocity. A similar expression is obtained for the bosonic contribution as

$$\Pi_T^B(q) = i\omega\sigma_{B1}^T(\boldsymbol{q},\omega) - \chi_B\boldsymbol{q}^2, \tag{68}$$

where $\chi_B = n(0)/48\pi m_B$ and $n(\epsilon)$ is the Bose occupation factor. χ_B diverges at the Bose condensation temperature $T_{\text{BE}}^{(0)} = 2\pi x/m_B$ when we assume a weak 3D transfer of the bosons. Assuming that the temperature is higher than $T_{\text{BE}}^{(0)}$, the boson conductivity is estimated as

$$\sigma_{B1}^T \cong x^{1/2}/|\boldsymbol{q}| \tag{69}$$

for $|\boldsymbol{q}| > \ell_B^{-1}$, where ℓ_B is the mean free path of the bosons. It can be seen from Eqs. (67) and (69) that $\sigma_{B1}^T \ll \sigma_{F1}^T$.

Summarizing, the propagator of the transverse gauge field is given by

$$\langle a_\alpha(q)a_\beta(-q)\rangle = (\delta_{\alpha\beta} - q_\alpha q_\beta/|\boldsymbol{q}|^2)D_T(q), \qquad (70)$$

$$D_T(q) = [\Pi_T^F(q) + \Pi_T^B(q)]^{-1} \cong [i\omega\sigma(\boldsymbol{q}) - \chi_d\boldsymbol{q}^2]^{-1}. \qquad (71)$$

Here

$$\sigma(\boldsymbol{q}) \cong \begin{cases} k_0/|\boldsymbol{q}| & \text{for } |\boldsymbol{q}|\ell > 1 \\ k_0\ell & \text{for } |\boldsymbol{q}|\ell < 1, \end{cases} \qquad (72)$$

where ℓ is the fermion mean free path and k_0 is of the order k_F of the fermions.

This gauge field is coupled to fermions and bosons and leads to their inelastic scatterings. By estimating the lowest-order self-energies of the fermion and boson propagators, it is found that these are diverging at any finite temperature. This is because of the singular behavior of $D_T(q)$ for small $|\boldsymbol{q}|$ and ω. This kind of singularity was first noted by Reizer (1989) for the problem of electrons coupled to a transverse electromagnetic field, even though related effects such as non-Fermi-liquid corrections for the specific heat were noted earlier (Holstein *et al.*, 1973). However, this does not cause any trouble since the propagators of fermions and bosons are not the gauge-invariant quantity and hence are not physical, as discussed above. As the representative of gauge-invariant quantities, we consider the conductivity of fermions and bosons. (Note that these are still not "physical" because one must combine these to obtain the physical conductivity, as discussed in the next section.) For example, the integral for the (inverse of) transport lifetime τ_{tr} contains the factor $1 - \cos\theta$, where θ is the angle between the initial and final momentum for the scattering. This factor scales with $|\boldsymbol{q}|^2$ for small $\boldsymbol{q}$ and removes the divergence. The explicit estimate gives

$$\frac{1}{\tau_{\text{tr}}^F} \cong \begin{cases} \xi_{\boldsymbol{k}}^{4/3} & \text{for } \xi_{\boldsymbol{k}} > kT \\ T^{4/3} & \text{for } \xi_{\boldsymbol{k}} < kT, \end{cases} \qquad (73)$$

for fermions while

$$\frac{1}{\tau_{\text{tr}}^B} \cong \frac{kT}{m_B\chi_d} \qquad (74)$$

for bosons. These results are interpreted as the scattering with fluctuating gauge flux whose propagator is given by the loop representing the particle-hole propagator for the two-particle current-current correlation function.

Now some words on the physical meaning of the gauge field are in order. For simplicity let us consider three sites and assume that the electron is moving around these. The quantum mechanical amplitude for this process is

$$P_{123} = \langle\chi_{12}\chi_{23}\chi_{31}\rangle = \langle f_{1\alpha}^\dagger f_{2\alpha} f_{2\beta}^\dagger f_{3\beta} f_{3\gamma}^\dagger f_{1\gamma}\rangle. \qquad (75)$$

One can prove that

$$(P_{123} - P_{132})/4i = \boldsymbol{S}_1 \cdot (\boldsymbol{S}_2 \times \boldsymbol{S}_3) \qquad (76)$$

and the right-hand side of the above equation corresponds to the solid angle subtended by the three vectors $\boldsymbol{S}_1, \boldsymbol{S}_2, \boldsymbol{S}_3$ and is called spin chirality (Wen *et al.*, 1989). The left-hand side of Eq. (76) is proportional to sin ϕ where ϕ is the flux of the gauge field seen by the fer-

mion. Therefore the gauge-field fluctuation is regarded as that of the spin chirality. It has been recently discussed that spin chirality will produce the anomalous Hall effect in some ferromagnets such as manganites and pyrochlore oxides in which noncoplanar spin configurations result from the thermal excitation of the Skyrmion or the strong spin anisotropy in the ground state (Ye *et al.*, 1999; Taguchi *et al.*, 2001). This phenomenon can be interpreted as the static limit of the gauge field, while the gauge field discussed here has both quantum and thermal fluctuations.

B. Ioffe-Larkin composition rule

In order to discuss the physical properties of the total system, we have to combine the information obtained for fermions and bosons. This was first discussed by Ioffe and Larkin (1989). Let us start with the physical conductivity σ, which is given by

$$\sigma^{-1} = \sigma_F^{-1} + \sigma_B^{-1} \qquad (77)$$

in terms of the conductivities of fermions (σ_F) and bosons (σ_B). This formula corresponds to the sequential circuit (not parallel) of the two resistances, and is intuitively understood from the fact that both fermions and bosons have to move the subject to the constraint. This formula can be derived in terms of the shift of the gauge field $\boldsymbol{a}$ and the resultant backflow effect. In the presence of the external electric field $\boldsymbol{E}$, the gauge field $\boldsymbol{a}$, and hence the internal electric field $\boldsymbol{e}$, is induced. Let us assume that the external electric field $\boldsymbol{E}$ is coupled to fermions. Then the effective electric field seen by fermions is

$$\boldsymbol{e}_F = \boldsymbol{E} + \boldsymbol{e} \qquad (78)$$

while that for bosons is

$$\boldsymbol{e}_B = \boldsymbol{e}. \qquad (79)$$

The fermion current $\boldsymbol{j}_F$ and the boson current $\boldsymbol{j}_B$ are induced, respectively, as

$$\boldsymbol{j}_F = \sigma_F\boldsymbol{e}_F, \quad \boldsymbol{j}_B = \sigma_B\boldsymbol{e}_B. \qquad (80)$$

The constraint $\boldsymbol{j}_F + \boldsymbol{j}_B = \boldsymbol{0}$ given by Eq. (62) leads to

$$\boldsymbol{e} = -\frac{\sigma_F}{\sigma_F + \sigma_B}\boldsymbol{E}. \qquad (81)$$

The physical current $\boldsymbol{j}$ is given by

$$\boldsymbol{j} = \boldsymbol{j}_F = -\boldsymbol{j}_B = \frac{\sigma_F\sigma_B}{\sigma_F + \sigma_B}\boldsymbol{E}, \qquad (82)$$

leading to the expression for the physical conductivity σ in Eq. (77). It is also noted here that the same result is obtained if instead we couple the electromagnetic field to bosons. In this case the internal electric field $\boldsymbol{e}$ is different, but $\boldsymbol{e}_F$ and $\boldsymbol{e}_B$ remain unchanged. Note that $\sigma_F \gg \sigma_B$ in the uRVB state, and we conclude that $\sigma \cong \sigma_B = x\tau_{\text{tr}}^B/m_B$, which is inversely proportional to the temperature T. Furthermore, the Drude weight of the opti-

cal conductivity is determined by x/m_B as observed experimentally. It remains true that the superfluidity density ρ_S in the superconducting state is given by the missing oscillator strength below the gap, which also means that $\rho_s \propto x$.

A more formal way of deriving the physical electromagnetic response follows. We can generalize the discussion of the effective action $S_{\text{eff}}(a)$ for the gauge field to include the external electromagnetic field A_μ. Let us again couple A_μ to the fermions. The effective action becomes, instead of Eq. (63),

$$S_{\text{eff}}^{\text{RPA}}(a,A) = \Pi_{\mu\nu}^F(q)[a_\mu(q) + A_\mu(q)][a_\nu(-q) + A_\nu(-q)] + \Pi_{\mu\nu}^B(q)a_\mu(q)a_\nu(-q). \quad (83)$$

After integrating over the gauge field a_μ, we end up with the effective action for A_μ only as

$$S_{\text{eff}}^{\text{RPA}}(A) = \Pi_{\mu\nu}(q)A_\mu(q)A_\nu(-q), \quad (84)$$

with the physical electromagnetic response function

$$\Pi_\alpha(q)^{-1} = [\Pi_\alpha^F(q)]^{-1} + [\Pi_\alpha^B(q)]^{-1}, \quad (85)$$

where $\alpha = 0$ or T stands for the longitudinal and transverse parts. Then the physical diamagnetic susceptibility $\tilde{\chi}$ is given by $\tilde{\chi}^{-1} = \chi_F^{-1} + \chi_B^{-1}$. Again in the superconducting state, $\Pi_T^F \propto \rho_s^F$ and $\Pi_T^B \propto \rho_s^B$, where ρ_s^F and ρ_s^B are the superfluidity density of the fermion pairing and boson condensation. This leads to the composition rule for ρ_s as $\rho_s^{-1} = (\rho_s^F)^{-1} + (\rho_s^B)^{-1} \cong (\rho_s^B)^{-1} \propto x^{-1}$, with $\rho_s^F \gg \rho_s^B$, reproducing the same result as suggested from the Drude weight. On the other hand, the temperature dependence of ρ_s^F is of the form $\rho_s^F(T) = \rho_s^F(0)(1 - aT)$, where a is given by the nodal fermion dispersion, while the temperature dependence of ρ_s^B is expected to follow higher powers in T and be negligible. The Ioffe-Larkin composition rule then predicts that

$$\rho_s(T) \approx \rho_s^B \left(1 - \frac{\rho_s^B}{\rho_s^F}\right) \approx \rho_s^B(0) - \frac{[\rho_s^B(0)]^2}{\rho_s^F(0)} aT. \quad (86)$$

Since $\rho_s^B(0) \sim xt$, this predicts that the temperature dependence of the superfluid density is proportional to x^2. Comparison with Eq. (5) implies that $\alpha \sim (t/J)x$ in the slave-boson theory. As shown in Fig. 14, this prediction does not agree with experiment and is probably an indication of the breakdown of Gaussian fluctuations, which underlines the Ioffe-Larkin rule.

We conclude this section by remarking that the Ioffe-Larkin rule can be extended to various other physical quantities. For example, the Hall constant R_H is given by

$$R_H = \frac{R_H^F \chi_B + R_H^B \chi_F}{\chi_B + \chi_F}, \quad (87)$$

while the thermopower $S = S_B + S_F$ and the electronic thermal conductivity $\kappa = \kappa_B + \kappa_F$ are sums of the bosonic and fermionic contributions (Lee and Nagaosa, 1992).

Compared with two-particle correlation functions discussed above, the single-particle Green's function is more complicated. At the mean-field level, the electron Green's function is given by the product of the fermion and boson Green's functions in the $(\boldsymbol{r}, \tau)$ space. Therefore in the momentum-frequency space, it is given by the convolution. The spectral function is composed of two contributions, one is the quasiparticle peak with weight $\sim x$ while the other is the incoherent background. Even the former one is broadened due to the momentum distribution of the noncondensed bosons, i.e., there is no quasiparticle peak in the strict sense. This absence of the delta-function peak also occurs in the SU(2) theory in Sec. XI indicating that fermions are not free and hence cannot be regarded as the quasiparticle. On the other hand, the dispersion of this quasiparticle peak is determined by that of fermions, and hence its locus of zero energy constitutes the large Fermi surface enclosing the area $1 - x$. However, this simple calculation does not reproduce some of the novel features in the ARPES experiments such as the Fermi arc in underdoped samples, and a more detailed treatment will be discussed in Sec. XI.

Combined with the discussion of the transport properties and the electron Green's function, the present uniform RVB state in the U(1) formulation offers an explanation of the dichotomy between the doped Mott insulator and the metal with large Fermi surface. In particular, the conclusion that the conductivity is dominated by the boson conductivity $\sigma \approx \sigma_B \approx x\tau_{tr}^B/m_B \approx xtT$ explains the linear T resistivity, which has been taken as a sign of non-Fermi-liquid behavior from the beginning of high-T_c research. However, we must caution the reader that this conclusion was reached for $T > T_{\text{BE}}^{(0)}$, while in experiments the linear T behavior persists to much lower temperature near optimal doping. It is possible that gauge fluctuations suppress the effective Bose condensation. Lee et al. (1996) have attempted to include the effect of strong gauge fluctuations on boson conductivity by assuming a quasistatic gauge fluctuation and treating the problem with quantum Monte Carlo calculations. The picture is that the boson tends to make self-retracing paths to cancel out the effect of the gauge field (Nagaosa and Lee, 1991). They indeed find that boson conductivity remains linear in T down to much lower temperature than $T_{\text{BE}}^{(0)}$.

C. Ginzburg-Landau theory and vortex structure

Up to now we have focused on the uRVB state where the pairing amplitude Δ of the fermions is zero. In this subsection we review the phenomenological Ginzburg-Landau theory to treat this pairing field (Nagaosa and Lee, 1992; Sachdev, 1992). The free energy for a single CuO_2 layer is given by

$$F = F_F[\psi, \boldsymbol{a}, \boldsymbol{A}] + F_B[\phi, \boldsymbol{a}] + F_{\text{gauge}}[\boldsymbol{a}], \quad (88)$$

with

$$F_F[\psi, \mathbf{a}, \mathbf{A}] = \frac{H_{cF}^2}{8\pi} \int d^2r \left[2\xi_F^2 \left| \left(\nabla - 2i\mathbf{a} - i\frac{2e}{c}\mathbf{A} \right) \psi \right|^2 \right.$$
$$\left. + 2\,\mathrm{sgn}(T - T_D^{(0)})|\psi|^2 + |\psi|^4 \right], \quad (89)$$

$$F_B[\psi, \mathbf{a}] = \frac{H_{cB}^2}{8\pi} \int d^2r [2\xi_B^2 |(\nabla - i\mathbf{a})\phi|^2$$
$$+ 2\,\mathrm{sgn}(T - T_{BE}^{(0)})|\phi|^2 + |\phi|^4], \quad (90)$$

and

$$F_{\mathrm{gauge}}[\mathbf{a}] = \int d^2r [\chi_F \{\nabla \times [\mathbf{a} + (e/c)\mathbf{A}]\}^2$$
$$+ \chi_B (\nabla \times \mathbf{a})^2], \quad (91)$$

where $\mathbf{A}$ is the electromagnetic vector potential, c is the velocity of light, and $\hbar$ is set to unity. In the above equations, the optimal value of the order parameter is scaled to be unity, and hence the correlation lengths ξ_B, ξ_F and the thermodynamic critical fields H_{cF}, H_{cB} are temperature dependent for both fermion pairing and Bose condensation. It is noted that the penetration length of the fermion pairing (boson condensation) λ_F (λ_B) is related to H_{cF} (H_{cB}) as $H_{cF} = \phi_0/2\sqrt{2}\pi\xi_F\lambda_F$ ($H_{cB} = \phi_0/\sqrt{2}\pi\xi_B\lambda_B$). We take the lattice constant as the unit of length. Then $\xi_F(0) \sim J/\Delta$, $\xi_B \sim x^{-1/2}$, and the condensation energy per unit area is given by $H_{cF}(0)^2/(8\pi) \sim \Delta^2/J$ and $H_{cB}(0)^2/(8\pi) \sim tx^2$.

Now we consider the consequences derived from this Ginzburg-Landau free energy. One is the interplay between the Berezinskii-Kosterlitz-Thouless transitions for the fermion pairing and boson condensation. We consider the type-II limit, and neglect $\mathbf{A}$ for the moment. As is well known, the binding or unbinding of the topological vortex excitations leads to the novel phase transition (Berezinskii-Kosterlitz-Thouless transition) in two dimensions. This is due to the logarithmic divergence of the vortex energy with respect to the sample size. This energy is competing with the entropy term which is also logarithmically diverging. Above some critical temperature the entropy dominates, and free vortex excitations are liberated resulting in the exponential decay of the order parameter. However, this logarithmic divergence is cut off when the order parameter is coupled to the massless gauge field $\mathbf{a}$. Namely, the gauge field screens the vortex current, and $|(\nabla - i\mathbf{a})\phi|$ and $|(\nabla - 2i\mathbf{a})\psi|$ decay exponentially beyond some penetration lengths. This means that the Berezinskii-Kosterlitz-Thouless transition for the fermion pairing and boson condensation disappear when the gauge field $\mathbf{a}$ is massless. In other words, these two order parameters are coupled through the gauge field, and the Berezinskii-Kosterlitz-Thouless transition occurs only simultaneously when the gauge field becomes massive due to the Higgs mechanism. Therefore the phase-transition lines for fermion pairing and boson condensation in the phase diagram of Fig. 21

become crossover lines and only the superconducting transition remains as the real Berezinskii-Kosterlitz-Thouless transition.

Now we turn to vortex structures in the superconducting state. The most intriguing issue here is the quantization of the magnetic flux. Because the boson has charge e while the fermion pairing $-2e$, the question is whether the hc/e vortex may be more stable than the conventional $hc/2e$ vortex. To study this issue, we compare the energy cost of the two types of vortex structure: (i) Type A: the fermion-pairing order parameter ψ vanishes at the core with its phase winding around it. The boson condensation does not vanish and the vortex core state is the Fermi liquid. The flux quantization is $hc/2e$. (ii) Type B: the Bose condensation is destroyed at the core and fermion pairing remains finite. Then the vortex core state is the spin-gap state. The flux quantization is hc/e in this case. The energy of each vortex is estimated as follows. First the Ioffe-Larkin composition rule results in the penetration length λ of the magnetic field as

$$\lambda^2 = \lambda_F^2 + \lambda_B^2, \quad (92)$$

which is equivalent to $\rho_s^{-1} = (\rho_s^F)^{-1} + (\rho_s^B)^{-1}$ derived in the previous subsection. The contribution from the region where the distance from the core is larger than ξ_F, ξ_B is estimated similarly to the usual case,

$$E_0 = \left[\frac{\phi_0}{4\pi\lambda} \right]^2 \ln \left[\frac{\lambda}{\max(\xi_F, \xi_B)} \right], \quad (93)$$

for the type-A vortex, and $4E_0$ for the type-B vortex because the quantized flux is doubled in the latter case. The core energy E_c is given by the condensation energy per area times the area of the core. For a type-A vortex

$$E_c^{(A)} \approx H_{cF}^2 \xi_F^2 \approx J, \quad (94)$$

while for a type-B vortex

$$E_c^{(B)} \approx H_{cB}^2 \xi_B^2 \approx tx. \quad (95)$$

Then the vortex energies are estimated to be $E^{(A)} \approx E_0 + E_c^{(A)}$ and $E^{(B)} = 4E_0 + E_c^{(B)}$, respectively. Note that E_0 is proportional to λ^{-2}, which is dominated by $\lambda_B^{-2} \approx x$ and hence E_0, $E_c^{(B)}$ are proportional to x while $E_c^{(A)}$ is a constant of order J. The latter energy is in agreement with the estimate of the vortex in the BCS theory discussed in Sec. V.B and is the dominant energy for sufficiently small x. We come to the conclusion that the type-B vortex (with hc/e flux quantization) will be more stable in the underdoped region. This conclusion was reached by Sachdev (1992) and by Nagaosa and Lee (1992) and appears to be a general feature of the U(1) gauge theory. Unfortunately, the experimental search for stable hc/e vortices has so far come up negative (Wynn et al., 2001). In Sec. XII.C we describe how this problem is fixed by the SU(2) gauge theory, which is designed to be more accurate for small doping.

D. Confinement-deconfinement problem

Despite the qualitative success of the mean-field and U(1) gauge-field theories, there are several difficulties with this picture. One is that the gauge fluctuations are strong and one cannot have a well-controlled small expansion parameter, except rather formal ones such as the large-N expansion. This issue is closely related to the confinement problem in lattice gauge theory and will be discussed below and also in Secs. X.H and XI.F.

The coupling constant of the gauge field is defined as the inverse of the coefficient of $f_{\mu\nu}^2$ in the Lagrangian. It is well known that the strong-coupling gauge field leads to confinement. In the confining phase, only the gauge singlet particles appear in the physical spectrum, which corresponds, for example, to the physical electron and the antiferromagnetic magnon in the present context. Below we give a brief introduction to this issue. For more details, see Nagaosa (1995).

Up to now the discussion is at the Gaussian fluctuation level where the effective action for the gauge field has been truncated at quadratic order in the continuum approximation. However, we are starting from the infinite-coupling limit, and even if finite coupling is produced by integrating over the matter field, the strong-coupling effect must be seriously considered. In the original problem the gauge field is defined on the lattice and the periodicity with respect to $a_{ij} \to a_{ij} + 2\pi$ must be taken into account. Namely, the relevant model is that of the compact lattice gauge theory. Let us first consider the most fundamental model without the matter field,

$$S_{\text{gauge}} = -\frac{1}{g} \sum_{\text{plaquette}} (1 - \cos f_{\mu\nu}), \qquad (96)$$

where

$$f_{\mu\nu} = a_{i,i+\mu} + a_{i+\mu,i+\mu+\nu} - a_{i+\nu,i+\mu+\nu} - a_{i,i+\nu} \qquad (97)$$

is the flux penetrating through the plaquette in the $(d+1)$-dimensional space and $\mu, \nu = x, y, \dots$. Now S_{gauge} is a periodic function of $f_{\mu\nu}$ with period 2π and one can consider tunneling between different potential minima. This leads to the "Bloch state" of $f_{\mu\nu}$ when the potential barrier height $1/g$ is low enough, while it is "localized" near one minimum when $1/g$ is high. The former corresponds to the quantum disordered $f_{\mu\nu}$ and leads to the linear confining force as shown below (confining state). On the other hand, in the latter case, one can neglect the compact nature of the gauge field and the analysis in previous sections is justified (deconfining state). For this confinement-deconfinement transition, one can define the following order parameter, i.e., the Wilson loop:

$$W(C) = \left\langle \exp\left(iq \oint_C dx_\mu a_\mu(x) \right) \right\rangle, \qquad (98)$$

where the loop C consists of the paths of length T along the time direction and those of length R along the spatial direction. It is related to the gauge potential $V(R)$ between the two static gauge charges $\pm q$ with opposite sign at distance R as

$$W(C) = \exp[-V(R)T]. \qquad (99)$$

There are two types of behavior of $W(C)$: (i) area law, $W(C) \sim e^{-\alpha RT}$; and (ii) perimeter law, $W(C) \sim e^{-\beta(R+T)}$, where α, β are constants. In the case (i), the potential $V(R)$ is increasing linearly in R, and hence the two gauge charges can never be free. Therefore it corresponds to confinement, while case (ii) corresponds to deconfinement.

It is known that the compact QED (pure gauge) model in (2+1)D is always confining however small the coupling constant is (Polyakov, 1987). The argument is based on the instanton configuration, which is enabled by the compactness of the gauge field. This instanton is the source of the flux with the field distribution

$$b(x) = \frac{x}{2|x|^3}, \qquad (100)$$

where $x = (r, \tau)$ are the (2+1)D coordinates in the imaginary-time formalism, and $b(x) = (e_y(x), -e_x(x), b(x))$ is the combination of the "electric field" $e_\alpha(x)$ and the "magnetic field" $b(x)$. This corresponds to the tunneling phenomenon of the flux because the total flux slightly above (future) or below (past) the instanton differs by 2π. The anti-instanton corresponds to the sink of the flux. This instanton or anti-instanton corresponds to the singular configuration in the continuous approximation but is allowed in the compact model on a lattice. Therefore (anti-)instantons take into account the compact nature of the original model in the continuum approximation. It is also clear from Eq. (100) that the instanton behaves as the positive magnetic charge and the anti-instanton behaves as the negative. Then it is evident that when we substitute the (anti-)instanton configuration into the action

$$S = \int d^3x \frac{1}{2g} [b(x)]^2 \qquad (101)$$

(g is the coupling constant), we obtain the Coulomb $1/|x|$ interaction between the (anti-)instantons as

$$S_{\text{inst}} = \sum_{i<j} \frac{q_i q_j}{|x_i - x_j|}, \qquad (102)$$

where q_i is the magnetic charge, which is $\sqrt{g}/2$ for the instanton and $-\sqrt{g}/2$ for the anti-instanton.

It is well known that the Coulomb gas in three dimensions is always in the screening phase, namely, the long-range Coulomb interaction is screened to be the short-range one due to the cloud of the opposite charges surrounding the charge. Therefore the creation energy of the (anti-)instanton is finite and the free magnetic charges are liberated. These free magnetic charges disorder the gauge field and make the Wilson loop exhibit the area law, i.e., confinement.

The discussion up to now is for the pure gauge model without the matter field. With the matter field the con-

finement issue becomes very subtle since the Wilson loop does not work as the order parameter any more. This is because a particle-antiparticle pair can be excited out of the vacuum to screen the static charges and the area law cannot be sustained. Furthermore, confinement disappears above some transition temperature even in the pure gauge model. In the presence of the matter field, the confinement-deconfinement transition at finite temperature is replaced by the gradual crossover to the plasma phase in the high-temperature limit (Polyakov, 1978; Susskind, 1979; Svetitsky, 1986). Therefore we can expect that the slave-boson theory without confinement describes the physics of the intermediate energy scale even though the ground state is the confining state. Indeed, within the U(1) gauge theory, the ground states are either antiferromagnetic, superconducting, or Fermi liquid and are all confining. Nevertheless, the pseudogap region which exists only at finite temperatures may be considered "deconfined" and describable by fermions and bosons coupled to noncompact gauge fields. We emphasize once again that in this scenario fermions and bosons are not to be considered free physical objects. Their interactions with gauge fields are important and physical gauge-invariant quantities are governed by the Ioffe-Larkin rule within the Gaussian approximation.

It is of great interest to ask the question of whether a deconfined ground state is possible in a U(1) gauge theory in the presence of a matter field. This issue was first addressed in a seminal paper by Fradkin and Shenker (1979), who considered a boson field coupled to a compact U(1) gauge field. The following bosonic action is added to S_{gauge}:

$$S_B = t \sum_i \cos[\Delta_\mu \theta(\mathbf{r_i}) - q a_\mu(\mathbf{r_i})]. \tag{103}$$

Here the Bose field is represented by phase fluctuations only, Δ_μ is the lattice derivative, $a_\mu(\mathbf{r_i}) = a_{i,i+\mu}$ is the gauge field on the link $i, i+\mu$, and q is an integer. It is interesting to consider the phase diagram in the t-g plane. Along the $t=0$ line, we have pure gauge theory, which is always confining in 2+1 dimensions. For $g \ll 1$, gauge fluctuations are weak and S_B reduces to the XY model weakly coupled to a U(1) gauge field, which exhibits an ordered Higgs phase at zero temperature. Note that in the Higgs phase, the gauge field is gapped by the Anderson-Higgs mechanism. On the other hand, it is also gapped in the confinement phase due to the screening of magnetic charges described earlier. There is no easy way to distinguish between these two phases and the central result of Fradkin and Shenker is that for $q =1$ the Higgs phase and the confinement phases are smoothly connected to each other. Indeed, it was argued by Nagaosa and Lee (2000) that for the (1+2)D case the entire t-g plane is covered by the Higgs-confinement phase, with the exception of the line $g=0$ which contains the XY transition.

The situation is dramatically different for $q=2$, i.e., if the boson field corresponds to a pairing field such as in a superconductor. It is possible to distinguish between the

Higgs phase and the confinement phase by asking whether $q = \pm 1$ have a linear confinement potential between them or not. In this case there is a phase boundary between the confined and the Higgs phase, and the Higgs phase (the pairing phase) is deconfined. One way of understanding this deconfinement is that the paired phase has a residual Z_2 gauge symmetry, i.e., the pairing order parameter is invariant under a sign change of the underlying $q=1$ fields which make up the pair. Furthermore, it is known that the Z_2 gauge theory has a confinement-deconfinement transition in 2+1 dimensions. Thus the conclusion is that a compact U(1) gauge theory coupled to a pair field can have a deconfined phase. This is indeed the route to a deconfined ground state proposed by Read and Sachdev (1991) and Wen (1991). In the context of the U(1) gauge theory, the fermion pair field Δ plays the role of the $q=2$ boson field in Eq. (103). In such a phase, the spinon and holons are deconfined, leading to the phenomenon of spin and charge fractionalization. A third elementary excitation in this theory is the Z_2 vortex, which is gapped.

Senthil and Fisher (2000) pointed out that the square root of Δ carried unit gauge charge and one can combine this with the fermion to form a gauge-invariant spinon and with the boson to form a gauge-invariant "chargon." The spinon and chargon only carry Z_2 gauge charges and can be considered almost free. They proposed an experiment to look for the gapped Z_2 vortex but the results have so far been negative. The connection between the U(1) slave-boson theory and their Z_2 gauge theory was clarified by Senthil and Fisher (2001a).

There is yet another route to a deconfined ground state and that is a coupling of a compact U(1) gauge field to gapless fermions. Nagaosa (1993) has suggested that dissipation due to gapless excitations lead to deconfinement. The special case of coupling to gapless Dirac fermions is of special interest. This route [called the U(1) spin liquid] appears naturally in the SU(2) formulation and will be discussed in detail in Sec. XI.F. In Sec. XII we use the proximity on this deconfined state to understand the pseudogap state. This is a more attractive scenario compared with the reliance purely on finite temperature to see deconfinement effects as described earlier in this section.

In the literature there have been some confusing discussions of the role of confinement in the gauge-theory approach to strong correlations. In particular, Nayak (2000, 2001) claimed that slave particles are always confined in U(1) gauge theories. His argument is based on the fact that since these gauge fields are introduced to enforce constraint, they do not have restoring force and the coupling constant is infinite. What he overlooked is the possibility that partially integrating out the matter fields will generate restoring forces, which brings the problem to one of strong but finite coupling, and then sweeping conclusions can no longer be made. Comments by Ichinose and Matsui (2001), Ichinose et al. (2001), and Oshikawa (2003) have clarified the issues and answered Nayak's objections. For example, Ichinose and Matsui

(2001) pointed out that $(3+1)$-dimensional SU(3) gauge theory coupled to N fermions is in the deconfined phase even at infinite coupling for $N > 7$. Recently, an example of N bosonic fields coupled to a U(1) gauge field with infinite coupling, which shows deconfinement for sufficiently large N, has been worked out in some detail (Lee and Lee, 2005b). Another counterexample has been found by Rantner and Wen (2002), Wen (2002b), and Hermele, Senthil, Fisher, *et al.* (2004), who have shown that the U(1) gauge theory coupled to massless Dirac fermions is in a gapless phase (or the deconfined phase) for sufficiently large N (see Sec. XI.F). There is also numerical evidence from Monte Carlo studies that the SU(N) Hubbard-Heisenberg model at $N=4$ exhibits a gapless spin-liquid phase, i.e., a Mott insulator with power-law spin correlation, without breaking lattice translational symmetry (Assaad, 2005). This spin-liquid state is strongly suggestive of the stability of a deconfined phase with a U(1) gauge field coupled to Dirac fermions.

E. Limitations of the U(1) gauge theory

The U(1) gauge theory, which only includes Gaussian fluctuations about mean-field theory, suffers from several limitations which are important in the underdoped regime. Apart from the confinement issue discussed in the last section, we first mention a difficulty with the linear T coefficient of the superfluid density. As long as the gauge fluctuation is treated as Gaussian, the Ioffe-Larkin law holds and one predicts that the superfluid density $\rho_s(T)$ behaves as $\rho_s(T) \approx ax - bx^2 T$. The ax term agrees with experiment while the $-bx^2 T$ term does not (Lee and Wen, 1997; Ioffe and Millis, 2002a), as explained in Sec. V.A. This failure is traced to the fact that in the Gaussian approximation the current carried by quasiparticles in the superconducting state is proportional to $x v_F$. We believe this failure is a sign that nonperturbative effects again become important and confinement takes place, so that the low-energy quasiparticles near the nodes behave like BCS quasiparticles which carry the full current v_F. This is certainly beyond the Gaussian fluctuation treatment described here.

A second difficulty is that experimentally it is known from neutron scattering that spin correlations at (π, π) are enhanced in the underdoped regime. This happens at the same time that a spin gap is forming in the pseudogap regime. The U(1) mean-field theory explains the existence of the spin gap as due to fermion pairing. However, this reduces the fermion density of states and it is not clear how one can get an enhancement of the spin correlation unless one introduces phenomenologically random-phase-approximation interactions (Brinckmann and Lee, 2001). This problem is more serious because the gauge field is gapped in the fermion-paired state and one cannot use gauge fluctuations to enhance the spin correlation. The gapping of the gauge field also tends to suppress fermion pairing self-consistently

(Ubbens and Lee, 1994). We shall see that both these difficulties are resolved by the SU(2) formulation.

A third difficulty has to do with the structure of the vortex core in the underdoped limit (Wen and Lee, 1996). As mentioned in Sec. IX.C, U(1) gauge theory predicts the stability of hc/e vortices, which has not been observed. This is a serious issue because STM experiments have shown that the pseudogap remains in the vortex core. Therefore the vortex core should be type B in U(1) theory, which carries hc/e flux. On the other hand, the $hc/2e$ vortex is not "cheap" because the pairing amplitude vanishes and one has to pay with the pairing energy at the core. These difficulties arise because in U(1) theory fermions become "strong" superconductors at low temperature in the underdoped region. However, this contradicts the fact that at half-filling the d-wave RVB state is equivalent to the π-flux state, which is not "superconducting." In short, U(1) theory misses the important low-lying fluctuations related to SU(2) particle-hole symmetry at half-filling. By incorporating this symmetry into the gauge field even at finite doping, we are led to the SU(2) gauge theory of high-T_c superconductors, which we discuss next.

X. SU(2) SLAVE-BOSON REPRESENTATION FOR SPIN LIQUIDS

In this section we develop the SU(2) slave-boson theory for spin liquids and underdoped high-T_c superconductors. This theory is equivalent to the U(1) slave-boson theory discussed in the last section. However, the SU(2) formalism makes explicit more of the symmetries of the slave-boson theory. This makes it easier to see the low-energy collective modes in the SU(2) formalism, which in turn allows us to resolve some difficulties of the U(1) slave-boson theory.[2] To develop the SU(2) slave-boson theory, let us first describe another way to understand U(1) gauge fluctuations in the slave-boson theory. In this section we concentrate on the undoped case in which the model is just a pure spin system. Even though the theory involves only the fermionic representation of the spin in the underdoped case, we continue to refer to the theory as the slave-boson theory in anticipation of the doped case. We generalize the SU(2) slave-boson theory to the doped model in the next section.

A. Where does the gauge structure come from?

According to the U(1) slave-boson mean-field theory, fluctuations around the mean-field ground state are described by gauge fields and fermion fields. Remember that the original model is just an interacting spin model which is a purely bosonic model. How can a purely

---

[2]We point out that those difficulties are not because the U(1) slave-boson theory is incorrect. The difficulties are the results of the incorrect treatment of the U(1) slave-boson theory, for example, overlooking some low-energy soft modes.

bosonic model contain excitations described by gauge and fermion fields? Should we believe the result?

Let us examine how the results are obtained. We first split the bosonic spin operator into a product of two fermionic operators $S_i = \frac{1}{2} f_i^\dagger \sigma f_i$. We then introduce a gauge field to glue the fermions back into a bosonic spin. From this point of view it appears that gauge bosons and fermions are fake and their appearance is just a mathematical artifact. The appearance of the fermion field and the gauge field in a purely bosonic model seems to indicate that the slave-boson theory is incorrect.

However, we should not discard this theory too quickly. It is actually capable of producing pictures that agree with common sense: the excitations in a bosonic spin system are bosonic excitations corresponding to spin flips, provided that the gauge field is in a confining phase. In the confining phase of the U(1) gauge theory, fermions interact with each other through a linear potential and can never appear as quasiparticles at low energies. Gauge bosons have a large energy gap in the confining phase and are absent from the low-energy spectrum. Only low-energy excitations are the bound states of two fermions which carry spin 1 and are bosons. These are the familiar magnons in the antiferromagnet. The mean-field theory plus the gauge fluctuations may not be very useful, but is not wrong.

On the other hand, the slave-boson mean-field theory (plus gauge fluctuations) is also capable of producing pictures that defy common sense if the gauge field is in a deconfined phase. In this case fermions and gauge bosons may appear as well-defined quasiparticles. The question is do we believe the deconfined phase picture? Do we believe in the possibility of emergent gauge bosons and fermions from a purely bosonic model? Clearly, the slave-boson construction outlined above is far too formal to believe such results. However, it was recently realized that some models (Kitaev, 2003; Levin and Wen, 2003; Wen, 2003b) can be solved exactly with the slave-boson theory (Wen, 2003c). Those models are in deconfined phases and confirm the striking results of the emergence of gauge bosons and fermions from the slave-boson theory.

To gain an intuitive picture of the correlated ground state which leads to emergent gauge bosons and fermions, let us try to understand how a mean-field *Ansatz* χ_{ij} is connected to a physical spin wave function. We know that the ground state $|\Psi_{\text{mean}}^{(\chi_{ij})}\rangle$ of the mean-field Hamiltonian

$$H_{\text{mean}} = \tilde{J} \sum_{ij,\sigma} (\chi_{ji} f_{i\sigma}^\dagger f_{j\sigma} + \text{H.c.}) + \sum_{i,\sigma} a_0 (f_{i\sigma}^\dagger f_{i\sigma} - 1) \quad (104)$$

is not a valid wave function for the spin system since it may not have one fermion per site. To connect to a physical spin wave function, we need to include fluctuations of a_0 to enforce the one fermion per site constraint. With this understanding, we obtain a valid wave function of the spin system $\Psi_{\text{spin}}(\{\alpha_i\})$ by projecting the mean-field state to the subspace of one fermion per site:

$$\Psi_{\text{spin}}^{(\chi_{ij})}(\{\alpha_i\}) = \langle 0_f | \prod_i f_{i\alpha_i} | \Psi_{\text{mean}}^{(\chi_{ij})}\rangle, \quad (105)$$

where $|0_f\rangle$ is the state with no f fermions, $f_{i\alpha}|0_f\rangle = 0$. Equation (105) connects the mean-field *Ansatz* to the physical spin wave function. It allows us to understand the physical meaning of the mean-field *Ansatz* and mean-field fluctuations.

For example, the projection (105) gives the gauge transformation (39) a physical meaning. Usually, for different choices of χ_{ij} the ground states of H_{mean}, Eq. (104), correspond to different mean-field wave functions $|\Psi_{\text{mean}}^{(\chi_{ij})}\rangle$. After projection they lead to different physical spin wave functions $\Psi_{\text{spin}}^{(\chi_{ij})}(\{\alpha_i\})$. Thus we can regard χ_{ij} as labels for different physical spin states. However, two mean-field *Ansätze* $\tilde{\chi}_{ij}$ and $\tilde{\chi}_{ij}$ related by a gauge transformation

$$\tilde{\chi}_{ij} = e^{i\theta_i} \chi_{ij} e^{-i\theta_j} \quad (106)$$

give rise to the same physical spin state after the projection

$$\Psi_{\text{spin}}^{(\tilde{\chi}_{ij})}(\{\alpha_i\}) = e^{i\Sigma_i \theta_i} \Psi_{\text{spin}}^{(\chi_{ij})}(\{\alpha_i\}). \quad (107)$$

Thus χ_{ij} is not a one-to-one label, but a many-to-one label. This property is important for us in order to understand the unusual dynamical properties of χ_{ij} fluctuations. Using many labels to label the same physical state also makes our theory a gauge theory.

Let us consider how the many-to-one property or the gauge structure of χ_{ij} affects its dynamical properties. If χ_{ij} was a one-to-one label of physical states, then χ_{ij} would be like the condensed boson amplitude $\langle \phi(x,t)\rangle$ in a boson superfluid or the condensed spin moment $\langle S_i(t)\rangle$ in the spin-density-wave state. The fluctuations of χ_{ij} would correspond to a bosonic mode similar to a sound mode or a spin-wave mode.[3] However, χ_{ij} does not behave like local order parameters, such as $\langle \phi(x,t)\rangle$ and $\langle S_i(t)\rangle$, which label physical states without redundancy. χ_{ij} is a many-to-one label as discussed above. The many-to-one label creates an interesting situation when we consider the fluctuations of χ_{ij}—some fluctuations of χ_{ij} do not change the physical state and are unphysical. These fluctuations are called pure gauge fluctuations. The effective theory for χ_{ij} must be gauge invariant; for example, the energy for the *Ansatz* χ_{ij} satisfies

$$E(\chi_{ij}) = E(e^{i\theta_i} \chi_{ij} e^{-i\theta_j}).$$

If we consider phase fluctuations $\chi_{ij} = \bar{\chi}_{ij} e^{ia_{ij}}$, then the energy for fluctuations a_{ij} satisfies

$$E(a_{ij}) = E(a_{ij} + \theta_i - \theta_j).$$

This gauge-invariant property of the energy (or, more precisely, the action) drastically changes the dynamical properties of the fluctuations. It is this property that

---

[3]More precisely, the sound mode and spin-wave mode are so-called scalar bosons. The fluctuations of local order parameters always give rise to scalar bosons.

makes the fluctuations of a_{ij} behave as gauge bosons, which are very different from the sound mode and the spin-wave mode.[4]

If we believe that gauge bosons and fermions do appear as low-energy excitations in the deconfined phase, then a natural question will be what do those excitations look like? The slave-boson construction (105) allows us to construct an explicit physical spin wave function that corresponds to a gauge fluctuation a_{ij},

$$\Psi^{(a_{ij})}_{\text{spin}} = \langle 0_f | \prod_i f_{i\alpha_i} | \Psi^{(\bar\chi_{ij} e^{ia_{ij}})}_{\text{mean}} \rangle .$$

We would like to mention that the gauge fluctuations affect the average

$$P_{123} = \langle \chi_{12}\chi_{23}\chi_{31} \rangle = \langle \bar\chi_{12}\bar\chi_{23}\bar\chi_{31} \rangle e^{i(a_{12}+a_{23}+a_{31})} .$$

Thus the U(1) gauge fluctuations a_{ij}, or more precisely the flux of U(1) gauge fluctuations $a_{12}+a_{23}+a_{31}$, correspond to the fluctuations of the spin chirality $S_1 \cdot (S_2 \times S_3) = (P_{123} - P_{132})/4i$, as pointed out in the last section.

Similarly, the slave-boson construction also allows us to construct a physical spin wave function that corresponds to a pair of fermion excitations. We start with the mean-field ground state with a pair of particle-hole excitations. After the projection (105), we obtain the physical spin wave functions that contain a pair of fermions:

$$\Psi^{\text{ferm}}_{\text{spin}}(i_1,\lambda_1;i_2,\lambda_2) = \langle 0 | \left(\prod_i f_{i\alpha_i} \right) f^\dagger_{i_1\lambda_1} f_{i_2\lambda_2} | \Psi^{(\bar\chi_{ij})}_{\text{mean}} \rangle .$$

We see that the gauge fluctuation a_{ij} and fermion excitation do have a physical "shape" given by the spin wave functions $\Psi^{(a_{ij})}_{\text{spin}}$ and $\Psi^{\text{ferm}}_{\text{spin}}$, although the shape is too complicated to picture.

Certainly, two types of excitations, gauge fluctuations and fermion excitations, interact with each other. The form of the interaction is determined by the fact that fermions carry the unit charge of the U(1) gauge field. The low-energy effective theory is given by Eq. (38) with $\Delta_{ij}=0$ and $b_i=0$.

B. What determines the gauge group?

We have mentioned that collective fluctuations around a slave-boson mean-field ground state are described by a U(1) gauge field. Here we would like to ask why the gauge group is U(1)? The reason is that the fermion Hamiltonian and the mean-field Hamiltonian are invariant under the local U(1) transformation,

$$f_i \to e^{i\theta_i} f_i, \quad \chi_{ij} \to e^{-i\theta_i}\chi_{ij}e^{i\theta_j} .$$

The reason that the fermion Hamiltonian is invariant is that the fermion Hamiltonian is a function of the spin operator S_i and the spin operator $S_i = \frac{1}{2}f^\dagger_i \sigma f_i$ is invariant under the local U(1) transformation. So the gauge group is simply the group formed of all the transformations

___

[4]In the continuum limit, the gauge bosons are vector bosons—bosons described by vector fields.

between $f_{i\uparrow}$ and $f_{i\downarrow}$ that leave the physical spin operator invariant.

C. From U(1) to SU(2)

This deeper understanding of gauge transformation allows us to realize that U(1) is only part of the gauge group. The full gauge group is actually SU(2). To understand this let us introduce

$$\psi_{1i} = f_{i\downarrow}, \quad \psi_{2i} = f^\dagger_{i\downarrow} .$$

We find

$$S^+_i = f^\dagger_i \sigma^+ f_i = \frac{1}{2}(\psi^\dagger_{1i}\psi^\dagger_{2i} - \psi^\dagger_{2i}\psi^\dagger_{1i}) ,$$

$$S^z_i = \frac{1}{2}f^\dagger_i \sigma^z f_i = \frac{1}{2}(\psi^\dagger_{1i}\psi_{1i} + \psi^\dagger_{2i}\psi_{2i} - 1) .$$

Now it is clear that S_i and any Hamiltonian expressed in terms of S_i are invariant under the local SU(2) gauge transformation:

$$\begin{pmatrix} \psi_{1i} \\ \omega_{2i} \end{pmatrix} \to W_i \begin{pmatrix} \psi_{1i} \\ \psi_{2i} \end{pmatrix}, \quad W_i \in \text{SU}(2) .$$

The local SU(2) invariance of the spin Hamiltonian implies that the mean-field Hamiltonian not only should have U(1) gauge invariance, it should also have SU(2) gauge invariance.

To write down the mean-field theory with explicit SU(2) gauge invariance, we start with the mean-field *Ansatz* that includes the pairing correlation:

$$\chi_{ij}\delta_{\alpha\beta} = 2\langle f^\dagger_{i\alpha}f_{j\beta} \rangle, \quad \chi_{ij} = \chi^*_{ji} ,$$

$$\Delta_{ij}\epsilon_{\alpha\beta} = 2\langle f_{i\alpha}f_{j\beta} \rangle, \quad \Delta_{ij} = \Delta_{ji} . \qquad (108)$$

After replacing fermion bilinears with χ_{ij} and Δ_{ij} in Eq. (35), we obtain the following mean-field Hamiltonian with pairing:

$$H_{\text{mean}} = \sum_{\langle ij \rangle} -\frac{3}{8}J_{ij}[(\chi_{ji}f^\dagger_{i\alpha}f_{j\alpha} - \Delta_{ij}f^\dagger_{i\alpha}f^\dagger_{j\beta}\epsilon_{\alpha\beta})$$
$$+ \text{H.c.} - |\chi_{ij}|^2 - |\Delta_{ij}|^2] .$$

However, the above mean-field Hamiltonian is incomplete. We know that the physical Hilbert space is formed by states with one f fermion per site. Such states correspond to states with even numbers of ψ fermion per site. The states with even numbers of ψ fermions per site are SU(2) singlet, one every site. The operators $\psi^\dagger_i \tau \psi_i$ that generate local SU(2) transformations vanish within the physical Hilbert space, where $\tau = (\tau^1, \tau^2, \tau^3)$ are the Pauli matrices. In the mean-field theory, we replace the constraint $\psi^\dagger_i \tau \psi_i = 0$ by its average

$$\langle \psi^\dagger_i \tau \psi_i \rangle = 0 .$$

The averaged constraint can be enforced by including the Lagrange multiplier $\sum_i a^l_0(i)\psi^\dagger_i \tau^l \psi_i$ in the mean-field Hamiltonian. This way we obtain the mean-field Hamil-

tonian of SU(2) slave-boson theory (Affleck *et al.*, 1988; Dagotto *et al.*, 1988):

$$H_{\text{mean}} = \sum_{\langle ij \rangle} -\frac{3}{8} J_{ij} [(\chi_{ji} f_{i\alpha}^\dagger f_{j\alpha} - \Delta_{ij} f_{i\alpha}^\dagger f_{j\beta}^\dagger \epsilon_{\alpha\beta}) + \text{H.c.}$$

$$- |\chi_{ij}|^2 - |\Delta_{ij}|^2] + \sum_i \{a_0^3 (f_{i\alpha}^\dagger f_{i\alpha} - 1)$$

$$+ [(a_0^1 + i a_0^2) f_{i\alpha} f_{i\beta} \epsilon_{\alpha\beta} + \text{H.c.}]\}. \quad (109)$$

So the mean-field *Ansatz* that describes a SU(2) slave-boson mean-field state is really given by χ_{ij}, Δ_{ij}, and a_0. We note that χ_{ij}, Δ_{ij}, and a_0 are invariant under spin rotation. Thus the mean-field ground state of H_{mean} is a spin singlet. Such a state describes a spin-liquid state.

The SU(2) mean-field Hamiltonian (109) is invariant under a local SU(2) gauge transformation. To see such an invariance explicitly, we need to rewrite Eq. (109) in terms of ψ:

$$H_{\text{mean}} = \sum_{\langle ij \rangle} \frac{3}{8} J_{ij} \left[\frac{1}{2} \text{Tr}(U_{ij}^\dagger U_{ij}) + (\psi_i^\dagger U_{ij} \psi_j + \text{H.c.}) \right]$$

$$+ \sum_i a_0^l \psi_i^\dagger \tau^l \psi_i, \quad (110)$$

where

$$U_{ij} = \begin{pmatrix} -\chi_{ij}^* & \Delta_{ij} \\ \Delta_{ij}^* & \chi_{ij} \end{pmatrix} = U_{ji}^\dagger. \quad (111)$$

Note that $\det(U) < 0$, so that U_{jk} is not a member of SU(2), but iU_{jk} is a member up to a normalization constant. From Eq. (110) we now can see that the mean-field Hamiltonian is invariant under a local SU(2) transformation W_i:

$$\psi_i \rightarrow W_i \psi_i,$$

$$U_{ij} \rightarrow W_i U_{ij} W_j^\dagger. \quad (112)$$

We note that in contrast to $\Phi_{i\uparrow}$ and $\Phi_{i\downarrow}$ introduced in Eq. (44), the doublet ψ_i does not carry a spin index. Thus the redundancy in the $\Phi_{i\sigma}$ representation is avoided, which accounts for a factor of 2 difference in front of the bilinear ψ_i term in Eq. (110) versus Eq. (45). However, the spin-rotation symmetry is not explicit in our formalism and it is hard to tell if Eq. (110) describes a spin-rotation-invariant state or not. In fact, for a general U_{ij} satisfying $U_{ij} = U_{ji}^\dagger$, Eq. (110) may not describe a spin-rotation-invariant state. But if U_{ij} has a form

$$U_{ij} = \chi_{ij}^\mu \tau^\mu, \quad \mu = 0, 1, 2, 3,$$

$$\chi_{ij}^0 = \text{imaginary}, \quad \chi_{ij}^l = \text{real}, \quad l = 1, 2, 3, \quad (113)$$

then Eq. (110) will describe a spin-rotation-invariant state. This is because the above U_{ij} has the form of Eq. (111). In this case Eq. (110) can be rewritten as Eq. (109), where the spin-rotation invariance is explicit. In Eq. (113), τ^0 is the identity matrix.

Now the mean-field *Ansatz* can be more compactly represented by $(U_{ij}, a_0(i))$. Again the mean-field *Ansatz*

$(U_{ij}, a_0(i))$ can be viewed as a many-to-one label of physical spin states. The physical spin state labeled by $(U_{ij}, a(i))$ is given by

$$|\Psi_{\text{spin}}^{(U_{ij}, a_0(i))}\rangle = \mathcal{P} |\Psi_{\text{mean}}^{(U_{ij}, a_0(i))}\rangle,$$

where $|\Psi_{\text{mean}}^{(U_{ij}, a_0(i))}\rangle$ is the ground state of the mean-field Hamiltonian (110) and $\mathcal{P}$ is the projection that projects into the subspace with even numbers of ψ fermions per site. From the relation between the f fermion and the ψ fermion, we note that the state with zero ψ fermions corresponds to the spin-down state and the state with two ψ fermions corresponds to the spin-up state. Since the states with even numbers of ψ fermions per site are SU(2) singlet on every site, we find that two mean-field *Ansätze* $(U_{ij}, a_0(i))$ and $(\tilde{U}_{ij}, \tilde{a}(i))$ related by a local SU(2) gauge transformation,

$$\tilde{U}_{ij} = W_i U_{ij} W_j^\dagger, \quad \tilde{a}_0(i) \cdot \tau = W_i a_0(i) \cdot \tau W_i^\dagger,$$

label the same physical spin state

$$\mathcal{P} |\Psi_{\text{mean}}^{(U_{ij}, a_0(i))}\rangle = \mathcal{P} |\Psi_{\text{mean}}^{(\tilde{U}_{ij}, \tilde{a}_0(i))}\rangle,$$

This relation represents the physical meaning of the SU(2) gauge structure.

Just as with U(1) slave-boson theory, the fluctuations of the mean-field *Ansatz* correspond to collective excitations. In particular, the "phase" fluctuations of U_{ij} represent the potential gapless excitations. However, unlike the U(1) slave-boson theory, the phase of U_{ij} is described by a two-by-two Hermitian matrix $a_{ij}^l \tau^l$, $l = 1, 2, 3$, on each link. If $(\bar{U}_{ij}, \bar{a}(i))$ is the *Ansatz* that describes the mean-field ground state, then the potential gapless fluctuations are described by

$$U_{ij} = \bar{U}_{ij} e^{i a_{ij}^l \tau^l}, \quad a_0(i) = \bar{a}_0(i) + \delta a_0(i).$$

Since $(U_{ij}, a_0(i))$ is a many-to-one labeling, the fluctuations $(a_{ij}, \delta a_0(i))$ correspond to SU(2) gauge fluctuations rather than usual bosonic collective modes such as phonon modes and spin waves.

D. A few mean-field *Ansätze* for symmetric spin liquids

After a general discussion of the SU(2) slave-boson theory, let us discuss a few mean-field *Ansätze* that have spin rotation, translation $T_{x,y}$, and parity $P_{x,y,xy}$ symmetries. We call such a spin state a symmetric spin liquid. Here T_x and T_y are translations in the x and y directions, and P_x, P_y, and P_{xy} are parity transformations $(x, y) \rightarrow (-x, y)$, $(x, y) \rightarrow (x, -y)$, and $(x, y) \rightarrow (y, x)$, respectively. We note that $P_{x,y,xy}$ parity symmetries imply 90° rotational symmetry.

We concentrate on three simple mean-field *Ansätze* that describe symmetric spin liquids:

(i) π-flux liquid (πfL) state[5] (Affleck and Marston, 1988),

---

[5] This state was called the π-flux (πF) state in the literature.

$$U_{i,i+x} = -i(-)^{i_y}\chi, \quad U_{i,i+y} = -i\chi; \tag{114}$$

(ii) staggered flux liquid (sfL) state[6] (Affleck and Marston, 1988),

$$U_{i,i+x} = -\tau^3\chi - i(-)^i\Delta,$$

$$U_{i,i+y} = -\tau^3\chi + i(-)^i\Delta; \tag{115}$$

(iii) Z_2-gapped state (Wen, 1991),

$$U_{i,i+x} = U_{i,i+y} = -\chi\tau^3, \quad U_{i,i+x+y} = \eta\tau^1 + \lambda\tau^2,$$

$$U_{i,i-x+y} = \eta\tau^1 - \lambda\tau^2, \quad a_0^{2,3} = 0, \quad a_0^1 \neq 0, \tag{116}$$

where $(-)^i \equiv (-)^{i_x+i_y}$. Note that the Z_2 mean-field state has pairing along the diagonal bond.

At first sight, those mean-field *Ansätze* appear not to have all the symmetries. For example, the Z_2-gapped *Ansätze* are not invariant under the P_x and P_y parity transformations and the πfL and sfL *Ansätze* are not invariant under translation in the y direction. However, those *Ansätze* do describe spin states that have all the symmetries. This is because the mean-field *Ansätze* are many-to-one labels of the physical spin state; the noninvariance of the *Ansatz* does not imply the noninvariance of the corresponding physical spin state after the projection. We only require the mean-field *Ansatz* to be invariant up to a SU(2) gauge transformation in order for the projected physical spin state to have a symmetry. For example, a P_{xy} parity transformation changes the sfL *Ansatz* to

$$U_{i,i+x} = -\tau^3\chi + i(-)^i\Delta,$$

$$U_{i,i+y} = -\tau^3\chi - i(-)^i\Delta.$$

The reflected *Ansatz* can be transformed into the original *Ansatz* via a SU(2) gauge transformation $W_i = (-)^i i\tau^1$. Therefore, after the projection the sfL *Ansatz* describes a P_{xy} parity symmetric spin state. Using a similar approach one can show that the above three *Ansätze* are invariant under translation $T_{x,y}$ and parity $P_{x,y,xy}$ symmetry transformations followed by corresponding SU(2) gauge transformations G_{T_x,T_y} and $G_{P_x,P_y,P_{xy}}$, respectively. Thus the three *Ansätze* all describe symmetric spin liquids. In the following, we list the corresponding gauge transformations G_{T_x,T_y} and $G_{P_x,P_y,P_{xy}}$ for the above three *Ansätze*:

(i) πfL state,

$$G_{T_x}(i) = (-)^{i_x}G_{T_y}(i) = \tau^0, \quad G_{P_{xy}}(i) = (-)^{i_x i_y}\tau^0,$$

$$(-)^{i_x}G_{P_x}(i) = (-)^{i_y}G_{P_y}(i) = \tau^0, \quad G_0(i) = e^{i\theta_i\tau^l}; \tag{117}$$

[6]Wen and Lee (1996) and Lee *et al.* (1998) called this phase the staggered flux (sF) state. In this paper we reserve sF to denote the U(1) mean-field state which explicitly breaks translational symmetry and which exhibits staggered orbital currents, as originally described by Hsu *et al.* (1991). This latter state is also called *d*-density wave, following Chakravarty, Laughlin, *et al.* (2002).

(ii) sfL state,

$$G_{T_x}(i) = G_{T_y}(i) = i(-)^i\tau^1, \quad G_{P_{xy}}(i) = i(-)^i\tau^1,$$

$$G_{P_x}(i) = G_{P_y}(i) = \tau^0, \quad G_0(i) = e^{i\theta\tau^3}; \tag{118}$$

(iii) Z_2-gapped state,

$$G_{T_x}(i) = G_{T_y}(i) = i\tau^0, \quad G_{P_{xy}}(i) = \tau^0,$$

$$G_{P_x}(i) = G_{P_y}(i) = (-)^i\tau^1, \quad G_0(i) = -\tau^0. \tag{119}$$

In the above we also list the pure gauge transformation $G_0(i)$ that leave the *Ansätze* invariant.

E. Physical properties of the symmetric spin liquids at mean-field level

To understand the physical properties of the above three symmetric spin liquids, let us first ignore the mean-field fluctuations of U_{ij} and consider the excitations at mean-field level.

At mean-field level, the excitations are spin-1/2 fermions ψ (or f). Their spectrum is determined by the mean-field Hamiltonian (110) [or Eq. (109)]. In the πfL state, the fermions have a dispersion

$$E_k = \pm\frac{3}{4}J|\chi|\sqrt{\sin^2 k_x + \sin^2 k_y}.$$

In the sfL state, the dispersion is given by

$$E_k = \pm\frac{3}{4}J\sqrt{\chi^2(\cos k_x + \cos k_y)^2 + \Delta^2(\cos k_x - \cos k_y)^2}. \tag{120}$$

In the Z_2-gapped state, we have

$$E_k = \pm\sqrt{\epsilon_k^2 + \Delta_{1k}^2 + \Delta_{2k}^2}, \quad \epsilon_k = -\frac{3}{4}J\chi(\cos k_x + \cos k_y),$$

$$\Delta_{1k} = \frac{3}{4}\eta J'\cos(k_x + k_y) + a_0^1, \Delta_{2k} = \frac{3}{4}\lambda J'\cos(-k_x + k_y),$$

where J is the nearest-neighbor spin coupling and J' is the next-nearest-neighbor spin coupling. We find that the πfL and sfL states, at mean-field level, have gapless spin-1/2 fermion excitations, while the Z_2-gapped state has gapped spin-1/2 fermion excitations.

Should we trust the mean-field results from slave-boson theory? The answer is that it depends on the importance of the gauge fluctuations. Unlike usual mean-field theory, the fluctuations in slave-boson theory include gauge fluctuations which can generate confining interactions between the fermions. In this case the gauge interactions represent relevant perturbations and the mean-field state is said to be unstable. The mean-field results from an unstable mean-field *Ansatz* cannot be trusted and cannot be applied to a real physical spin state. In particular, spin-1/2 fermionic excitations in mean-field theory in this case will not appear in the physical spectrum of a real spin state.

If the dynamics of the gauge fluctuations is such that the gauge interaction is short ranged, then the gauge interactions represent irrelevant perturbations and can be ignored. In this case the mean-field state is said to be stable and the mean-field results can be applied to real physical spin liquids. In particular, the corresponding physical spin state contains fractionalized spin-1/2 fermionic excitations.

F. Classical dynamics of the SU(2) gauge fluctuations

We have seen that the key to understanding the physical properties of a spin liquid described by a mean-field *Ansatz* (U_{ij}, a_0^l) is to understand the dynamics of the SU(2) gauge fluctuations. To gain some intuitive understanding, let us treat the mean-field *Ansätze* $(U_{ij}, a_0(i))$ as classical fields and study the classical dynamics of their fluctuations. The dynamics of the fluctuations is determined by the effective Lagrangian $L_{\mathrm{eff}}(U_{ij}(t), a_0(i,t))$. To obtain the effective Lagrangian, we start with the Lagrangian representation of the mean-field Hamiltonian

$$L(\psi_i, U_{ij}, a_0) = \sum_i i\psi_i^\dagger \partial_t \psi_i - H_{\mathrm{mean}},$$

where H_{mean} is given in Eq. (110). The effective Lagrangian L_{eff} is then obtained by integrating out ψ:

$$e^{i\int dt L_{\mathrm{eff}}(U_{ij}, a_0)} = \int \mathcal{D}\psi \mathcal{D}\psi^\dagger e^{i\int dt L(\psi, U_{ij}, a_0)}.$$

We note that L describes a system of fermions ψ_i and SU(2) gauge fluctuations U_{ij}. Thus the effective Lagrangian is invariant under the SU(2) gauge transformation:

$$L_{\mathrm{eff}}(\tilde{U}_{ij}, \tilde{a}_0) = L_{\mathrm{eff}}(U_{ij}, a_0), \quad \tilde{U}_{ij} = W_i(U_{ij})W_j^\dagger,$$

$$\tilde{a}_0^l(i)\tau^l = W_i a_0^l(i)\tau^l W_i^\dagger, \quad W_i \in \mathrm{SU}(2). \tag{121}$$

The classical equation of motion obtained from $L_{\mathrm{eff}}(U_{ij}, a_0)$ determines the classical dynamics of the fluctuations.

To see if the collective fluctuations are gapless, we would like to determine if the frequencies of the collective fluctuations are bound from below. We know that the time-independent saddle point of $L_{\mathrm{eff}}(U_{ij}, a_0)$, $(\bar{U}_{ij}, \bar{a}_0)$, corresponds to a mean-field ground-state *Ansatz*, and $-L_{\mathrm{eff}}(\bar{U}_{ij}, \bar{a}_0)$ is the mean-field ground-state energy. If we expand $-L_{\mathrm{eff}}(\bar{U}_{ij}e^{ia_{ij}^l\tau^l}, \bar{a}_0)$ to second order in the fluctuation a_{ij}, then the presence or the absence of the mass term a_{ij}^2 will determine if the collective SU(2) gauge fluctuations have an energy gap or not.

To understand how the mean-field *Ansätze* $\bar{U}_{ij}$ affect the dynamics of the gauge fluctuations, it is convenient to introduce the loop variable of the mean-field solution,

$$P(C_i) = (i\bar{U}_{ij})(i\bar{U}_{jk})\cdots(i\bar{U}_{ki}). \tag{122}$$

Following the comment after Eq. (111), $P(C_i)$ belongs to the SU(2) group and we can write $P(C_i)$ as $P(C_i) = e^{i\Phi(C_i)}$, where Φ is the SU(2) flux through the loop C_i: $i \to j \to k \to \cdots \to l \to i$, with base point i. The SU(2) flux corresponds to the gauge-field strength in the continuum limit. Compared with the U(1) flux, the SU(2) flux has two new features. First, the flux Φ is a two-by-two traceless Hermitian matrix. If we expand Φ as $\Phi = \Phi^l\tau^l$, $l = 1, 2, 3$, we can say that the flux is represented by a vector Φ^l in the τ^l space. Second, the flux is not gauge invariant. Under the gauge transformations, $\Phi(C_i)$ transforms as

$$\Phi(C_i) \to W_i\Phi(C_i)W_i. \tag{123}$$

Such a transformation rotates the direction of the vector Φ^l. Since the direction of the SU(2) flux for loops with different base points can be rotated independently by the local SU(2) gauge transformations, it is meaningless to directly compare the directions of SU(2) flux for different base points. However, it is quite meaningful to compare the directions of SU(2) flux for loops with the same base point. We can divide different SU(2) flux configurations into three classes based on the SU(2) flux through loops with the same base point: (a) trivial SU(2) flux where all $P(C) \propto \tau^0$, (b) collinear SU(2) flux where all the SU(2) fluxes point in the same direction, and (c) noncollinear SU(2) flux where the SU(2) flux for loops with the same base point are in different directions. We show below that different SU(2) fluxes can lead to different dynamics for the gauge field (Wen, 1991; Mudry and Fradkin, 1994).

1. Trivial SU(2) flux

First let us consider an *Ansatz* $\bar{U}_{ij}$ with trivial SU(2) flux $\Phi(C) = 0$ for all the loops [such as the πfL *Ansatz* in Eq. (114)]. We shall call the state described by such an *Ansatz* the SU(2) state. We perform a SU(2) gauge transformation to transform the *Ansatz* into a form where all $\bar{U}_{ij} \propto \tau^0$. In this case, the gauge invariance of the effective Lagrangian implies that

$$L_{\mathrm{eff}}(\bar{U}_{ij}e^{ia_{ij}^l\tau^l}) = L_{\mathrm{eff}}(\bar{U}_{ij}e^{i\theta_i^l\tau^l}e^{ia_{ij}^l\tau^l}e^{-i\theta_j^l\tau^l}). \tag{124}$$

Under gauge transformation $e^{i\theta_i^1\tau^1}$, a_{ij}^1 transforms as $a_{ij}^1 \to a_{ij}^1 + \theta_i^1 - \theta_j^1$. The mass term $(a_{ij}^1)^2$ is not invariant under such a transformation and is thus not allowed. Similarly, we can show that none of the mass terms $(a_{ij}^1)^2$, $(a_{ij}^2)^2$, and $(a_{ij}^3)^2$ are allowed in the expansion of L_{eff}. Thus the SU(2) gauge fluctuations are gapless and appear at low energies.

We note that all the pure gauge transformations $G_0(i)$ that leave the *Ansatz* invariant form a group. We call this an invariant gauge group. For the *Ansatz* $\bar{U}_{ij} \propto \tau^0$, the invariant gauge group is a SU(2) group formed by a uniform SU(2) gauge transformation $G_0(i) = e^{i\theta^l\tau^l}$. We recall from the last paragraph that the (classical) gapless

gauge fluctuations are also SU(2). Such a relation between the invariant gauge group and the gauge group of the gapless classical gauge fluctuations is general and applies to all the *Ansätze* (Wen, 2000b).

To understand the dynamics of the gapless gauge fluctuations beyond the classical level, we need to treat two cases separately. In the first case, fermions have a finite energy gap. Those fermions will generate the following low-energy effective Lagrangian for the gauge fluctuations,

$$\mathcal{L} = \frac{g}{8\pi}\mathrm{Tr}f_{\mu\nu}f^{\mu\nu},$$

where $f_{\mu\nu}$ is a 2×2 matrix representing the field strength of the SU(2) gauge field a_{ij} in the continuum limit. At the classical level, such an effective Lagrangian leads to an $\sim g\ln(r)$ interaction between SU(2) charges in two spatial dimensions. So the gauge interaction at the classical level is not confining (i.e., not described by a linear potential). However, if we go beyond the classical level (i.e., beyond the quadratic approximation) and include the interactions between gauge fluctuations, the picture is completely changed. In $(1+2)$D, the interactions between gauge fluctuations change the $g\ln(r)$ interaction to a linear confining interaction, regardless of the value of the coupling constant g. So the SU(2) mean-field states with gapped fermions are not stable. The mean-field results from such *Ansätze* cannot be trusted.

In the second case, the fermions are gapless and have a linear dispersion. In the continuum limit, those fermions correspond to massless Dirac fermions. Those fermions will generate a nonlocal low-energy effective Lagrangian for the gauge fluctuations, which is roughly $\mathcal{L} = (g/8\pi)\mathrm{Tr}\, f_{\mu\nu}(1/\sqrt{-\partial^2})f^{\mu\nu}$. Due to the screening of massless fermions, the interaction potential between SU(2) charges becomes $\sim g/r$ at the classical level. Such an interaction represents a marginal perturbation. It is a quite complicated matter to determine if the SU(2) states with gapless Dirac fermions are stable or not beyond the quadratic approximation.

2. Collinear SU(2) flux

Second, let us assume the SU(2) flux is collinear. This means the SU(2) fluxes for different loops with the same base point all point in the same direction. However, the SU(2) fluxes for loops with different base points may still point in different directions [even for the collinear SU(2) flux]. Using the local SU(2) gauge transformation we can rotate the SU(2) flux for different base points in the same direction, and pick this direction to be the τ^3 direction. In this case the SU(2) fluxes have the form $P(C) \propto \chi^0(C) + i\chi^3(C)\tau^3$. We can choose a gauge such that the mean-field *Ansätze* have the form $\bar{U}_{ij} = ie^{i\phi_{ij}\tau^3}$. The gauge invariance of the energy implies that

$$L_{\mathrm{eff}}(\bar{U}_{ij}e^{ia^l_{ij}\tau^l}) = L_{\mathrm{eff}}(\bar{U}_{ij}e^{i\theta_i\tau^3}e^{ia^l_{ij}\tau^l}e^{-i\theta_j\tau^3}). \quad (125)$$

When $a^{1,2}_{ij} = 0$, the above reduces to

$$L_{\mathrm{eff}}(\bar{U}_{ij}e^{ia^3_{ij}\tau^3}) = L_{\mathrm{eff}}(\bar{U}_{ij}e^{i(a^3_{ij}+\theta_i-\theta_j)\tau^3}). \quad (126)$$

We find that the mass term $(a^3_{ij})^2$ is incompatible with Eq. (126). Therefore at least the gauge field a^3_{ij} is gapless. How about the a^1_{ij} and a^2_{ij} gauge fields? Let $P_A(i)$ be the SU(2) flux through a loop with base point i. If we assume the gauge-invariant terms that can appear in the effective Lagrangian do appear, then $L_{\mathrm{eff}}(U_{ij})$ will contain the following term:

$$L_{\mathrm{eff}} = a\mathrm{Tr}[P_A(i)iU_{i,i+x}P_A(i+x)iU_{i+x,i}] + \cdots. \quad (127)$$

If we write $iU_{i,i+x}$ as $\chi e^{i\phi_{ij}\tau^3}e^{ia^l_x\tau^l}$, using the fact $U_{i,i+x} = U^\dagger_{i+x,i}$ [see Eq. (111)] and expand to $(a^l_x)^2$ order, Eq. (127) becomes

$$L_{\mathrm{eff}} = -\frac{1}{2}a\chi^2\mathrm{Tr}([P_A, a^l_x\tau^l]^2) + \cdots. \quad (128)$$

We see from Eq. (128) that the mass terms for a^1_{ij} and a^2_{ij} are generated if $P_A \propto \tau^3$.

To summarize, we find that if the SU(2) flux is collinear, then the *Ansatz* is invariant only under a U(1) rotation $e^{i\theta n\cdot\tau}$, where n is the direction of the SU(2) flux. Thus the invariant gauge group is U(1). The collinear SU(2) flux also breaks the SU(2) gauge structure down to a U(1) gauge structure, i.e., the low-lying gauge fluctuations are described by a U(1) gauge field. Again we see that the invariant gauge group of the *Ansatz* is the gauge group of the (classical) gapless gauge fluctuations. We call the states with collinear SU(2) flux the U(1) states. The sfL *Ansatz* in Eq. (115) is an example of collinear SU(2) flux.

For the U(1) states with gapped fermions, fermions will generate the following effective Lagrangian for the gauge fluctuations:

$$\mathcal{L} = \frac{g}{8\pi}(e^2 - b^2),$$

where e is the "electric" field and b is the "magnetic" field of the U(1) gauge field. Again at the classical level the effective Lagrangian leads to an $\sim g\ln(r)$ interaction between U(1) charges and the gauge interaction at the classical level is not confining. If we go beyond the classical level and include interactions between gauge fluctuations induced by the space-time monopoles, the $g\ln(r)$ interaction will be changed to a linear confining interaction, regardless of the value of the coupling constant g (Polyakov, 1977). So the U(1) mean-field states with gapped fermions are not stable.

If the fermions in the U(1) state are gapless and are described by massless Dirac fermions (such as those in the sfL state), those fermions will generate a nonlocal low-energy effective Lagrangian, which at the quadratic level has the form

$$\mathcal{L} = \frac{g}{8\pi}f_{\mu\nu}\frac{1}{\sqrt{-\partial^2}}f^{\mu\nu}. \quad (129)$$

Again the screening of massless fermions changes the $g\ln(r)$ interaction to g/r interactions between U(1)

charges, at least at the classical level. Such an interaction represents a marginal perturbation. Beyond the classical level, we show in Secs. XI.D and XI.F that when there are many Dirac fermions the U(1) gauge interactions with Dirac fermions are exact marginal perturbations. So the U(1) states with enough gapless Dirac fermions are not unstable. Mean-field theory can give us a good starting point for studying the properties of the corresponding physical spin state (see Sec. XI.D).

3. Noncollinear SU(2) flux

Third, we consider the situation where the SU(2) flux is noncollinear. In the above, we have shown that a SU(2) flux P_A can induce a mass term of the form $\text{Tr}([P_A, a_x^l \tau^l]^2)$. For a noncollinear SU(2) flux configuration, we can have in Eq. (127) another SU(2) flux, P_B, pointing in a different direction from P_A. The mass term will contain, in addition to Eq. (128), a term $\text{Tr}([P_B, a_x^l \tau^l]^2)$. In this case, the mass terms for the SU(2) gauge fields $(a_{ij}^1)^2$, $(a_{ij}^2)^2$, and $(a_{ij}^3)^2$ will be generated. All SU(2) gauge bosons will gain an energy gap.

We note that *Ansatz* U_{ij} is always invariant under the global Z_2 gauge transformation $-\tau^0$. So the invariant gauge group always contains a Z_2 subgroup and the Z_2 gauge structure is unbroken at low energies. The global Z_2 gauge transformation is the only invariance for the noncollinear *Ansatz*. Thus the invariant gauge group is Z_2 and the low-energy effective theory is a Z_2 gauge theory. We can show that the low-energy properties of noncollinear states, such as the existence of a Z_2 vortex and ground-state degeneracy, are indeed identical to those of a Z_2 gauge theory. So we call the state with noncollinear SU(2) flux a Z_2 state.

In a Z_2 state, all the gauge fluctuations are gapped. Those fluctuations can only mediate short-range interactions between fermions. Low-energy fermions interact weakly and behave like free fermions. Therefore including mean-field fluctuations does not qualitatively change the properties of the mean-field state. The gauge interactions are irrelevant and the Z_2 mean-field state is stable at low energies.

A stable mean-field spin-liquid state implies the existence of a real physical spin liquid. The physical properties of the stable mean-field state apply to the physical spin liquid. If we believe these two statements, then we can study the properties of a physical spin liquid by studying its corresponding stable mean-field state. Since fermions are not confined in mean-field Z_2 states, the physical spin liquid derived from this state contains neutral spin-1/2 fermions as its excitation.

The Z_2-gapped *Ansatz* in Eq. (116) is an example in which the SU(2) flux is noncollinear. To see this, let us consider the SU(2) flux through two triangular loops $(i, i+y, i-x)$ and $(i, i+x, i+y)$ with the same base point i:

$$U_{i,i+y}U_{i+y,i-x}U_{i-x,i} = -\chi^2(\eta\tau^1 + \lambda\tau^2),$$

$$U_{i,i+x}U_{i+x,i+y}U_{i+y,i} = -\chi^2(\eta\tau^1 - \lambda\tau^2).$$

We see that when η and λ are nonzero, the SU(2) flux is not collinear. Therefore, after projection, the Z_2-gapped *Ansatz* gives rise to a real physical spin liquid, which contains fractionalized spin-1/2 neutral fermionic excitations (Wen, 1991). The spin liquid also contains a Z_2 vortex excitation. The bound state of a spin-1/2 fermionic excitation and a Z_2 vortex gives us a spin-1/2 bosonic excitation (Read and Chakraborty, 1989; Wen, 1991).

G. The relation between different versions of slave-boson theory

We have discussed two versions of slave-boson theory, the U(1) slave-boson theory and the SU(2) slave-boson theory. Senthil and Fisher (2000) proposed a third slave-boson theory—the Z_2 slave-boson theory. Here we point out that all three versions are equivalent descriptions of the same spin-1/2 Heisenberg model on a square lattice, if we treat the SU(2), U(1), or Z_2 gauge fluctuations exactly.

To understand the relation between the three versions, we point out that the SU(2), U(1), or Z_2 gauge structures were introduced in order to project the fermion Hilbert space (which has four states per site) to the smaller spin-1/2 Hilbert space (which has two states per site). In SU(2) slave-boson theory, we regard two fermions ψ_{1i} and ψ_{2i} as a SU(2) doublet. Among the four fermion states on each site, $|0\rangle$, $\psi_{1i}^\dagger|0\rangle$, $\psi_{2i}^\dagger|0\rangle$, and $\psi_{1i}^\dagger\psi_{2i}^\dagger|0\rangle$, only the SU(2)-invariant state corresponds to the physical spin state. There are only two SU(2)-invariant states on each site: $|0\rangle$ and $\psi_{1i}^\dagger\psi_{2i}^\dagger|0\rangle$, which correspond to the spin-up and spin-down states. So the spin-1/2 Hilbert space is obtained from the fermion Hilbert space by projecting onto the local SU(2) singlet subspace.

In U(1) slave-boson theory, we regard ψ_{1i} as a charge $+1$ fermion and ψ_{2i} as a charge -1 fermion. The spin-1/2 Hilbert space is obtained from the fermion Hilbert space by projecting onto the local charge-neutral subspace. Among the four fermion states on each site, only two states $|0\rangle$ and $\psi_{1i}^\dagger\psi_{2i}^\dagger|0\rangle$ are charge neutral.

In Z_2 slave-boson theory, we regard ψ_{ai} as a fermion that carries a unit Z_2 charge. The spin-1/2 Hilbert space is obtained from the fermion Hilbert space by projecting onto the local Z_2-charge-neutral subspace. Again the two states $|0\rangle$ and $\psi_{1i}^\dagger\psi_{2i}^\dagger|0\rangle$ are the only Z_2-charge-neutral states.

In the last subsection we discussed Z_2, U(1), and SU(2) spin-liquid states. These must not be confused with Z_2, U(1), and SU(2) slave-boson theories. We stress that Z_2, U(1), and SU(2) in the Z_2, U(1), and SU(2) spin-liquid states are gauge groups that appear in low-energy effective theories of those spin liquids. We call those gauge groups low-energy gauge groups. They should not be confused with the Z_2, U(1), and SU(2) gauge groups in the Z_2, U(1), and SU(2) slave-boson theories. We call

the latter high-energy gauge groups. The high-energy gauge groups have nothing to do with the low-energy gauge groups. A high-energy Z_2 gauge theory (or a Z_2 slave-boson approach) can have a low-energy effective theory that contains SU(2), U(1), or Z_2 gauge fluctuations. Even the Heisenberg model, which has no gauge structure at lattice scale, can have a low-energy effective theory that contains SU(2), U(1), or Z_2 gauge fluctuations. The spin liquids studied in this paper all contain some kind of low-energy gauge fluctuations. Despite their different low-energy gauge groups, all those spin liquids can be constructed from any one of the SU(2), U(1), or Z_2 slave-boson approaches. After all, all those approaches describe the same Heisenberg model and are equivalent.

The high-energy gauge group is related to the way in which we write down the Hamiltonian. We can write the Hamiltonian of the Heisenberg model in many different ways which can contain an arbitrary high-energy gauge group of our choice. We just need to split the spin into two, four, six, or some other even number of fermions. While the low-energy gauge group is a property of the ground state of the spin model, it has nothing to do with how we are going to write down the Hamiltonian. Thus we should not regard Z_2 spin liquids as the spin liquids constructed using the Z_2 slave-boson approach. A Z_2 spin liquid can be constructed and was first constructed within the U(1) or SU(2) slave-boson and slave-fermion approaches. However, when we study a particular spin-liquid state, a certain version of the slave-boson theory may be more convenient than other versions. Although a spin liquid can be described by slave-boson theory, sometimes a particular version of the theory may have the weakest fluctuations.

H. The emergence of gauge bosons and fermions in condensed-matter systems

In the early days, it was believed that a pure boson system can never generate gauge bosons and fermions. Rather, gauge bosons and fermions were regarded as fundamental. The spin liquids discussed in this paper suggest that gauge bosons (or gauge structures) and fermions are not fundamental and can emerge from a local bosonic model. Here we discuss how those ideas were developed historically.

Let us first consider gauge bosons. In the standard picture of gauge theory, the gauge potential a_μ is viewed as a geometrical object—a connection of a fiber bundle. However, there is another point of view on gauge theory. Many thinkers in theoretical physics were not happy with the redundancy of the gauge potential a_μ. It was realized in the early 1970s that one can use gauge-invariant loop operators to characterize different phases of gauge theory (Wegner, 1971; Wilson, 1974; Kogut and Susskind, 1975). It was later found that one can formulate the entire gauge theory using closed strings (Banks *et al.*, 1977; Foerster, 1979; Gliozzi *et al.*, 1979; Mandelstam, 1979; Polyakov, 1979; Savit, 1980). Those studies revealed the intimate relation between gauge theories

and closed-string theories—a point of view very different from the geometrical notion of vector potential.

In a related development, it was found that gauge fields can emerge from a local bosonic model if the model is in certain quantum phases. This phenomenon is also called the dynamical generation of gauge fields. The emergence of gauge fields from local bosonic models has a long and complicated history. The emergent U(1) gauge field was introduced in the quantum disordered phase of the (1+1)D CP^N model (D'Adda *et al.*, 1978; Witten, 1979). In condensed-matter physics, the U(1) gauge field has been found in the slave-boson approach to spin-liquid states (Affleck and Marston, 1988; Baskaran and Anderson, 1988). The slave-boson approach not only has a U(1) gauge field, it also has gapless fermion fields.

It is well known that the compact U(1) gauge theory is confining in (1+1)D and (1+2)D (Polyakov, 1975). The concern about confinement led to an opinion that the U(1) gauge field and gapless fermion fields are just unphysical artifacts of the "unreliable" slave-boson approach. Thus the key to finding emergent gauge bosons and emergent fermions is not to write down a Lagrangian that contains gauge fields and Fermi fields, but to show that gauge bosons and fermions actually appear in the physical low-energy spectrum. However, only when the dynamics is such that the gauge field is in the deconfined phase can the gauge boson appear as a low-energy quasiparticle. Thus after the initial finding of D'Adda *et al.* (1978), Witten (1979), Affleck and Marston (1988), and Baskaran and Anderson (1988), many researchers have been trying to find the deconfined phase of the gauge field.

One way to obtain a deconfined phase is to give the gauge boson a mass. In 1988 it was shown that if we break the time-reversal symmetry in a 2D spin-1/2 model, then the U(1) gauge field from the slave-boson approach can be in a deconfined phase due to the appearance of a Chern-Simons term (Khveshchenko and Wiegmann, 1989; Wen *et al.*, 1989). The deconfined phase corresponds to a spin-liquid state of the spin-1/2 model (Kalmeyer and Laughlin, 1987), which is called a chiral spin liquid. The chiral spin state contains neutral spin-1/2 excitations that carry fractional statistics. A second deconfined phase was found by breaking the U(1) or SU(2) gauge structure down to a Z_2 gauge structure. Such a phase contains a deconfined Z_2 gauge theory (Read and Sachdev, 1991; Wen, 1991; Mudry and Fradkin, 1994) and is called a Z_2 spin liquid (or a short-ranged RVB state).[7] The Z_2 spin state also contains neutral spin-1/2 excitations. But now the spin-1/2 excitations are fermions and bosons.

The above Z_2 spin liquids have a finite energy gap for their neutral spin-1/2 excitations. Balents *et al.* (1998) constructed a spin liquid with gapless spin-1/2 excita-

----

[7]The Z_2 state obtained in Read and Sachdev (1991) breaks the 90° lattice rotational symmetry while the Z_2 state in Wen (1991) has all the lattice symmetries.

tions by studying a quantum disordered d-wave super-conductor. Such a spin liquid was identified as a Z_2 spin liquid using Z_2 slave-boson theory (Senthil and Fisher, 2000). The mean-field *Ansatz* is given by

$$U_{i,i+x} = \chi\tau^3 + \eta\tau^1, \quad U_{i,i+y} = \chi\tau^3 - \eta\tau^1,$$

$$a_0^3 \neq 0, \quad a_0^{1,2} = 0, \quad U_{i,i+x+y} = U_{i,i+x-y} = \gamma\tau^3. \quad (130)$$

The diagonal hopping breaks particle-hole symmetry and breaks the U(1) symmetry of the $a_0^3=0$ d-wave pairing *Ansatz* down to Z_2. We call such an *Ansatz* a Z_2-gapless *Ansatz*. The *Ansatz* describes a symmetric spin liquid since it is invariant under the combined transformations $(G_{T_x}T_x, G_{T_y}T_y, G_{P_x}P_x, G_{P_y}P_y, G_{P_{xy}}P_{xy}, G_0)$ with

$$G_{T_x} = \tau^0, \quad G_{T_y} = \tau^0, \quad G_0 = -\tau^0,$$

$$G_{P_x} = \tau^0, \quad G_{P_y} = \tau^0, \quad G_{P_{xy}} = i\tau^3. \quad (131)$$

The fermion excitations are gapless only at four k points with a linear dispersion.

The Z_2-gapped state and the Z_2-gapless state are just two Z_2 states among over 100 Z_2 states that can be constructed within the SU(2) slave-boson theory (Wen, 2002b). The chiral spin liquid and the Z_2 spin liquids provide examples of emergent gauge structure and emergent fermions (or anyons). However, those results were obtained using slave-boson theory, which is not very convincing to many people.

In 1997, an exact soluble spin-1/2 model (Kitaev, 2003),

$$H_{\text{exact}} = 16g\sum_i S_i^y S_{i+\hat{x}}^x S_{i+\hat{x}+\hat{y}}^y S_{i+\hat{y}}^x,$$

was found. The SU(2) slave-boson theory turns out to be exact for such a model (Wen, 2003c). That is, by choosing a proper SU(2) mean-field *Ansatz* the corresponding mean-field state gives rise to an exact eigenstate of H_{exact} after the projection. In fact all the eigenstates of H_{exact} can be obtained this way by choosing a different mean-field *Ansatz*. The exact solution allows us to show the excitations of H_{exact} to be fermions and Z_2 vortices. This confirms the results obtained from the slave-boson theory.

More exactly soluble or quasiexactly soluble models were found for the dimer model (Moessner and Sondhi, 2001), the spin-1/2 model on a Kagomé lattice (Balents *et al.*, 2002), the boson model on a square lattice (Senthil and Motrunich, 2002), and the Josephson-junction array (Ioffe *et al.*, 2002). A model of electrons coupled to pairing fluctuations, with a local constraint which results in a Mott insulator that obeys the spin SU(2) symmetry, was also constructed (Motrunich and Senthil, 2002). Those models realize the Z_2 states. A boson model that realizes Z_3 gauge structure (Motrunich, 2003) and U(1) gauge structure (Senthil and Motrunich 2002; Wen, 2003a) were also found. Fifteen years after the slave-boson approach to spin liquids, it is now easy to construct (quasi)exactly soluble spin or boson models that have emergent gauge bosons and fermions.

We point out that spin liquids are not the first examples of emergent fermions from local bosonic models. The first example of emergent fermions, or more generally emergent anyons, is given by the fractional quantum Hall states. Although Arovas *et al.* (1984) only discussed how anyons can emerge from a fermion system in a magnetic field, the same argument can be easily generalized to show how fermions and anyons can emerge from a boson system in a magnetic field. Also in 1987, in a study of resonating-valence-bond (RVB) states, emergent fermions (the spinons) were proposed in a nearest-neighbor dimer model on a square lattice (Kivelson *et al.*, 1987; Rokhsar and Kivelson, 1988; Read and Chakraborty, 1989). But according to the deconfinement picture, the results in Kivelson *et al.* (1987) and Rokhsar and Kivelson (1988) are valid only when the ground state of the dimer model is in the Z_2 deconfined phase. It appears that the dimer liquid on a square lattice with only nearest-neighbor dimers is not a deconfined state (Rokhsar and Kivelson, 1988; Read and Chakraborty, 1989), and thus it is not clear if the nearest-neighbor dimer model on a square lattice (Rokhsar and Kivelson, 1988) has the deconfined quasiparticles or not (Read and Chakraborty, 1989). However, on a triangular lattice the dimer liquid is indeed a Z_2 deconfined state (Moessner and Sondhi, 2001). Therefore the results of Kivelson *et al.* (1987) and Rokhsar and Kivelson (1988) are valid for the triangular-lattice dimer model and deconfined quasiparticles do emerge in a dimer liquid on a triangular lattice.

The above models with emergent fermions are 2D models in which emergent fermions can be understood from binding flux to a charged particle (Arovas *et al.*, 1984). Recently, it was pointed out by Levin and Wen (2003) that the key to emergent fermions is a string structure. Fermions can generally appear as ends of open strings in any dimension if the ground state has a condensation of closed strings. The string picture allows a construction of a 3D local bosonic model that has emergent fermions (Levin and Wen, 2003). According to this picture, models with emergent fermions contain closed-string condensation in their ground states. Since fluctuations of condensed closed strings are gauge fluctuations (Banks *et al.*, 1977; Savit, 1980; Wen, 2003a), this explains why the model with emergent fermions also has emergent gauge structures. Since gauge charges are ends of open strings, this also explains why emergent fermions always carry gauge charges.

The second way to obtain a deconfined phase is to simply go to higher dimensions. In 3+1 dimensions, the gapless U(1) fluctuations do not generate confining interactions. In 4+1 dimensions and above, even non-Abelian gauge theory can be in a deconfined phase. So it is not surprising that one can construct bosonic models on a cubic lattice that have emergent gapless photons [U(1) gauge bosons] (Motrunich and Senthil, 2002; Wen, 2002a, 2003a).

The third way to obtain a deconfined phase is to include gapless excitations which carry gauge charges. The charged gapless excitations can screen the gauge interaction to make it less confining. We remark that deconfinement in this case has different behavior than the previous two cases. In the previous two cases the charged particles in the deconfined phases become noninteracting quasiparticles at low energies. In the present case deconfinement only means that those gapless charged particles remain gapless. Those particles may not become noninteracting quasiparticles at low energies. The spin liquids obtained from the sfL *Ansatz* and the uRVB *Ansatz* [given by Eq. (115) with $\Delta=0$] belong to this case. Those spin liquids are gapless. But the gapless excitations are not described by free fermionic quasiparticles or free bosonic quasiparticles at low energies. The uRVB state (upon doping) leads to strange-metal states (Lee and Nagaosa, 1992) with a large Fermi surface. We discuss the spin liquid obtained from the sfL *Ansatz* in Secs. XI.D and XI.F.

Finally, we remark that what is common among these three ways to achieve deconfinement is that instantons are irrelevant and a certain gauge flux is a conserved quantity. We shall exploit this property in Sec. XII.E.

I. The projective symmetry group and quantum order

The Z_2-gapped *Ansatz* (116) and the Z_2-gapless *Ansatz* (130), after the projection, give rise to two spin-liquid states, which have exactly the same symmetry. The question here is whether there is a way to classify these as distinct phases. According to Landau's symmetry-breaking theory, two states with the same symmetry belong to the same phase. However, after the discovery of fractional quantum Hall states, we now know that Landau's symmetry-breaking theory does not describe all the phases. Different quantum Hall states have the same symmetry, yet they can belong to different phases since they contain different topological orders (Wen, 1995). So it is possible that the two Z_2 spin liquids contain different orders that cannot be characterized by symmetry breaking and local order parameters. The issue here is to find a new set of universal quantum numbers that characterize the new orders.

To find a new set of universal quantum numbers, we note that although the projected wave functions of the two Z_2 spin liquids have the same symmetry, their *Ansätze* are invariant under the same set of symmetry transformations but they are followed by different gauge transformations [see Eqs. (119) and (131)]. So the invariant group of the mean-field *Ansatz* for the two spin liquids are different. The invariant group is called the projective symmetry group. This group is generated by the combined transformations $(G_{T_x} T_x, G_{T_y} T_y, G_{P_x} P_x, G_{P_y} P_y, G_{P_{xy}} P_{xy})$ and G_0. We note that the projective symmetry group is the symmetry group of the mean-field Hamiltonian. Since the mean-field fluctuations in the Z_2 states are weak and perturbative in nature, those fluctuations cannot change the symmetry group of the mean-field theory. Therefore the projective symmetry group of an *Ansatz* is a universal property, at least against perturbative fluctuations. This group can be used to characterize the new order in the two Z_2 spin liquids (Wen, 2002b). Such an order is called the quantum order. The two Z_2 spin liquids belong to two different phases since they have different projective symmetry groups and hence different quantum orders.

We know that the symmetry characterization of phases (or orders) has some important applications. It allows us to classify 230 crystal orders in three dimensions. The symmetry also produces and protects gapless collective excitations—the Nambu-Goldstone bosons. The projective symmetry group characterization of quantum orders has similar applications. Using the projective symmetry group we can classify over 100 different 2D Z_2 spin liquids that all have the same symmetry (Wen, 2002b). Just like the symmetry group, the projective symmetry group can also produce and protect gapless excitations. However, unlike the symmetry group, the projective symmetry group can produce and protect gapless gauge bosons and fermions (Wen, 2002a, 2002b; Wen and Zee, 2002).

XI. SU(2) SLAVE-BOSON THEORY OF DOPED MOTT INSULATORS

In order to apply the SU(2) slave-boson theory to high-T_c superconductors, we need to first generalize the theory to the case with finite doping. Then we discuss how to use the theory to explain some of those properties in detail.

A. SU(2) slave-boson theory at finite doping

The SU(2) slave-boson theory can be generalized to describe doped spin liquids (Wen and Lee, 1996; Lee *et al.*, 1998). The generalized SU(2) slave-boson theory involves two SU(2) doublets ψ_i and $h_i = \binom{b_{1i}}{b_{2i}}$. Here b_{1i} and b_{2i} are two spin-0 boson fields. The additional boson fields allow us to form a SU(2) singlet to represent the electron operator c_i:

$$c_{\uparrow i} = \frac{1}{\sqrt{2}} h_i^\dagger \psi_i = \frac{1}{\sqrt{2}}(b_{1i}^\dagger f_{i\uparrow} + b_{2i}^\dagger f_{i\downarrow}^\dagger),$$

$$c_{\downarrow i} = \frac{1}{\sqrt{2}} h_i^\dagger \bar{\psi}_i = \frac{1}{\sqrt{2}}(b_{1i}^\dagger f_{i\downarrow} - b_{2i}^\dagger f_{i\uparrow}^\dagger), \tag{132}$$

where $\bar{\psi} = i\tau^2 \psi^*$, which is also a SU(2) doublet. The *t-J* Hamiltonian

$$H_{tJ} = \sum_{\langle ij \rangle} \left[J \left(\mathbf{S}_i \cdot \mathbf{S}_j - \frac{1}{4} n_i n_j \right) - t(c_{i\alpha}^\dagger c_{\alpha j} + \text{H.c.}) \right]$$

can now be written in terms of our fermion-boson fields. The Hilbert space of the fermion-boson system is larger than that of the *t-J* model. However, the local SU(2) singlets satisfying $(\psi_i^\dagger \boldsymbol{\tau} \psi_i + h_i^\dagger \boldsymbol{\tau} h_i)|\text{phys}\rangle = 0$ form a subspace that is identical to the Hilbert space of the *t-J*

model. On a given site, there are only three states that satisfy the above constraint. They are $f_\uparrow^\dagger|0\rangle$, $f_\downarrow^\dagger|0\rangle$, and $(1/\sqrt{2})(b_1^\dagger + b_2^\dagger f_\downarrow^\dagger f_\uparrow^\dagger)|0\rangle$, corresponding to a spin-up and spin-down electron, and a vacancy, respectively. Furthermore, the fermion-boson Hamiltonian H_{tJ}, as a SU(2) singlet operator, acts within the subspace and has the same matrix elements as the t-J Hamiltonian.

We note that as in Eq. (36) our treatment of the $\frac{1}{4}n_i n_j$ term introduces a nearest-neighbor boson attraction term which we shall ignore from now on.[8] Now the partition function Z is given by

$$Z = \int D\psi D\psi^\dagger Dh Da_0^1 Da_0^2 Da_0^3 DU \exp\left(-\int_0^\beta d\tau L_2\right),$$

with the Lagrangian taking the form

$$L_2 = \tilde{J}\sum_{\langle ij\rangle} \mathrm{Tr}[U_{ij}^\dagger U_{ij}] + \tilde{J}\sum_{\langle ij\rangle} (\psi_i^\dagger U_{ij}\psi_j + \mathrm{c.c.})$$
$$+ \sum_i \psi_i^\dagger(\partial_\tau - ia_{0i}^\ell\tau^\ell)\psi_i + \sum_i h_i^\dagger(\partial_\tau - ia_{0i}^\ell\tau^\ell + \mu)h_i$$
$$- \frac{1}{2}\sum_{\langle ij\rangle} t_{ij}(\psi_i^\dagger h_i h_j^\dagger\psi_j + \mathrm{c.c.}). \tag{133}$$

Following the standard approach with the choice $\tilde{J} = \frac{3}{8}J$, we obtain the following mean-field Hamiltonian for the fermion-boson system, which is an extension of Eq. (110) to the doped case:

$$H_{\mathrm{mean}} = \sum_{\langle ij\rangle} \frac{3}{8}J\left[\frac{1}{2}\mathrm{Tr}(U_{ij}^\dagger U_{ij}) + (\psi_i^\dagger U_{ij}\psi_j + \mathrm{H.c.})\right]$$
$$- \frac{1}{2}\sum_{\langle ij\rangle} t(h_i^\dagger U_{ij} h_j + \mathrm{H.c.}) - \mu\sum_i h_i^\dagger h_i$$
$$+ \sum_i a_0^l(\psi_i^\dagger\tau^l\psi_i + h_i^\dagger\tau^l h_i). \tag{134}$$

The value of the chemical potential μ is chosen such that the total boson density (which is also the density of the holes in the t-J model) is

$$\langle h_i^\dagger h_i\rangle = \langle b_{1i}^\dagger b_{1i} + b_{2i}^\dagger b_{2i}\rangle = x.$$

The values of $a_0^l(i)$ are chosen such that

$$\langle \psi_i^\dagger\tau^l\psi_i + h_i^\dagger\tau^l h_i\rangle = 0.$$

For $l=3$ we have

---

[8]Lee and Salk (2001) have introduced a different formulation in which the combination $(\boldsymbol{S}_i\cdot\boldsymbol{S}_j - \frac{1}{4}n_i n_j)$ is written as $-\frac{1}{2}|(f_{\uparrow i}^\dagger f_{\downarrow j}^\dagger - f_{\downarrow i}^\dagger f_{\uparrow j}^\dagger)|^2(1 - h_i^\dagger h_i)(1 - h_j^\dagger h_j)$. The last two factors are the boson projections, which are needed when both sites i and j are occupied by holes. While the formulations are equivalent, the mean-field phase diagram is a bit different in that a nearest-neighbor attraction term may lead to boson pairing. The competition between boson condensation and boson pairing needs further studies but we shall proceed without the boson interaction term.
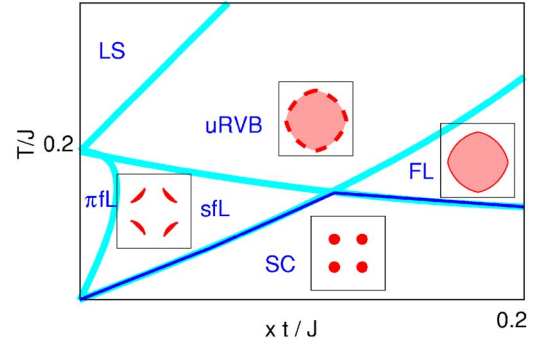
FIG. 22. (Color online) SU(2) mean-field phase diagram for $t/J=1$. The phase diagram for $t/J=2$ is quantitatively similar to the $t/J=1$ phase diagram when plotted in terms of the scaled variable xt/J, except the πfL phase disappears at a lower-scaled doping concentration. Also plotted are the Fermi surface, the Fermi arcs, or the Fermi points in phases. From Wen and Lee, 1996.

$$\langle f_{i\alpha}^\dagger f_{i\alpha} + b_{1i}^\dagger b_{1i} - b_{2i}^\dagger b_{2i}\rangle = 1. \tag{135}$$

We see that unlike the U(1) slave-boson theory, the density of the fermion $\langle f_{i\alpha}^\dagger f_{i\alpha}\rangle$ is not necessarily equal to 1 $-x$. This is because a vacancy in the t-J model may be represented by an empty site with a b_1 boson, or a doubly occupied site with a b_2 boson.

B. The mean-field phase diagram

To obtain the mean-field phase diagram, we have searched the minima of the mean-field free energy for the mean-field *Ansatz* with translational, lattice, and spin-rotational symmetries. We find a phase diagram with six different phases (see Fig. 22; Wen and Lee, 1996).

(i) The d-wave superconducting phase is described by the following mean-field *Ansatz*:

$$U_{i,i+\hat{x}} = -\chi\tau^3 + \Delta\tau^1, \quad U_{i,i+\hat{y}} = -\chi\tau^3 - \Delta\tau^1,$$
$$a_0^3 \neq 0, \quad a_0^{1,2} = 0, \quad \langle b_1\rangle \neq 0, \quad \langle b_2\rangle = 0. \tag{136}$$

Notice that the boson condenses in the superconducting phase despite the fact that in our mean-field theory the interactions between bosons are ignored. In the superconducting phase, the fermion and boson dispersion are given by $\pm E_f$ and $\pm E_b - \mu$, where

$$E_f = \sqrt{(\epsilon_f + a_0^3)^2 + \eta_f^2}, \quad \epsilon_f = -\frac{3J}{4}(\cos k_x + \cos k_y)\chi,$$

$$\eta_f = -\frac{3J}{4}(\cos k_x - \cos k_y)\Delta, \quad E_b = \sqrt{(\epsilon_b + a_0^3)^2 + \eta_b^2},$$

$$\epsilon_b = -2t(\cos k_x + \cos k_y)\chi,$$

$$\eta_b = -2t(\cos k_x - \cos k_y)\Delta. \tag{137}$$

(ii) The Fermi-liquid phase is similar to the superconducting phase except that there is no fermion pairing ($\Delta = 0$).

(iii) The staggered flux liquid (sfL) phase is described by the following:

$$U_{i,i+\hat{x}} = -\tau^3 \chi - i(-)^i \Delta, \quad U_{i,i+\hat{y}} = -\tau^3 \chi + i(-)^i \Delta,$$

$$a_0^l = 0, \quad \langle b_{1,2} \rangle = 0. \tag{138}$$

The U matrix is the same as that of the staggered flux phase in the U(1) slave-boson theory, which breaks transitional symmetry. Here the breaking of translational invariance is a gauge artifact. In fact, a site-dependent SU(2) gauge transformation $W_i = e^{-i\pi\tau^1/4} e^{-i\pi(i_x+i_y)(\tau^1/2+1)}$ maps the sfL *Ansatz* to the *d*-wave pairing *Ansatz*

$$U_{i,i+\hat{x}} = -\chi\tau^3 + \Delta\tau^1, \quad U_{i,i+\hat{y}} = -\chi\tau^3 - \Delta\tau^1,$$

$$a_0^l = 0, \quad \langle b_{1,2} \rangle = 0, \tag{139}$$

which is explicitly translation invariant. However, the staggered flux representation of Eq. (138) is more convenient because the gauge symmetry is immediately apparent. Since this U matrix commutes with τ^3, it is clearly invariant under τ^3 rotation, but not τ^1 and τ^2, and the gauge symmetry has been broken from SU(2) down to U(1) following the discussion in Sec. X.F. For this reason we shall refer to this state as the staggered flux liquid (sfL).

In the sfL phase, the fermion and boson dispersion are given by $\pm E_f$ and $\pm E_b - \mu$ with E_f and E_b in Eq. (137), but now $a_0^3 = 0$. Since $a_0^3 = 0$ we have $\langle f_{i\alpha}^\dagger f_{i\alpha} \rangle = 1$ and $\langle b_1^\dagger b_1 \rangle = \langle b_2^\dagger b_2 \rangle = x/2$.

(iv) The π-flux liquid (πfL) phase is the same as the sfL phase except here $\chi = \Delta$.

(v) The uniform RVB (uRVB) phase is described by Eq. (138) with $\Delta = 0$.

(vi) A localized spin phase has $U_{ij} = 0$ and $a_{0i}^l = 0$, where the fermions cannot hop.

C. Simple properties of the mean-field phases

Note that the topology of the phase diagram is similar to that of U(1) mean-field theory shown in Fig. 21. The uRVB, sfL, πfL, and localized spin phases contain no boson condensation and correspond to unusual metallic states. As the temperature is lowered, the uRVB phase changes into the sfL or πfL phase. A gap is opened at the Fermi surface near $(\pi,0)$, which reduces the low-energy spin excitations. Thus the sfL and πfL phases correspond to the pseudogap phase.

The Fermi-liquid phase contains boson condensation. In this case the electron Green's function $\langle c^\dagger c \rangle \propto \langle (\psi^\dagger h) \times (h^\dagger \psi) \rangle$ is proportional to the fermion Green's function $\langle \psi^\dagger \psi \rangle$. Thus the electron spectral functions contain a δ-function peak in the Fermi-liquid phase. Therefore the low-energy excitations in the Fermi-liquid phase are de-

scribed by electronlike quasiparticles and the Fermi-liquid phase corresponds to a Fermi-liquid phase of electrons.

The superconducting phase contains both the boson and fermion-pair condensations and corresponds to a *d*-wave superconducting state of the electrons. Just as in the U(1) slave-boson theory, the superfluid density is given by $\rho_s = \rho_s^b \rho_s^f / (\rho_s^b + \rho_s^f)$, where ρ_s^b and ρ_s^f are the superfluid density of bosons and condensed fermion pairs, respectively. We see that in the low-doping limit, $\rho_s \sim x$ and one needs the condensation of both bosons and fermion pairs to achieve a superconducting state.

We point out that the different mean-field phases contain different gapless gauge fluctuations at the classical level, i.e., the gauge groups for gapless gauge fluctuations are different in different mean-field phases. The uRVB and πfL phases have trivial SU(2) flux and the gapless gauge fluctuations are SU(2) gauge fluctuations. In the sfL phase, the collinear SU(2) flux breaks the SU(2) gauge structure to a U(1) gauge structure. In this case the gapless gauge fluctuations are U(1) gauge fluctuations. In the superconducting and Fermi-liquid phases, $\langle b_a \rangle \neq 0$. Since b_a transform as a SU(2) doublet, there is no pure SU(2) gauge transformation that leaves mean-field *Ansatz* (U_{ij}, a_0^l, b_a) invariant. Thus the invariant gauge group is trivial. As a result, the SU(2) gauge structure is completely broken and there are no low-energy gauge fluctuations.

D. Effect of gauge fluctuations: Enhanced (π, π) spin fluctuations in the pseudogap phase

The pseudogap phase has a very puzzling property which seems hard to explain. As the doping is lowered, it was found experimentally that both the pseudogap and the antiferromagnetic spin correlation in the normal state increase. Naively one expects the pseudogap and the antiferromagnetic correlations to work against each other. That is, the larger the pseudogap, the lower the single-particle density of states, the fewer the low-energy spin excitations, and the weaker the antiferromagnetic correlations.

It turns out that the gapless U(1) gauge fluctuations present in the sfL phase play a key role in resolving the above puzzle (Kim and Lee, 1999; Rantner and Wen, 2002). Due to the U(1) gauge fluctuations, the antiferromagnetic spin fluctuations in the sfL phase are as strong as those of a nested Fermi surface, despite the presence of the pseudogap.

To see how the U(1) gauge fluctuations in the sfL phase enhance the antiferromagnetic spin fluctuations, we map the lattice effective theory for the sfL state onto a continuum theory. In the low-doping limit, the bosons do not affect the spin fluctuations much. So we ignore the bosons and effectively consider the undoped case. In the sfL phase, the low-energy fermions only appear near $k = (\pm\pi/2, \pm\pi/2)$. Since the fermion dispersion is linear near $k = (\pm\pi/2, \pm\pi/2)$, those fermions are described by massless Dirac fermions in the continuum limit:

$$S = \int d^3x \sum_\mu \sum_{\alpha=1}^N \bar{\Psi} v_{\alpha,\mu} \partial_\mu \gamma_\mu \Psi_\alpha, \tag{140}$$

where $v_{\alpha,0}=1$ and $N=2$, but in the following we treat N as an arbitrary integer, which gives a large-N limit of the sfL state. In general, $v_{\alpha,1} \neq v_{\alpha,2}$. However, for simplicity we shall here assume $v_{\alpha,i}=1$. The Fermi field Ψ_α is a 4×1 spinor which describes lattice fermions f_i with momenta near $(\pm\pi/2, \pm\pi/2)$. The 4×4 γ_μ matrices form a representation of the $\{\gamma_\mu, \gamma_\nu\}=2\delta_{\mu\nu}$ $(\mu, \nu=0,1,2)$ and are taken to be

$$\gamma_0 = \begin{pmatrix} \sigma_3 & 0 \\ 0 & -\sigma_3 \end{pmatrix}, \quad \gamma_1 = \begin{pmatrix} \sigma_2 & 0 \\ 0 & -\sigma_2 \end{pmatrix}, \tag{141}$$

$$\gamma_2 = \begin{pmatrix} \sigma_1 & 0 \\ 0 & -\sigma_1 \end{pmatrix}, \tag{142}$$

with σ_μ the Pauli matrices. Finally, note that $\bar{\Psi}_\sigma \equiv \Psi_\sigma^\dagger \gamma_0$.

The fermion field Ψ couples to the U(1) gauge field in the sfL phase. To determine the form of the coupling, we note that the U(1) gauge transformation takes the following form: $f_i \rightarrow e^{i\theta_i} f_i$ if we choose Eq. (138) to describe the sfL phase. By requiring U(1) gauge invariance of the continuum model, we find the continuum Euclidean action to be

$$S = \int d^3x \sum_\mu \sum_{\sigma=1}^N \bar{\Psi}_\sigma v_{\sigma,\mu} (\partial_\mu - i a_\mu) \gamma_\mu \Psi_\sigma. \tag{143}$$

The dynamics for the U(1) gauge field arises solely due to the screening by bosons and fermions, both of which carry gauge charges. In the low-doping limit, however, we include only the screening by fermion fields. After integrating out Ψ in Eq. (143), we obtain the following effective action for the U(1) gauge field (Kim and Lee, 1999):

$$\mathcal{Z} = \int Da_\mu \exp\left(-\frac{1}{2} \int \frac{d^3q}{(2\pi)^3} a_\mu(q) \Pi_{\mu\nu} a_\nu(-q)\right),$$

$$\Pi_{\mu\nu} = \frac{N}{8} \sqrt{q^2}\left(\delta_{\mu\nu} - \frac{q_\mu q_\nu}{q^2}\right). \tag{144}$$

By simple power counting we can see that the above polarizability makes the gauge coupling $a_\mu j^\mu$ a marginal perturbation at the free fermion fixed point. Since the conserved current j^μ cannot have any anomalous dimension, this interaction is an exact marginal perturbation protected by current conservation.

For $N=2$, the spin operator with momenta near $q=(0,0)$, (π,π), and $(\pi,0)$ has a different form when expressed in terms of Ψ_α. Near $q=(0,0)$,

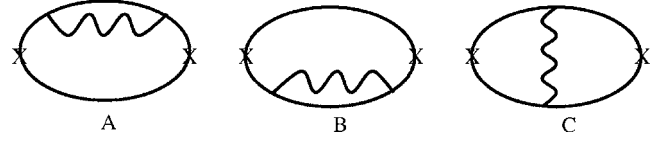$$S_u(x) = \frac{1}{2}\bar{\Psi}_\alpha \gamma^0 \sigma_{\alpha\beta}\Psi_\beta.$$

Near $q=(\pi,\pi)$,

FIG. 23. Nonzero leading $1/N$ corrections to the staggered spin-correlation function. x denotes the vertex, which is the 4×4 unit matrix in the case of interest.

$$S_s(x) = \frac{1}{2}\bar{\Psi}_\alpha \sigma_{\alpha\beta}\Psi_\beta.$$

Near $q=(\pi,0)$,

$$S_{(\pi,0)}(x) = \frac{1}{2}\bar{\Psi}_\alpha \begin{pmatrix} 0 & \sigma_1 \\ \sigma_1 & 0 \end{pmatrix} \sigma_{\alpha\beta}\Psi_\beta.$$

At the mean-field level, the above spin operators have algebraic correlations $1/r^4$ with decay exponent 4. The effect of gauge fluctuations can be included at $1/N$ order by calculating the diagrams in Fig. 23. We find that (Rantner and Wen, 2002; Franz *et al.*, 2003) these spin correlators still have algebraic decays, indicating that the gauge interaction is indeed marginal. The decay exponents of the spin correlation near $q=(0,0)$ and $q=(\pi,0)$ are not changed and remain 4. This result is expected for the spin correlation near $q=(0,0)$ since $S_u(x)$ is proportional to the conserved density operator that couples to the U(1) gauge field. Therefore $S_u(x)$ cannot have an anomalous dimension. $S_{(\pi,0)}(x)$ does not have any anomalous dimensions either (at $1/N$ order). In fact, this result holds to all orders in $1/N$ for the case of isotropic velocities due to a SU(4) symmetry (Hermele, Senthil, and Fisher, 2005). Thus the spin fluctuations near $(\pi,0)$ are also not enhanced by the gauge interactions. This may explain why it is so hard to observe any spin fluctuations near $(\pi,0)$ in experiments.

$S_s(x)$ is found to have a nonzero anomalous dimension. The spin correlation near $q=(\pi,\pi)$ is found to be $1/r^{4-2\alpha}$ with

$$\alpha = \frac{32}{3\pi^2 N}. \tag{145}$$

In the ω-k space, the imaginary part of the spin susceptibility near (π,π) is given by

$$\text{Im}\,\chi(\omega,q) \equiv \text{Im}\langle S^+(\omega, q+Q)S^-(-\omega, -q+Q)\rangle$$

$$= \frac{C_s}{2}\sin(2\alpha\pi)\Gamma(2\alpha-2)\Theta(\omega^2-q^2)$$

$$\times (\omega^2 - q^2)^{1/2-\alpha}, \tag{146}$$

where C_s is a constant depending on the physics at the lattice scale.

From Eq. (146) it is clear that the gauge fluctuations have reduced the mean-field exponent. If we set $N=2$, which is the physically relevant case, we find $\alpha=0.54 > 1/2$, which signals the divergence of χ $(\omega=0, q=0)$. Thus after including the gauge fluctuations, the (π,π) spin fluctuations are enhanced in the sfL phase despite
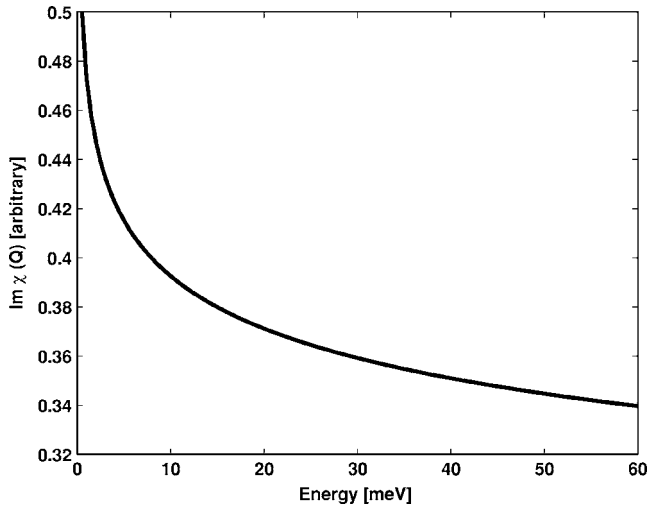
FIG. 24. Imaginary part of the spin susceptibility at (π, π). Note the divergence at small ω. From Rantner and Wen, 2002.

the pseudogap. In Fig. 24 we plot the imaginary part of the spin susceptibility at (π, π). The ω dependence of the spin susceptibility at (π, π) is similar to the one of a nested Fermi surface.

The enhancement of the staggered spin correlation follows the trend found in the Gutzwiller projection of the staggered flux (or equivalently the d-wave pairing) state. Ivanov (2000) and Paramekanti *et al.* (2004) reported a power-law decay of the equal-time staggered spin-correlation function as $r^{-\nu}$, where $\nu = 1.5$ for the undoped case and 2.5 for 5% doping, which are considerably slower than the r^{-4} behavior before projection.

We remark that with doping Lorentz invariance is broken by the presence of bosons. In this case the Fermi velocity receives a logarithmic correction which enhances the specific heat coefficient and the uniform susceptibility (Kim *et al.*, 1997).

E. Electron spectral function

One of the striking properties of the high-T_c superconductor is the appearance of the pseudogap in the electron spectral function for underdoped samples, even in the nonsuperconducting state. To understand this property within the SU(2) slave-boson theory, we calculate the physical electron Green's function. Since the nonsuperconducting state for small x is described by the sfL phase in SU(2) slave-boson theory, we need to calculate the electron Green's function in the sfL phase.

1. Single-hole spectrum

The electron Green's function is given by

$$G_e(\mathbf{x}) \propto \langle h^\dagger(\mathbf{x}) \psi(\mathbf{x}) h(0) \psi^\dagger(0) \rangle.$$

If we ignore the gauge interactions between bosons and fermions, the electron Green's function can be written as
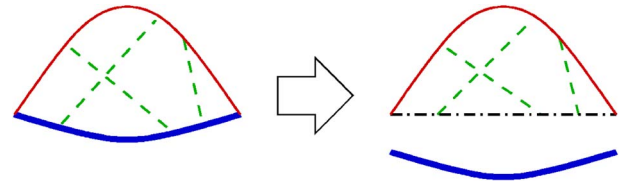

FIG. 25. (Color online) The electron Green's function in the slave-boson theory. The thick line represents the boson world line, the thin line represents the fermion world line, and the dashed line represents the gauge interaction. The dash-dotted line is the straight return path. The U(1) gauge interaction is caused by the extra phase term $e^{i\oint d\mathbf{x}\cdot\mathbf{a}}$ due to the U(1) flux through the loop formed by the boson and the fermion world lines. Such flux can be approximated through the loop formed by the fermion world line and the straight return path.

$$G_{e0} \propto \langle h^\dagger h \rangle_0 \langle \psi \psi^\dagger \rangle_0,$$

where the subscript 0 indicates to ignore gauge fluctuations when calculating $\langle \cdots \rangle_0$.

The effect of the U(1) gauge fluctuations is an extra phase term $e^{i\oint d\mathbf{x}\cdot\mathbf{a}}$ determined by the U(1) flux through the loop formed by the boson and fermion world lines (see Fig. 25). Since the fermion has a linear dispersion relation, the area between the boson and fermion world lines is of order $|\mathbf{x}|^2$, where $|\mathbf{x}|$ is the separation between the two points of the Green's function. Such an area is about the same as the area between the fermion world line and the straight return path (see Fig. 25). We may approximate the effect of U(1) gauge fluctuations as the effect caused by the U(1) flux through the fermion world line and the straight return path (Rantner and Wen, 2001b). This corresponds to an approximation of the electron Green's function as

$$G_e(\mathbf{x}) \propto \langle h^\dagger(\mathbf{x}) h(0) \rangle_0 \langle \psi(\mathbf{x}) \psi^\dagger(0) e^{i\int_0^{\mathbf{x}} d\mathbf{x}\cdot\mathbf{a}} \rangle,$$

where $\int_0^{\mathbf{x}} d\mathbf{x}$ is the integration along the straight return path and $\langle \cdots \rangle$ includes integrating out the gauge fluctuations.

First, let us consider the fermion Green's function. At the leading order of a large-N approximation, it was found that (Rantner and Wen, 2001a, 2001b)[9]

$$\langle \psi(\mathbf{x}) \psi^\dagger(0) e^{i\int_0^{\mathbf{x}} d\mathbf{x}\cdot\mathbf{a}} \rangle \propto (\mathbf{x}^2)^{-(2-\alpha)/2}, \qquad (147)$$

where α is given in Eq. (145). We note that Eq. (147) becomes the Green's function for a free massless Dirac

---

[9]Note that the usual fermion Green's function $\langle \psi(\mathbf{x}) \psi^\dagger(0) \rangle$ is not gauge invariant. As a result, the Green's function is not well defined and depends on the choices of gauge-fixing conditions (Franz and Tesanovic, 2001; Franz *et al.*, 2002; Khveshchenko, 2002; Ye, 2003). If one incorrectly identifies $\langle \psi(\mathbf{x}) \psi^\dagger(0) \rangle$ as the electron Green's function, then the function will have different decay exponents for different gauge-fixing conditions. In contrast, the combination $\langle \psi(\mathbf{x}) \psi^\dagger(0) e^{i\int_0^{\mathbf{x}} d\mathbf{x}\cdot\mathbf{a}} \rangle$ is gauge invariant and well defined. The resulting electron Green's function does not depend on gauge-fixing conditions.
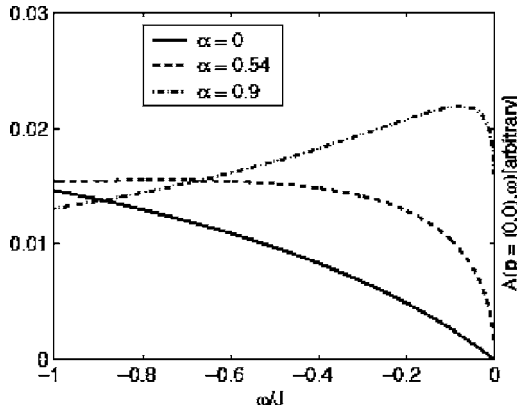
FIG. 26. The single-hole spectral function at $(\pi/2, \pi/2)$. Increasing α corresponds to increasing attraction between fermions and bosons due to gauge-field fluctuations. From Rantner and Wen, 2001b.

fermion when $\alpha = 0$. The finite α is the effect of gauge fluctuations.

For a single hole, the boson Green's function is simply that of a classical particle. The electron Green's function $G_e(\boldsymbol{r}, \tau)$ is readily calculated using Eq. (147) and its Fourier transform yields the electron spectral function. The result at the nodal position $(\pi/2, \pi/2)$ is shown in Fig. 26. The $\alpha = 0$ curve is the result without gauge fluctuations. It is the convolution of the fermion and Bose spectra and is extremely broad. The gauge field leads to an effective attraction between the fermion and boson in order to minimize the gauge flux enclosed by the fermion on boson vortex lines as shown in Fig. 25. The result is a piling up of spectral weight at low energy with increasing α. Still, the one-hole spectrum remains incoherent, as is appropriate for a deconfined U(1) spin-liquid state. This calculation can be extended to finite-hole density, which requires making certain assumptions about the boson Green's function (Franz and Tesanovic, 2001; Rantner and Wen, 2001b). Under certain conditions one obtains power-law-type spectral functions similar to those of the Luttinger liquid.

2. Finite-hole density: pseudogap and Fermi arcs

Here we consider the mean-field electron Green's function G_0 at finite doping. Using the expression of c_α in Eq. (132), the mean-field electron Green's function is given by the product of the fermion and boson Green's functions. So the electron spectral function is a convolution of the boson and the fermion spectral functions.

Let us consider the pseudogap phase above T_c but at a temperature which is not too high that the boson can be considered as nearly condensed. The boson spectral function contains a peak at $\omega = 0$ and $\boldsymbol{k} = 0$ and $\boldsymbol{k} = (\pi, \pi)$. The weight of the peak is of order x and the width is of order T. At high energies, the boson Green's function is given by the single-boson Green's function G_b^s as if no other bosons are present. The boson spectral function contains a broad background which extends the whole bandwidth of the boson band. Such a boson spec-

FIG. 27. Diagram for a renormalized electron Green's function. The solid line is the fermion propagator and the dashed line the boson propagator.

tral function leads to a mean-field electron Green's function which has the form (Wen and Lee, 1996; Lee *et al.*, 1998)

$$G_0 = \frac{x}{2}\left(\frac{u_{\boldsymbol{k}}^2}{\omega - E_f} + \frac{v_{\boldsymbol{k}}^2}{\omega + E_f}\right) + G_{\mathrm{in}}, \qquad (148)$$

where u and v are the coherent factors:

$$u_{\boldsymbol{k}} = \sqrt{\frac{E_f + \epsilon_f}{2E_f}}\,\mathrm{sgn}(\eta_f), \quad v_{\boldsymbol{k}} = \sqrt{\frac{E_f - \epsilon_f}{2E_f}}.$$

The second term G_{in} gives rise to a broad background in the electron. It comes from the convolution of the background part of the boson and fermion spectral functions. The first term is the coherent part since its imaginary part is a peak of width T, which is approximated by a δ function here. The quasiparticle dispersion is given by $\pm E_f$. The peak in the electron spectral function crosses zero energy at four points at $\boldsymbol{k} = (\pm\pi/2, \pm\pi/2)$. Thus the mean-field sfL phase has four Fermi points. Also, in the sfL phase, $\mathrm{Im}\,G_{\mathrm{in}}$ is nonzero only for $\omega < 0$ and contributes $1/2$ to a total spectral weight which is $(1+x)/2$.

From the dispersion relation of the peak $\omega = E_f(\boldsymbol{k})$ and the fact that $\mathrm{Im}\,G_{\mathrm{in}} \approx 0$ when $\omega < -E_f(\boldsymbol{k})$, we find that the electron spectral function contains a gap of order Δ at $(0, \pi)$ and $(\pi, 0)$ even in the nonsuperconducting state. So the mean-field electron spectral function of SU(2) slave-boson theory can explain the pseudogap in the underdoped samples. However, if we examine the mean-field electron spectral function more closely, we see that the Fermi surface of the quasiparticles is just four isolated points $(\pm\pi/2, \pm\pi/2)$. This property does not agree with experiments.

In reality there is a strong attraction between bosons and fermions due to the fluctuation around the mean-field state. The dominant effect comes from gauge fluctuations, which attempt to bind bosons and fermions into electrons. This corresponds to an effective attraction between bosons and fermions. In the case of a single hole, the interaction with gauge fields can be treated as discussed in the last section. Here we proceed more phenomenologically. One way to include this effect is to use the diagram in Fig. 27 to approximate the electron Green's function which leads to

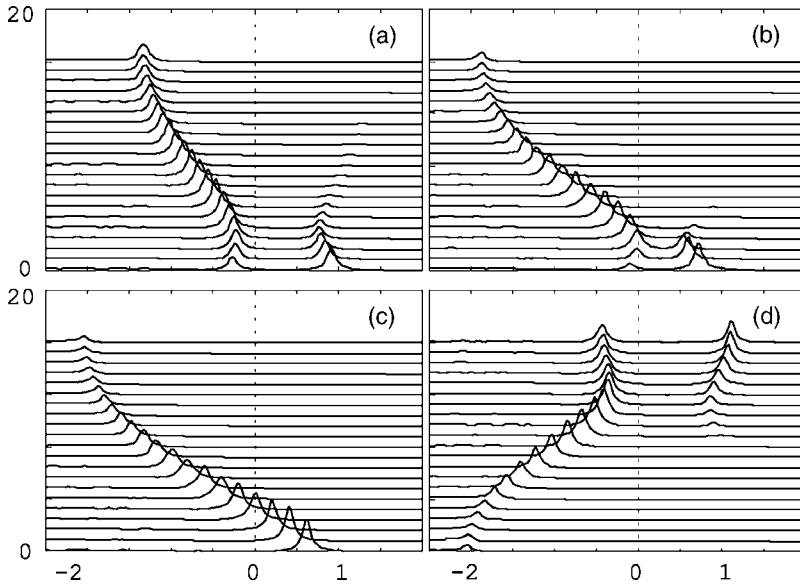$$G(\omega, \boldsymbol{k}) = \frac{1}{G_0^{-1}(\omega, \boldsymbol{k}) + V(\boldsymbol{k})} \qquad (149)$$

with

FIG. 28. The electron spectral function for (a) $k=(-\pi/4,\pi/4)\rightarrow(\pi/4,3\pi/4)$, (b) $k=(-\pi/8,\pi/8)\rightarrow(3\pi/8,5\pi/8)$, (c) $k=(0,0)$ $\rightarrow(\pi/2,\pi/2)$, and (d) $k=(0,\pi)\rightarrow(0,0)$. We have chosen $J=1$. The paths of the four momentum scans are shown in Fig. 29.

$$V(\mathbf{k}) = U + 2t(\cos k_x + \cos k_y). \tag{150}$$

The first term U comes from the fluctuations of a_0^ℓ, which is approximated by an on-site attraction $\delta H = -(U/2) \times (\psi^\dagger h)(h^\dagger \psi) = -Uc^\dagger c$. The second term [whose importance was pointed out by Laughlin (1995)] is due to the fluctuations of $|\chi_{ij}|$, which induces

$$\delta H = -t(\psi^\dagger h)_j(h^\dagger \psi)_i = -2tc_j^\dagger c_i. \tag{151}$$

This is nothing but the original hopping term. In Figs. 28 and 30 we plot the electron spectral function calculated from Eq. (149) (Wen and Lee, 1996; Lee *et al.*, 1998).

We have chosen $t=2J$, $\chi=1$, $\Delta/\chi=0.4$, $x=0.1$, and $T=0.1J$. The value of U is determined by requiring that the renormalized electron Greens function satisfy the sum rule

$$\int_0^\infty \frac{d\omega}{2\pi} \int \frac{d^2k}{(2\pi)^2} \, \mathrm{Im}\, G = x. \tag{152}$$

We find that the gap near $(0,\pm\pi)$ and $(\pm\pi,0)$ survives the binding potential $V(\mathbf{k})$. However, the spectral functions near $(\pm\pi/2,\pm\pi/2)$ are modified (see Fig. 28). By marking the position where the spectral peak crosses zero energy, we find that the Fermi point at the nodal point $(\pi/2,\pi/2)$ for the mean-field electron Green's function G_0 is stretched into a Fermi segment as shown in Fig. 29. As we approach the uRBV phase, Δ decreases and the Fermi arcs are elongated. Eventually the arcs join together to form a large closed Fermi surface. Such an evolution of Fermi arcs agrees with what is observed in experiments.

While the phenomenological binding picture successfully produces the observed quasiparticle spectral peak and Fermi arcs near the nodal points, the results are not as satisfactory for antinodal points. STM experiments in underdoped samples reveal a rather broad structure for both particle and hole excitations suggesting that there is no sharp quasiparticle spectral peak near the gap maximum (Hanaguri *et al.*, 2004). ARPES measure-

ments, which can measure only the occupied states, show a reduction of the density of states over a broad energy range near antinodal points (Ronning *et al.*, 2003). These line shapes are more reminiscent of those shown in Fig. 26 for intermediate α. This again indicates that there is no well-defined quasiparticle spectral peak near antinodal points for underdoped samples. The observed electron spectral function shows a nodal-antinodal dichotomy: the presence of a quasiparticle peak near the nodal points and the absence of a quasiparticle peak near the antinodal points.

While an energy gap is produced by SU(2) theory near the antinodal point $(0,\pi)$, the theory gives a rather sharp quasiparticle peak at the gap and the asymmetric gaps above and below the Fermi energy (see Fig. 30); both disagree with experiments. The simple spin-charge binding picture in SU(2) theory fails to explain the nodal-antinodal dichotomy of quasiparticles. The sharp hole spectra in SU(2) theory at both the nodal and antinodal points are due to the assumption of "almost Bose condensation" in our phenomenological approach outlined above.

Recently, Ribeiro and Wen (2005) have developed a fully fermionic mean-field theory which can reproduce the nodal-antinodal dichotomy as well as the symmetric gap at antinodal points. The new mean-field theory is
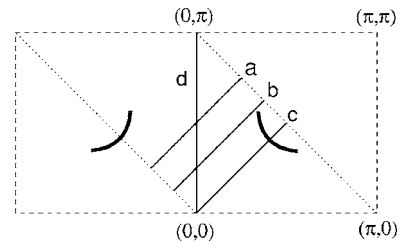

FIG. 29. The solid lines a, b, c, and d are paths of the four momentum scans in Fig. 28. The solid curves are schematic representations of the Fermi segments where the quasiparticle peak crosses the zero energy.
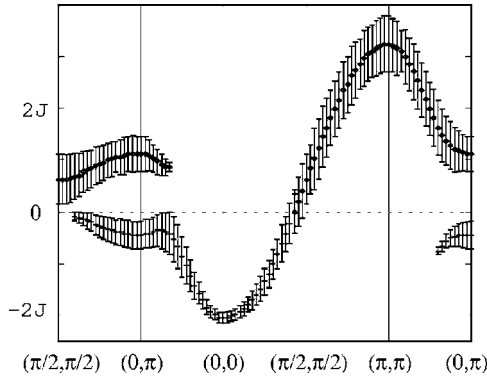
FIG. 30. The points describe the dispersion of the quasiparticle peaks for the s-flux liquid phase in Fig. 30. The vertical bars are proportional to the peak values of $\text{Im}G_U$, which are proportional to the quasiparticle weight.

motivated by the fact that at low energies electrons appear as well-defined quasiparticles. To capture this low-energy property, the new mean-field theory uses fermionic spinons and fermionic electrons to describe the doped Mott insulator. The bosonic holons are bound states of spinons and electrons. In contrast, the SU(2) slave-boson approach starts with the spinons and the holons, and electrons appear as the bound states of the spinons and the holons. In the new mean-field theory, electron spectral weight comes from two bands, a low-energy spinon band [see Eq. (120)] and a high-energy electron band. The spectral weight from the spinon band is a sharp peak which corresponds to the coherent peak in the SU(2) approach. The spectral weight from the electron band is broad due to many decay channels at high energy. Such a broad spectrum corresponds to the incoherent background discussed above. The nodal-antinodal dichotomy is due to the strong mixing between the spinons and electrons near the nodal point and the lack of mixing near the antinodal point. Without the spinon-electron mixing, the spinon band cannot contribute to the electron spectral function.

We also mention that the assumption of Bose condensation leads to a decoupling of the electron to the electromagnetic field, and as a result the current carried by the quasiparticles $j=edE_k(A)/dA$ is strongly reduced from ev_F to xev_F which disagrees with experiments (see Sec. IX.B). Wen and Lee (1998) took a first step towards addressing this problem by assuming that the binding between bosons and fermions and/or between the b_1 and b_2 bosons prevents single-boson condensation. The superconducting state characterized by $\langle cc\rangle\neq0$ contains only boson-pair condensation, i.e., $\langle b_1b_2\rangle\neq0$ while $\langle b\rangle=0$. They showed that with this assumption the quasiparticle current can be a finite fraction of ev_F, i.e., the parameter in Eq. (6) does not have to go as x. The competition between fermion-boson binding, boson-boson binding, and Bose condensation is a complicated problem which is still poorly understood at present.

We point out that Honerkamp *et al.* (2001) have proposed another machanism for the pseudogap and the

nodal-antinodal dichotomy. They emphasized the role of umklapp scattering, which in their N patch renormalization-group approach leads to a gapping of the saddle-point area near $(0,\pi)$ and Fermi segments near the nodes.

F. Stability of algebraic spin liquids

The sfL mean-field *Ansatz* leads to a gapless spin liquid. We call this a U(1) spin liquid, and it is an example of a class which we call an algebraic spin liquid since the spin correlations have algebraic decay. We stress that the algebraic spin liquid is a phase of matter, not a critical point at a phase transition between two phases.

The algebraic spin liquid has a striking property: its low-energy excitations interact with each other even down to zero energy. This can be seen from the correlation functions at low energies. Those correlation functions have noninteger exponents and always contain a branch cut without any poles. This implies that we cannot use free bosonic or free fermionic quasiparticles to describe the low-energy excitations. For other commonly known gapless states, such as solids, superfluids, Fermi liquids, etc., the gapless excitations are always described by free bosons or free fermions. The only exception is the 1D Luttinger liquid. Thus the algebraic spin liquid can be viewed as an example of Luttinger liquids beyond one dimension.[10]

We know that interactions tend to open up energy gaps. From this point of view, one might have thought that the only self-consistent gapless excitations are the ones described by free quasiparticles. Knowing that the gapless excitations in the algebraic spin liquid interact down to zero energy, we may wonder does it really exist? Have we overlooked some effects which open up energy gaps and make algebraic spin liquids unstable?

Indeed, in the above calculation we have overlooked two effects and both of them can potentially destabilize the algebraic spin liquids. First, the self-energy in Figs. 23(a) and 23(b) contains a cutoff-dependent term which gives the fermion Ψ a cutoff-dependent mass $m(\Lambda)\bar{\Psi}\Psi$. In the above calculation, we have dropped such a term. If such a cutoff-dependent term was kept, fermions would gain a mass which would destabilize the algebraic spin liquids.

Second, we have overlooked the effects of instantons described by the space-time monopoles of the U(1)

---

[10]We point out that in their gauge-theory description algebraic spin liquids and Luttinger liquids are neither confined phases nor deconfined phases. They are not confined phases since the gauge fluctuations are gapless. They are not deconfined phases since there are no well-defined quasiparticles. Also note that the concept of "spin-charge separation" in a 1D Luttinger liquid has nothing to do with deconfinement. It simply means that the collective modes, which are the only low-lying excitations in one-dimension and correspond to spin- and charge-density fluctuations, are decoupled and have different velocities.

gauge field. After integrating out massless fermions, the effective action of the U(1) gauge field has a form similar to Eq. (129). Unlike the Maxwell term discussed in Sec. IX.D, which produced a $1/r$ potential, in this case the interaction of the space-time monopoles is described by a $\ln(r)$ potential. That is, the action of the pair of space-time monopoles separated by a distance r is given by $C \ln(r)$. Just as in the Coulomb gas in two dimensions, if the coefficient C is larger than 6, then the instanton effect is an irrelevant perturbation and the inclusion of the instantons will not destabilize the algebraic spin liquid (Ioffe and Larkin, 1989). If the coefficient C is less than 6, then the instanton effect is a relevant perturbation and the inclusion of the instantons will destabilize the algebraic spin liquid.

Recently, it has been argued by Herbut and Seradjah (2003) and Herbut et al. (2003) that the instanton effect always represents a relevant perturbation due to a screening effect of the 3D Coulomb gas, regardless of the value of C. This led to a conclusion by Herbut and Seradjah (2003) that the algebraic spin liquid described by the sfL state does not exist. The easiest way to understand the screening effect of the 3D Coulomb gas is to note that the partition function of the Coulomb gas can be written as a path integral

$$\int \prod d^3 \boldsymbol{x}_i e^{-C \Sigma q_i q_j \ln |\boldsymbol{x}_i - \boldsymbol{x}_j|}$$

$$= \int \mathcal{D} \phi e^{-\int d^3 \boldsymbol{x}(2\pi/C) \partial \phi \sqrt{-\partial^2} \partial \phi - g \cos(\phi)}. \qquad (153)$$

If we integrate out short-distance fluctuations of ϕ, a counterterm $K(\partial \phi)^2$ can be generated. The counterterm changes the long-distance interaction of the space-time monopoles from $\ln(r)$ to $1/r$. The space-time monopoles with $1/r$ interaction always represent a relevant perturbation, which will destabilize the algebraic spin liquid. Physically, the change of the interaction from $\ln(r)$ to $1/r$ is due to the screening effect of monopole-antimonopole pairs. Thus the counterterm $K(\partial \phi)^2$ represents the screening effect.

The issue of the stability of the algebraic spin liquid has been examined by Rantner and Wen (2002), Wen (2002b), and more carefully by Hermele, Senthil, Fisher, et al. (2004) using an argument based on the projective symmetry group. They came to the conclusion that the U(1) spin liquid is stable for large enough N if the SU(2) spin symmetry is generalized to SU(N). They have shown that there is no relevant operator which can destabilize the deconfined fixed point which consists of $2N$ two-component Dirac fermions coupled to noncompact U(1) gauge fields, for N sufficiently large. Hermele, Senthil, Fisher, et al. (2004) have also pointed out the fallacy of the monopole screening argument. We summarize some of the salient points below.

The operators which perturb the noncompact fixed point can be classified into two types, those which preserve the flux and those which change the flux by 2π. The latter are instanton creation operators which restore the compactness of the gauge field. Among the first type there are four fermion terms which are readily seen to be irrelevant, but as mentioned earlier the dangerous term is the quadratic fermion mass term. The important point is that the mass terms are forbidden by the special symmetry described by the projective symmetry group. The discrete symmetry (such as translational and rotational) of the sfL state defined on the lattice imposes a certain symmetry on the continuum Dirac field which forbids the mass term. Another way of seeing this is that after integrating out the short-distance fluctuations, if a mass term is generated it can be described in the lattice model as a deformation of the mean-field Ansatz δU_{ij}. Since the short-distance fluctuations are perturbative in nature, the deformation δU_{ij} cannot change the symmetry of the Ansatz $\bar{U}_{ij}$ that describes the ground state, i.e., if $\bar{U}_{ij}$ is invariant under a projective symmetry group, δU_{ij} must be invariant under the same projective symmetry group. One can show that for the possible deformations invariant under the sfL projective symmetry group described by Eq. (117), none of them can generate the mass term for fermions. Thus the masslessness of fermions are protected by the sfL projective symmetry group.

As for the second type of operators which change the flux, Hermele, Senthil, Fisher, et al. (2004) have appealed to a result in conformal field theory which relates the scaling dimension of such operators to the eigenvalues of states on a sphere with a magnetic flux through the surface (Borokhov et al., 2002). This is easily bound by the ground-state energy of $2N$ component Dirac fermions on the sphere which clearly scale as N. Thus the creation of instantons is also irrelevant for sufficiently large N.

As far as the monopole screening argument goes, the fallacy is that in that argument fermions are first integrated out completely in order to derive an effective action for the field ϕ shown in Eq. (153). Then renormalization-group arguments generate a $K(\partial \phi)^2$ term. However, implicit in this procedure is the assumption that fermions are rapidly changing variables compared with the monopoles. The fact that fermions are gapless makes this procedure unreliable. (One could say that the screening argument implicitly assumes mass generation for fermions.) A better approach is to renormalize the monopoles and fermions on the same footing, i.e., let the infrared cutoff length scale for the fermion (L_f) and the monopoles (L_m) approach infinity with a fixed ratio, e.g., $L_f/L_m = 1$. In this case integrating out fermions down to scale L_f will produce an effective action for the U(1) gauge field of the form

$$\frac{g(L_f)}{16\pi} f_{\mu\nu} f^{\mu\nu},$$

where the running coupling constant $g(L_f) \sim L_f$. This in turn generates an interaction between two monopoles separated by a distance r, which is of order $g(L_f)/r$. To calculate such an interaction, we should integrate out all

fermions with wavelength less than r. We find the interaction to be $g(r)/r \sim r^0$, indicating a logarithmic interaction between monopoles. Thus the logarithmic interaction is constantly being rejuvenated and cannot be screened. This can be cast into a renormalization group language and we can see that the flow equation for the coupling constant g is modified from the form used by Herbut and Seradjah (2003). The extra term leads to the conclusion that the instanton fugacity scales to zero and the instanton becomes irrelevant for N larger than a certain critical value.

To summarize, the algebraic spin liquid derived from the sfL *Ansatz* contains a quantum order characterized by the sfL projective symmetry group (117). The sfL projective symmetry group forbids the mass term of fermions. The continuum limit misses such an effect. To capture such an effect by hand, we must drop the mass term in the self-energy in our calculation in the continuum model (Rantner and Wen, 2002). Ignoring the mass term is a way to include the effects of the projective symmetry group in the continuum model. Just like the fermion mass term, we believe that the $K(\partial\phi)^2$ term is also forbidden by the sfL projective symmetry group Eq. (117). Thus we must ignore the screening effect described by the $K(\partial\phi)^2$ term when we consider instantons. We are then assured that instanton effects are irrelevant in the large-N limits. So the algebraic spin liquid exists and is stable at least in the large-N limit. The interacting gapless excitations in the algebraic spin liquid are protected by the sfL projective symmetry group. It is well known that the symmetry can protect gapless Nambu-Goldstone modes. The above example shows that the projective symmetry group and the associated quantum order can also protect gapless excitations (Rantner and Wen, 2002; Wen, 2002b; Wen and Zee, 2002).

XII. APPLICATION OF GAUGE THEORY TO THE HIGH-T_c SUPERCONDUCTIVITY PROBLEM

Now we summarize how gauge-theory concepts described above may be applied to the high-T_c problem. The central observation is that high-T_c superconductivity emerges upon doping a Mott insulator. The antiferromagnetic order of the Mott insulator disappears rather rapidly and is replaced by the superconducting ground state. The "normal" state above the superconducting transition temperature exhibits many unusual properties, which we refer to as pseudogap behavior. How does one describe the simultaneous suppression of the Néel order and the emergence of the pseudogap and the superconductor from the Mott insulator? The approach we take is to first understand the nature of a possible nonmagnetic Mott state at zero doping, the spin-liquid state, which naturally becomes a singlet superconductor when doped. This is the central idea behind the RVB proposal (Anderson, 1987) and is summarized in Fig. 31. The idea is that doping effectively frustrates the Néel order so that the system is pushed across the transition where the Néel order is lost. In the real system, the loss of Néel
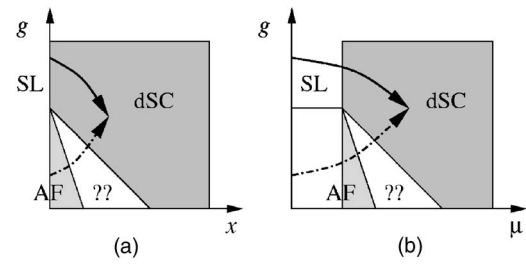

FIG. 31. Schematic zero-temperature phase diagram showing the route between the antiferromagnetic Mott insulator and the *d*-wave superconductor. The vertical axis is labeled by a parameter g, which represents a measure of the frustration in the interaction between the spins in the Mott insulator. AF represents the antiferromagnetically ordered state. SL is a spin-liquid insulator reached by increasing the frustration. The path taken by the cuprate materials as a function of doping x is shown as a dash-dotted line. The question marks represent regions where the physics is not clear at present. Doping the spin liquid naturally leads to the dSC state. The idea behind the spin-liquid approach is to regard the superconducting system at nonzero x as resulting from doping the spin liquid as shown with the solid line, though this is not the path actually taken by the material. (b) Same as in (a) but as a function of chemical potential rather than hole doping. Here the AF includes an insulating and a lightly doped (light shaded) regions.

order may proceed through complicated states, such as incommensurate charge and spin order, stripes, or inhomogeneous charge segregation (Carlson *et al.*, 2003). However, in this direct approach the connection with superconductivity is not at all clear. Instead it is conceptually useful to arrive at the superconducting state via a different path, starting from a spin-liquid state. Recently, Senthil and Lee (2005) have elaborated upon this point of view which we summarize below.

A. Spin liquid, quantum critical point, and the pseudogap

It is instructive to consider the phase diagram as a function of the chemical potential rather than hole doping as shown in Fig. 31(b).

Consider any spin-liquid Mott state that when doped leads to a *d*-wave superconductor. As a function of chemical potential, there will then be a zero-temperature phase transition where the holes first enter the system. For concreteness we refer to this as the Mott transition. The associated quantum critical fixed point will control the physics in a finite nonzero range of parameters. The various crossovers expected near such transitions are well known and are shown in Fig. 32.

Sufficiently close to this zero-temperature critical point many aspects of the physics will be universal. The regime in which such universal behavior is observed will be limited by "cutoffs" determined by microscopic parameters. In particular, we may expect that the cutoff scale is provided by an energy of a fraction of J (the exchange energy for the spins in the Mott insulator). We note that this corresponds to a reasonably high temperature scale.
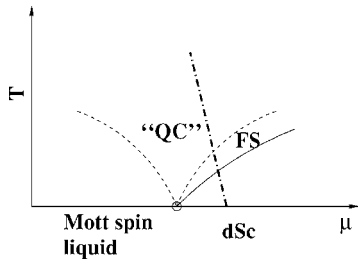
FIG. 32. Schematic phase diagram for a doping-induced Mott transition between a spin-liquid insulator and a d-wave superconductor. The bold dot-dashed line is the path taken by a system at hole density x that has a superconducting ground state. The region marked FS represents the fluctuation regime of the superconducting transition. The region marked QC is the quantum critical region associated with the Mott critical point. It is separated from the Mott spin-liquid state by a crossover line (dashed line). The QC region may be identified with the high-temperature pseudogap phase in the experiments.

Now consider an underdoped cuprate material at fixed doping x. Upon increasing the temperature this will follow a path in Fig. 32 that is shown schematically. The properties of the system along this path may be usefully discussed in terms of the various crossover regimes. In particular it is clear that the normal state above the superconducting transition is to be understood directly as the finite-temperature quantum critical region associated with the Mott transition. Empirically this region corresponds to the pseudogap regime. Thus our assertion is that the pseudogap regime is controlled by the unstable zero-temperature fixed point associated with the (Mott) transition to a Mott insulator.

What are the candidates for the spin-liquid phase? There have been several proposals in the literature. One proposal is the dimer phase (Sachdev, 2003). Strictly speaking, this is a valence-bond solid and not a spin liquid: it is a singlet state which breaks translational symmetry. It was shown by Read and Sachdev (1990) that within the large-N Schwinger boson approach the dimer phase emerges upon disordering the Néel state. Sachdev and collaborators showed that doping the dimer state produces a d-wave superconductor (Vojta and Sachdev, 1999). However, such a superconductor also inherits the dimer order and has a full gap to spin excitations, at least for low doping. As we have seen in this review, there is strong empirical evidence for gapless nodal quasiparticles in the superconducting state. In our view, it is more natural to start with translationally invariant spin-liquid states which produce d-wave superconductors with nodal quasiparticles when doped.

We see from Sec. X that the spin-liquid states are rather exotic in that their excitations are conveniently described in terms of fractionalized spin-1/2 spinon degrees of freedom. We have discussed in Sec. X.G that spin liquids are characterized by their low-energy gauge group. Among spin liquids with nodal fermionic spinons, two versions, the Z_2 and the U(1) spin liquids, have been proposed. The Z_2 gauge theory was advocated by Senthil and Fisher (2000). It can be considered as growing

out of the fermion pairing phase of the U(1) mean-field phase diagram shown in Fig. 21. The pairing of fermions $\Delta_{ij}=\langle f_{i\uparrow}f_{i\downarrow}-f_{i\downarrow}f_{i\uparrow}\rangle$ breaks the U(1) gauge symmetry down to Z_2, i.e., only $f\to -f$ remains unbroken. One feature of this theory is that in the superconducting state hc/e vortices tend to have lower energy than $hc/2e$ vortices, particularly at low doping. We have seen in Sec. IX.C that $hc/2e$ vortices involve suppression of the pairing amplitude $|\Delta_{ij}|$ at the center and cost a large energy of order J. On the other hand, one can form an hc/e vortice by winding the boson phase by 2π, leaving the fermion pairing intact inside the core. Another way of describing this from the point of view of Z_2 gauge theory is that the $hc/2e$ vortex necessarily involves the presence of a Z_2 gauge flux (called a vison by Senthil and Fisher) in its core. The finite-energy cost of the Z_2 flux dominates in the low-doping limit and raises the energy of the $hc/2e$ vortices. Experimental proposals were made (Senthil and Fisher, 2001b) to provide for a critical test of such a theory by detecting the vison excitation or by indirectly looking for signatures of stable hc/e vortices. To date, all such experiments have yielded negative results and have provided fairly tight bounds on the vison energy (Bonn $et\ al.$, 2001).

We are then left with the U(1) spin liquid as the final candidate. The mean-field basis of this state is the staggered flux liquid state of the SU(2) mean-field phase diagram (Fig. 22). The low-energy theory of this state consists of fermions with massless Dirac spectra (nodal quasiparticles) interacting with a U(1) gauge field. Note that this U(1) gauge field refers to the low-energy gauge group and is not to be confused with the U(1) gauge theory in Sec. IX, which refers to the high-energy gauge group in the nomenclature of Sec. X.G. This theory was treated in some detail in Sec. XI. This state has enhanced (π,π) spin fluctuations but no long-range Néel order, and the ground state becomes a d-wave superconductor when doped with holes. As we shall see, a low-energy $hc/2e$ vortex can be constructed, thus overcoming a key difficulty of the Z_2 gauge theory. Furthermore, an objection in the literature about the stability of the U(1) spin liquid has been overcome, at least for sufficiently large N (see Sec. IX.F). It has also been argued by Senthil and Lee (2005) that even if the physical spin-1/2 case does not possess a stable U(1) liquid phase, it can exist as a critical state separating the Néel phase from a Z_2 spin liquid and may still have the desired property of dominating the physics of the pseudogap and the superconducting states. An example of deconfinement appearing at the critical point between two ordered phases was recently pointed out by Senthil $et\ al.$ (2004).

In the next section we shall further explore the properties of the U(1) spin liquid upon doping. We approach the problem from the low-temperature limit and work our way up in temperature. This regime is conveniently described by a nonlinear σ-model effective theory.

B. σ-model effective theory and new collective modes in the superconducting state

Here we attempt to reduce the large number of degrees of freedom in the partition function in Eq. (133) to the few which dominate the low-energy physics. We shall ignore the amplitude fluctuations in the fermionic degrees of freedom, which are gapped on the scale of J. The bosons tend to Bose condense. We shall ignore the amplitude fluctuations and assume that its phase is slowly varying on the fermionic scale, given by $\xi = \epsilon_F/\Delta$ in space. In this case we can have an effective-field theory (σ-model) description in which the local boson phases are slow variables and the fermionic degrees of freedom are assumed to follow them. We begin by picking a mean-field representation $U_{ij}^{(0)}$. The choice of the staggered flux state U_{ij}^{SF} given by Eq. (138) is most convenient because U_{ij}^{SF} commutes with τ^3, making explicit the residual U(1) gauge symmetry, which corresponds to a τ^3 rotation. Thus we choose $U_{ij}^{(0)} = U_{ij}^{\text{SF}} e^{i a_{ij}^3 \tau^3}$ and replace the integral over U_{ij} by an integral over the gauge field a_{ij}^3. It should be noted that any $U_{ij}^{(0)}$ which are related by SU(2) gauge transformations will give the same result. At the mean-field level, bosons form a band with minima at Q_0. Writing $h = \tilde{h} e^{i Q_0 \cdot r}$, we expect $\tilde{h}$ to be slowly varying in space and time. We transform to the radial gauge, i.e., we write

$$\tilde{h}_i = g_i \begin{pmatrix} b_i \\ 0 \end{pmatrix}, \tag{154}$$

where b_i can be taken as real and positive and g_i is a SU(2) matrix parametrized by

$$g_i = \begin{pmatrix} z_{i1} & -z_{i2}^* \\ z_{i2} & z_{i1}^* \end{pmatrix}, \tag{155}$$

where

$$z_{i1} = e^{i\alpha_i} e^{-i\phi_i/2} \cos \frac{\theta_i}{2} \tag{156}$$

and

$$z_{i2} = e^{i\alpha_i} e^{i\phi_i/2} \sin \frac{\theta_i}{2}. \tag{157}$$

We ignore the boson amplitude fluctuations and replace b_i by a constant b_0.

An important feature of Eq. (133) is that L_2 is invariant under the SU(2) gauge transformation,

$$\tilde{h}_i = g_i^\dagger h_i, \tag{158}$$

$$\tilde{\psi}_i = g_i^\dagger \psi_i, \tag{159}$$

$$\tilde{U}_{ij} = g_i^\dagger U_{ij}^{(0)} g_j, \tag{160}$$

and

$$\tilde{a}_{0i}^\ell \tau^\ell = g^\dagger a_{0i}^\ell \tau^\ell g - g(\partial_\tau g^\dagger). \tag{161}$$

Starting from Eq. (133) and making the above gauge transformation, the partition function is integrated over g_i instead of h_i and the Lagrangian takes the form

$$
\begin{aligned}
L_2' = {} & \frac{\tilde{J}}{2} \sum_{\langle ij \rangle} \text{Tr}(\tilde{U}_{ij}^\dagger \tilde{U}_{ij}) + \tilde{J} \sum_{\langle ij \rangle} \psi_i^\dagger \tilde{U}_{ij} \psi_j + \text{c.c.} \\
& + \sum_i \psi_i^\dagger (\partial_\tau - i a_{0i}^\ell \tau^\ell) \psi_i + \sum_i (-i a_{0i}^3 + \mu_B) b_0^2 \\
& - \sum_{ij,\sigma} \tilde{t}_{ij} b_0^2 f_{j\sigma}^\dagger f_{i\sigma}.
\end{aligned}
\tag{162}
$$

We have removed the tilde from $\tilde{\psi}_{i\sigma}$, $\tilde{f}_{i\sigma}$, and $\tilde{a}_0^\ell$ because these are integration variables and $\tilde{t}_{ij} = t_{ij}/2$. Note that g_i appears only in $\tilde{U}_{ij}$. For every configuration $\{g_i(\tau), a_{ij}^3(\tau)\}$ we can, in principle, integrate out fermions and a_0^ℓ to obtain an energy functional. This will constitute the σ-model description. In practice, we can make the slowly varying g_i approximation and solve the local mean-field equation for a_{0i}^ℓ. This was the approach taken by Lee et al. (1998).

The σ model depends on $\{g_i(\tau), a_{ij}^3(\tau)\}$, i.e., it is characterized by α_i, θ_i, and ϕ_i, and the gauge field a_{ij}^3. α_i is the familiar overall phase of the electron operator, which becomes half of the pairing phase in the superconducting state. To help visualize the remaining dependence of freedom, it is useful to introduce the local quantization axis,

$$\boldsymbol{I}_i = z_i^\dagger \boldsymbol{\tau} z_i = (\sin \theta_i \cos \phi_i, \sin \theta_i \sin \phi_i, \cos \theta_i). \tag{163}$$

Note that $\boldsymbol{I}_i$ is independent of the overall phase α_i, which is the phase of the physical electron operator. Then different orientations of $\boldsymbol{I}$ represent different mean-field states in U(1) mean-field theory. This is shown in Fig. 33. For example, $\boldsymbol{I}$ pointing to the north pole corresponds to $g_i = I$ and the staggered flux state. This state has $a_0^3 \neq 0$, $a_0^1 = a_0^2 = 0$, and has small Fermi pockets. It also has orbital staggered currents around the plaquettes. $\boldsymbol{I}$ pointing to the south pole corresponds to the degenerate staggered flux state whose staggered pattern is shifted by one unit cell. On the other hand, when $\boldsymbol{I}$ is in the equator, it corresponds to a d-wave superconductor. Note that the angle ϕ is a gauge degree of freedom and states with different ϕ anywhere along the equator are gauge equivalent. A general orientation of $\boldsymbol{I}$ corresponds to some combination of d-wave superconductor and staggered flux.

At zero doping, all orientations of $\boldsymbol{I}$ are energetically the same. This symmetry is broken by doping and the $\boldsymbol{I}$ vector has a small preference to lie on the equator. At low temperature, there is a phase transition to a state where $\boldsymbol{I}$ lies on the equator, i.e., the d-superconductor ground state. It is possible to carry out a small expansion about this state and explicitly work out the collective modes (Lee and Nagaosa, 2003). In an ordinary superconductor, there is a single complex order parameter Δ and we expect an amplitude mode and a phase mode.
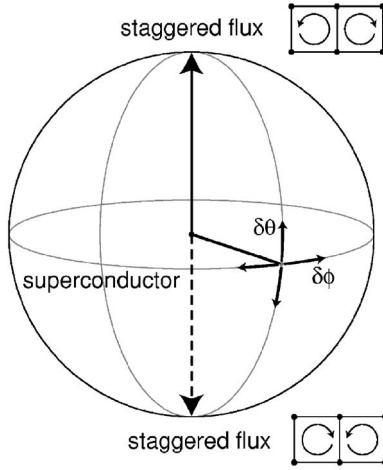
FIG. 33. The quantization axis I in the SU(2) gauge theory. The north and south poles correspond to the staggered-flux phases with shifted orbital current patterns. All points on the equators are equivalent and correspond to the d-wave super-conductor. In the superconducting state one particular direction is chosen on the equator. There are two important collective modes. The θ modes correspond to fluctuations in the polar angle $\delta\theta$ and the ϕ gauge mode to a spatially varying fluctuation in $\delta\phi$.

For a charged superconductor, the phase mode is pushed up to the plasma frequency and one is left with the amplitude mode only. In gauge theory we have, in addition to Δ_{ij}, the order parameter χ_{ij}. Thus it is natural to expect additional collective modes. From Fig. 33 we see that two modes of special interest are those corresponding to small θ and ϕ fluctuations. Physically the θ mode corresponds to local fluctuations of the staggered-flux states which generate local orbital current fluctuations. These currents generate a small magnetic field (estimated to be ~ 10 G) which couples to neutrons. Lee and Nagaosa (2003) have predicted a peak in the neutron-scattering cross section at (π, π), at energy just below $2\Delta_0$, where Δ_0 is the maximum d-wave gap. This is in addition to the resonance mode discussed in Sec. III.B, which is purely spin fluctuation in origin. The orbital origin of this mode can be distinguished from the spin fluctuation by its distinct form factor (Hsu *et al.*, 1991; Chakravarty, Kee, and Nayak, 2002).

The ϕ mode is more subtle because ϕ is the phase of a Higgs field, i.e., it is part of the gauge degrees of freedom. It turns out to correspond to a relative oscillation of the amplitudes of χ_{ij} and Δ_{ij} and is again most prominent at (π, π). Since $|\chi_{ij}|$ couples to the bond density fluctuation, inelastic Raman scattering is the tool of choice for studying this mode once the technology reaches the requisite 10-meV energy resolution. Lee and Nagaosa (2003) have pointed out that due to the special nature of the buckled layers in LSCO this mode couples to photons and may show up as a transfer of spectral weight from a buckling phonon to a higher frequency peak. Such a peak was reported experimentally (Kuz-menko *et al.*, 2003), but it is apparently not unique to

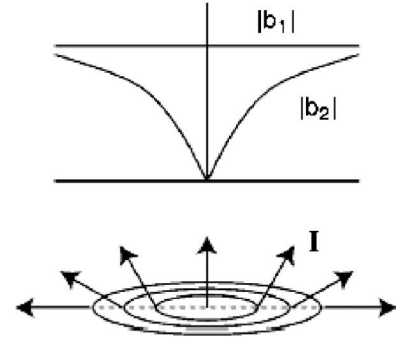
FIG. 34. Structure of the superconducting vortex. Top: b_1 is constant while b_2 vanishes at the center and its phase winds by 2π. Bottom: The isospin quantization axis points to the north pole at the center and rotates towards the equatorial plane as one moves out radially. The pattern is rotationally symmetric around the $\hat{z}$ axis.

LSCO as the theory would predict, and hence its interpretation remains unclear at this point.

From Fig. 33 it is clear that the σ-model representation of SU(2) gauge theory is a useful way of parametrizing the myriad U(1) mean-field states which become almost degenerate for small doping. The low-temperature d-superconducting phase is the ordered phase of the σ model, while in the high-temperature limit we expect the I vector to be disordered in space and time, to the point at which the σ-mode approach fails and one crosses over to the SU(2) mean-field description. The disordered phase of the σ model then corresponds to the pseudogap phase. How does this phase transition take place? It turns out that the destruction of superconducting order proceeds via the usual route of the Berezinskii-Kosterlitz-Thouless proliferation of vortices. To see how this comes about in the σ-model description, we have to first understand the structure of vortices.

C. Vortex structure

The σ-model picture leads to a natural model for a low-energy $hc/2e$ vortex (Lee and Wen, 2001). It takes advantage of the existence of two kinds of bosons, b_1 and b_2, with opposite gauge charges but with the same coupling to electromagnetic fields. Far away from the vortex core, $|b_1| = |b_2|$ and b_1 has constant phase while b_2 winds its phase by 2π around the vortex. As the core is approached $|b_2|$ must vanish in order to avoid a divergent kinetic energy, as shown in Fig. 34 (top). The quantization axis I provides a nice way to visualize this structure [Fig. 34 (bottom)]. It smoothly rotates to the north pole at the vortex core, indicating that at this level of approximation the core consists of the staggered flux state. The azimuthal angle winds by 2π as we go around the vortex. It is important to remember that I parametrizes only the internal gauge degrees of freedom θ and ϕ and the winding of ϕ by 2π is different from the usual winding of the overall phase α by π in an $hc/2e$ vortex. To better understand the phase winding we use the fol-

lowing continuum model for the phase θ_1, θ_2 of b_1 and b_2, valid far away from the core:

$$D = \int d^2x \frac{K}{2}[(\nabla\theta_1 - \boldsymbol{a} - \boldsymbol{A}) + (\nabla\theta_2 + \boldsymbol{a} - \boldsymbol{A})^2] + \cdots,$$

(164)

where $\boldsymbol{a}$ stands for the continuum version of a_{ij}^3 in the last section, and $\boldsymbol{A}$ is the electromagnetic field (e/c has been set to be unity). We now see that the $hc/2e$ vortex must contain a half-integer vortex of the $\boldsymbol{a}$ gauge flux with an opposite sign. Then θ_1 sees zero flux while θ_2 sees 2π flux, consistent with the windings chosen in Fig. 34. This vortex structure has low energy for small x because the fermion degrees of freedom remain gapped in the core and one does not pay the fermionic energy of order J as in U(1) gauge theory. Physically, the above description takes advantage of the states with almost degenerate energies (in this case the staggered flux state), which is guaranteed by the SU(2) symmetry near half-filling. There is direct evidence from STM tunneling that the energy gap is preserved in the core (Maggio-Aprile *et al.*, 1995; Pan *et al.*, 2000). This is in contrast to theoretical expectations for conventional *d*-wave vortex cores in which a large resonance is expected to fill in the gap in the tunneling spectra (Wang and MacDonald, 1995).

We can clearly reverse the roles of b_1 and b_2 to produce another vortex configuration which is degenerate in energy. In this case $\boldsymbol{I}$ in Fig. 34 points to the south pole. These configurations are sometimes referred to as merons (half of a hedgehog) and the two halves can tunnel to each other via the appearance of instantons in space-time. The time scale of the tunneling event is difficult to estimate, but should be considerably less than J. Depending on the time scale, the orbital current of the staggered flux state in the core generates a physical staggered magnetic field which may be experimentally observable by NMR (almost static), muon spin rotation (intermediate time scale), and neutron scattering (short time scale). The experiment must be performed in a large magnetic field so that a significant fraction of the area consists of vortices and the signal of the staggered field should be proportional to H. A muon spin rotation experiment on underdoped YBCO has detected such a field-dependent signal with a local field of ± 18 G (Miller *et al.*, 2002). However, muon spin rotation is not able to determine whether the field has an orbital or spin origin and this experiment is only suggestive, but by no means definitive proof of orbital currents in the vortex core. In principle, neutron scattering is a more definitive probe because one can use the form factor to distinguish between orbital and spin effects. However, due to the small expected intensity, neutron scattering has so far not yielded any definite results.

As discussed in Sec. XI.E, we expect enhanced (π, π) fluctuations to be associated with the staggered flux liquid phase. Indeed, the staggered-flux liquid state is our route to Néel order and if gauge fluctuations are large, we may expect to have quasistatic Néel order inside the vortex core. Experimentally, there are reports of enhanced spin fluctuations in the vortex core by NMR experiments (Curro *et al.*, 2000; Mitrovic *et al.*, 2001; Kakuyanagi *et al.*, 2002; Mitrovic *et al.*, 2003). There are also reports of the static incommensurate spin order forming a halo around the vortex in the LSCO family (Kitano *et al.*, 2000; Lake *et al.*, 2001, 2002; Khaykovich *et al.*, 2002). One possibility is that these halos are the condensation of preexisting soft incommensurate modes known to exist in LSCO, driven by quasistatic Néel order inside the core. We emphasize that the staggered-flux liquid state is our way of producing antiferromagnetic order starting from microscopies and hence is fully consistent with the appearance of static or dynamical antiferromagnetism in the vortex core. Our hope is that gauge fluctuations (including instanton effects) are sufficiently reduced in doped systems to permit a glimpse of the staggered orbital current. The detection of such current fluctuations will be a strong confirmation of our approach.

Finally, we note that the orbital current does not show up directly in STM experiments, which are sensitive to the local density of states. Kishine *et al.* (2002) have considered the possibility of interference between Wannier orbitals on neighboring lattice sites, which could lead to modulations of STM signal between lattice positions. STM experiments have detected 4×4 modulated patterns in the vortex core region and also in certain underdoped regions. Such patterns appear to require density modulations which are in addition to our vortex model.

D. Phase diagram

We can now construct a phase diagram of underdoped cuprates starting from the *d*-wave superconductor ground state at low temperatures. The vortex structure allows us to unify the σ-model picture with the conventional picture of the destruction of superconducting order in two dimensions, i.e., the Berezinskii-Kosterlitz-Thouless transition via the unbinding of vortices. The σ model contains, in addition to the pairing phase 2α, the phases θ and ϕ. However, we have seen in Sec. XII.C that a particular configuration of θ and ϕ is favored inside the vortex core. SU(2) gauge theory provides a mechanism for cheap vortices, which are necessary for a Berezinskii-Kosterlitz-Thouless description, as discussed in Sec. V.B. If the core energy is too large, the system will behave like a superconductor on any reasonable length scale above T_{BKT}, which is not in accord with experiment. On the other hand, if the core energy is small compared with T_c, vortices will proliferate rapidly. They overlap and lose their identity. As discussed in Sec. V.B, there is strong experimental evidence that vortices survive over a considerable temperature range above T_c. These experiments require the vortex core energy to be cheap, but not too cheap, i.e., of the order of T_c. Honerkamp and Lee (2004) have attempted a microscopic modeling of the proliferation of vortices. They assume a staggered-flux core and estimate the energy
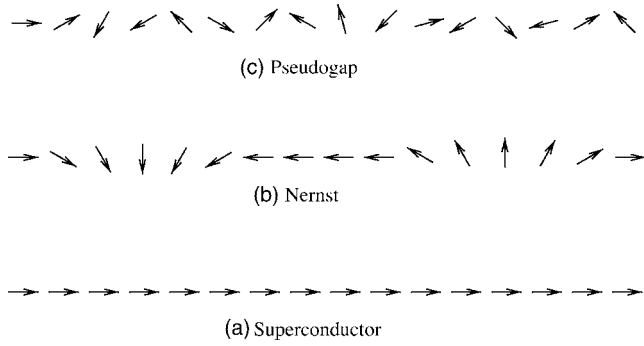
(c) Pseudogap

(b) Nernst

(a) Superconductor

FIG. 35. Schematic picture of the quantization axis I in different parts of the phase diagram shown in Fig. 18. (a) In the superconducting phase I is ordered in the x-y plane. (b) In the Nernst phase, I points to the north or south pole inside the vortex core. (c) The pseudogap corresponds to a completely disordered arrangement of I. (I is a three-dimensional vector and only a two-dimensional projection is shown.)

from projected wave-function calculations. They found that there is a large range of temperatures above the Berezinskii-Kosterlitz-Thouless transition where vortices grow in number but still maintain their identity. This forms a region in the phase diagram which may be called the Nernst region as shown in Fig. 18. The corresponding picture of the I-vector fluctuation is shown in Fig. 35. Above the Nernst region the I vector is strongly fluctuating and is almost isotopic. This is the strongly disordered phase of the σ model. The vortices have lost their identity and indeed the σ-model description, which assumes well-defined phases of b_1 and b_2, begins to break down. Nevertheless, the energy gap associated with fermions remains. This is the pseudogap part of the phase diagram in Fig. 18. In SU(2) gauge theory this is understood as the U(1) spin liquid. There is no order parameter associated with this phase, as fluctuations including staggered orbital currents and d-wave pairing become short range. Is there a way to characterize this state of affairs other than the term spin liquid? This question is addressed in the next section.

E. Signature of the spin liquid

Senthil and Lee (2005) have pointed out that if the pseudogap region is controlled by the U(1) spin-liquid fixed point, it is possible to characterize this region in a certain precise way. The spin liquid is a deconfined state, meaning that instantons are irrelevant. Then the U(1) gauge flux is a conserved quantity. Unfortunately, it is not clear how to couple to this gauge flux using conventional probes. We note that the flux associated with the a^3 gauge field is different from the U(1) gauge flux considered in Sec. IX, which had the meaning of spin chirality. In the case in which bosons are locally condensed and their local phase is well defined, it is possible to identify the gauge flux in terms of the local phase variables. The gauge magnetic field B is given by

$$B = (\nabla \times a^3)_z = \frac{1}{2}\hat{n} \cdot \partial_x \hat{n} \times \partial_y \hat{n}, \qquad (165)$$

where

$$\hat{n} = (\sin\theta\cos\alpha, \sin\theta\sin\alpha, \cos\theta),$$

with θ and α defined in Eq. (156). Note that the azimuthal angle associated with $\hat{n}$ is now the pairing phase α, in contrast with the vector I we considered earlier. The gauge flux is thus related to the local pairing and staggered-flux order as

$$B = \frac{1}{2}(\nabla\hat{n}_z \times \nabla\alpha)_z, \qquad (166)$$

and it is easily checked that the vortex structure described in Sec. XII.C contains a half-integer gauge flux.

In the superconducting state the gauge flux is localized in the vortex core and fluctuations between ±half-integer vortices are possible via instantons because the instanton action is finite. The superconductor is in a confined phase as far as the U(1) gauge field is concerned. As the temperature is raised towards the pseudogap phase this gauge field leaks out of the vortex cores and begins to fluctuate homogeneously.

The asymptotic conservation of the gauge flux at the Mott transition fixed point potentially provides some possibilities for its detection. At nonzero temperatures in nonsuperconducting regions, flux conservation is only approximate (as the instanton fugacity is small but nonzero). Nevertheless, at low enough temperatures the conserved flux will propagate diffusively over a long range of length and time scales. Thus there should be an extra diffusive mode that is present at low temperatures in the nonsuperconducting state. It is, however, not clear at present how to design a probe that will couple to this diffusive mode.

Alternately the vortex structure described above provides a useful way to create and then detect the gauge flux in the nonsuperconducting normal state. We first describe this by ignoring the instantons completely in the normal state. The effects of instantons will then be discussed.

Consider first a large disk of cuprate material where the doping level changes as a function of the radial distance from the center, as shown in Fig. 36. The outermost annulus has the largest doping x_1. The inner annulus has a lower doping level x_2. The rest of the sample is at a doping level $x_3 < x_2 < x_1$. The corresponding transition temperatures $T_{c1,2,3}$ will be such that $T_{c3} < T_{c2} < T_{c1}$. We also imagine that the thickness $\Delta R_o, \Delta R_i$ of the outer and inner annuli are both much smaller than the penetration depth for the physical vector potential A. The penetration depth of the internal gauge field a is expected to be small and we expect it will be smaller than $\Delta R_o, \Delta R_i$. We also imagine that the radius of this inner annulus R_i is a substantial fraction of the radius R_o of the outer annulus.

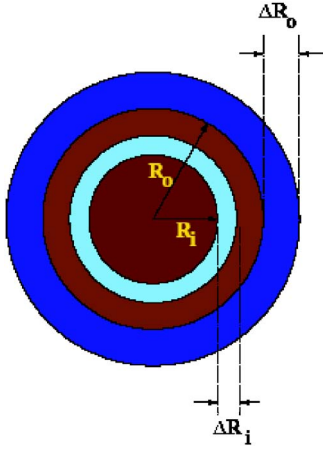Now consider the following set of operations on such a sample.

FIG. 36. (Color online) Structure of the sample needed for the proposed experiment. The outer annulus (in dark blue) has the highest T_c. The inner annulus (in light blue) has a smaller T_c. The rest of the sample (in brown) has even smaller T_c.

(i) First cool in a magnetic field to a temperature T_{in} such that $T_{c2} < T_{in} < T_{c1}$. The outer ring will then go superconducting while the rest of the sample stays normal. In the presence of the field the outer ring will condense into a state in which there is a net vorticity ongoing around the ring. We are interested in the case where this net vorticity is an odd multiple of the basic $hc/2e$ vortex. If, as assumed, the physical penetration depth is much bigger than the thickness ΔR_o, then the physical magnetic flux enclosed by the ring will not be quantized.

(ii) Now consider turning off the external magnetic field. The vortex present in the outer superconducting ring will stay (manifested as a small circulating persistent current) and will give rise to a small magnetic field. As explained above if the vorticity is odd, then it must be associated with a flux of the internal gauge field that is $\pm \pi$. This internal gauge flux must be in the inner "normal" region of the sample with very small penetration into the outer superconducting ring. It will spread out evenly over the full inner region. We have thus managed to create a configuration with a nonzero internal gauge flux in the nonsuperconducting state.

(iii) How do we detect the presence of this internal gauge flux? For that imagine now cooling the sample further to a temperature T_{fin} such that $T_{c3} < T_{fin} < T_{c2}$. Then the inner ring will also go superconducting. This is due to the condensation of the two boson species $b_{1,2}$. But this condensation occurs in the presence of some internal gauge flux. When bosons $b_{1,2}$ condense in the inner ring, they will do so in a manner that quantizes the internal gauge flux enclosed by this inner ring into an integer multiple of π. If, as assumed, the inner radius is a substantial fraction of the outer radius, then the net internal gauge flux will prefer the quantized values $\pm \pi$ rather than be zero (see below). However, configurations of the inner ring that enclose the quantized internal gauge flux of $\pm \pi$ also necessarily contain a physical vortex that is an odd multiple of $hc/2e$. With the thickness of the inner ring being smaller than the physical penetra-

tion depth, most of the physical magnetic flux will escape. There will still be a small residual physical flux due to the current in the inner ring associated with the induced vortex. This residual physical magnetic flux can then be detected.

Note that the sign of the induced physical flux is independent of the sign of the initial magnetic field. Furthermore, the effect is obtained only if the initial vorticity in the outer ring is odd. If, on the other hand, the initial vorticity is even, the associated internal gauge flux is zero and there will be no induced physical flux when the inner ring goes superconducting.

The preceding discussion ignores any effects of instantons. In contrast to a bulk vortex in the superconducting state, the vortices in the setup above have macroscopic cores. The internal gauge flux is therefore distributed over a region of macroscopic size. Consequently, if instantons are irrelevant at long scales in the normal state, their rate may be expected to be small. At any nonzero temperature (as in the proposed experiment) there will be a nonzero instanton rate which will be small for small temperature.

When such instantons are allowed the internal gauge flux created in the sample after step (ii) will fluctuate between the values $+\pi$ and $-\pi$. However, so long as the time required to form the physical vortex in step (iii), which we expect to be a short electronic time scale, is much shorter than the inverse of the instanton rate, we expect that the effect will be seen. Since the cooling is assumed to be slow enough that the system always stays in equilibrium, the outcome of the experiment is determined by thermodynamic considerations. Senthil and Lee (2005) have estimated the various energies of the operation and have concluded that for sample diameters under a micron and sufficiently low temperatures ($=10$ K) such an experiment may be feasible.

XIII. SUMMARY AND OUTLOOK

In this review we have summarized a large body of work which views high-temperature superconductivity as the problem of the doping of a Mott insulator. We have argued that the t-J model, supplemented by t' terms, contains the essence of the physics. We offer as evidence numerical work based on the projected trial wave functions, which correctly predicts the d-wave-pairing ground state and a host of properties such as the superfluid density and the quasiparticle spectral weight and dispersion. Analytic theory hinges on the treatment of the double occupation constraint. The redundancy in the representations used to enforce the constraint naturally leads to various gauge theories. We argue that with doping the gauge theory may be in a deconfined phase, in which case the slave boson and fermion degrees of freedom, which were introduced as mathematical devices, take on a physical meaning in that they are sensible starting points for describing physical phenomena. In the deconfined phase the coupling to gauge fluctuations is still of order unity and approximation schemes (such as large-N expansion) are needed to

calculate physical properties such as spin correlation and the electron spectral function. These results qualitatively capture the physics of the pseudogap phase, but certainly not at a quantitative level. Nevertheless, our picture of the vortex structure and how it proliferates gives us a reasonable account of the phase diagram and the onset of T_c.

One direction of future research is to refine the treatment of the low-energy effective model, i.e., fermions and bosons coupled to gauge fields, and attempt a more detailed comparison with experiments such as photoemission line shapes, etc. On the other hand, it is worthwhile to step back and take a broader perspective. What is really new and striking about the high-temperature superconductors is the strange "normal" metallic state for underdoped samples. The carrier density is small and the Fermi surface is broken up by the appearance of a pseudogap near $(0,\pi)$ and $(\pi,0)$, leaving a Fermi arc near the nodal points. All this happens without the doubling of the unit cell via breaking translational or spin-rotational symmetry. How this state comes into being in a lightly doped Mott insulator is the crux of the problem. We can distinguish between two classes of answers. The first, perhaps more conventional one, postulates the existence of a symmetry-breaking state which gaps the Fermi surface and further assumes that thermal fluctuations prevent this state from ordering. A natural candidate for the state is the superconducting state itself. However, it now appears that phase fluctuations of a superconductor can explain the pseudogap phenomenon only over a relatively narrow temperature range, which we have called the Nernst regime. Alternatively, a variety of competing states which have nothing to do with superconductivity have been proposed, often on a phenomenological level, as producing the pseudogap. We refer to this as the thermal explanation of the pseudogap.

A second class of answer, which we refer to as the quantum explanation, proposes that the pseudogap is connected with a fundamentally new quantum state. Thus despite its appearance at high temperatures it is argued that it is a high-frequency phenomenon which is best understood quantum mechanically. The gauge theory reviewed here belongs to this class and views the pseudogap state as derived from a new state of matter, the quantum spin-liquid state. The spin-liquid state is connected to the Néel state at half-filling by confinement. At the same time, with doping a d-wave superconducting ground state is naturally produced. We argue that rather than considering the cuprate as evolving directly from the antiferromagnet to the superconductor, it is better conceptually to start from the spin-liquid state and consider how the antiferromagnet and superconductivity develop from it. In this view the pseudogap is the closest we can get to obtaining a glimpse of the spin liquid, which up to now is unstable in the square-lattice t-J model.

Is there a "smoking gun" signature to prove or disprove the validity of this line of theory? Our approach is to make specific predictions as much as possible in the hope of stimulating experimental work. This is the reason we place emphasis on the staggered flux liquid with its orbital current fluctuations. It is a unique signature which may be experimentally detectable. Our predictions range from new collective modes in the superconducting state to quasistatic order in the vortex core. Unfortunately, the physical manifestation of the orbital current is a very weak magnetic field, which is difficult to detect, and to date we have not found experimental verification. Besides orbital current, we also propose an experiment involving flux generation in a special geometry. This experiment addresses the fundamental issue of the quantum spin liquid as the origin of the pseudogap phase.

The pseudogap metallic state is so strange that at the beginning it is not clear if a microscopic description is even possible. So the microscopic description provided by the SU(2) slave-boson theory, although still relatively qualitative, represents important progress and leads to some deep insights. A key finding is that the parent spin liquid is a new state of matter that cannot be described by Landau's symmetry-breaking theory. The description of the parent spin liquid, such as the SU(2) slave-boson theory, must involve gauge theory. Even if one starts with an ordered phase and later uses quantum fluctuations to restore the symmetry, the resulting description of the symmetry-restored state, if found, appears to always contain gauge fields (Wu *et al.*, 1998). Thus the appearance of the gauge field in the quantum description of the pseudogap metal is not a mathematical artifact of the slave-boson theory. It is a consequence of a new type of correlation in those states. The new type of correlation represents a new type of order (Wen, 2002b), which makes those states different from the familiar states described by Landau's symmetry-breaking theory.

From this perspective, the study of high-temperature superconductivity may have a much broader and deeper impact than merely understanding high-temperature superconductivity. Such a study is actually a study of new states of matter. It represents our entry into a new exciting world that lies beyond Landau's world of symmetry breaking. Hopefully the new states of matter will be discovered in some materials other than high-temperature superconductors. The slave-boson theory and the resulting gauge theory developed for high-temperature superconductivity may be useful for these new states of matter once they are discovered in experiments. [Examples of these new states of matter have already been discovered in many theoretical toy models (Moessner and Sondhi, 2001; Balents *et al.*, 2002; Kitaev, 2003; Wen, 2003c).] At the moment, gauge theory is the only known language for describing this new state of affairs. We believe the introduction of this subject to condensed-matter physics has enriched the field and will lead to many interesting further developments.

ACKNOWLEDGMENTS

REFERENCES

Abanov, A., A. Chubukov, M. Esehig, M. Norman, and J. Schmalian, 2002, Phys. Rev. Lett. **89**, 177002.

Aeppli, G., T. Mason, S. Hayden, and H. Mook, 1995, J. Phys. Chem. Solids **56**, 1911.

Affleck, I., and J. B. Marston, 1988, Phys. Rev. B **37**, 3774.

Affleck, I., Z. Zou, T. Hsu, and P. W. Anderson, 1988, Phys. Rev. B **38**, 745.

Alloul, H., T. Ohno, and P. Mendels, 1989, Phys. Rev. Lett. **63**, 1700.

Andersen, O. K., *et al.*, 1996, J. Low Temp. Phys. **105**, 285.

Anderson, P. W., 1973, Mater. Res. Bull. **8**, 153.

Anderson, P. W., 1987, Science **235**, 1196.

Anderson, P. W., 1997, *The Theory of Superconductivity in the High T_c Cuprates* (Princeton University Press, Princeton).

Anderson, P. W., M. Randeria, T. Rice, N. Trivedi, and F. Zhang, 2004, J. Phys.: Condens. Matter **16**, R755.

Armitage, N. P., *et al.*, 2001, Phys. Rev. Lett. **87**, 147003.

Arovas, D., J. R. Schrieffer, and F. Wilczek, 1984, Phys. Rev. Lett. **53**, 722.

Arovas, D. P., and A. Auerbach, 1988, Phys. Rev. B **38**, 316.

Arovas, D. P., A. Berlinsky, C. Kallin, and S.-C. Zhang, 1997, Phys. Rev. Lett. **79**, 2871.

Assaad, F., 2005, Phys. Rev. B **71**, 075103.

Balents, L., M. P. A. Fisher, and S. M. Girvin, 2002, Phys. Rev. B **65**, 224412.

Balents, L., M. P. A. Fisher, and C. Nayak, 1998, Int. J. Mod. Phys. B **12**, 1033.

Banks, T., R. Myerson, and J. B. Kogut, 1977, Nucl. Phys. B **129**, 493.

Barnes, S. E., 1976, J. Phys. F: Met. Phys. **6**, 1375.

Baskaran, G., and P. Anderson, 1998, J. Phys. Chem. Solids **59**, 1780.

Baskaran, G., and P. W. Anderson, 1988, Phys. Rev. B **37**, 580.

Baskaran, G., Z. Zou, and P. W. Anderson, 1987, Solid State Commun. **63**, 973.

Basov, D. N., A. Puchkov, R. Hughes, T. Strach, J. Preston, T. Timusk, D. Bonn, R. Liang, and W. Hardy, 1994, Phys. Rev. B **49**, 12165.

Basov, D. N., and T. Timusk, 2005, Rev. Mod. Phys. **77**, 721.

Bednorz, J. G., and K. A. Müller, 1986, Z. Phys. B: Condens. Matter **64**, 189.

Benfatto, L., S. Capara, C. Castellani, A. Paramekanti, and M. Randeria, 2001, Phys. Rev. B **63**, 174513.

Berezinskii, V. L., 1971, Sov. Phys. JETP **61**, 1144.

Bonn, D. A., J. Wynn, B. W. Gardner, R. Liang, W. Hardy, J. Kirtley, and K. Moler, 2001, Nature (London) **414**, 887.

Bonn, D. A., *et al.*, 1996, Czech. J. Phys. **46**, 3195.

Boris, A. V., N. N. Kovaleva, O. V. Dolgov, T. Holden, C. T. Lin, B. Keimer, and C. Berkhard, 2204, Science **304**, 708.

Borokhov, V., A. Kapustin, and X. Wu, 2002, J. High Energy Phys. 11, 49.

Bourges, P., Y. Sidis, H. Fong, L. Regnault, J. Bossy, A.

Ivanov, and B. Keimer, 2000, Science **288**, 1234.

Boyce, B. R., J. Skinta, and T. Lemberger, 2000, Physica C **341-348**, 561.

Brinckmann, J., and P. Lee, 2001, Phys. Rev. B **65**, 014502.

Brinckmann, J., and P. A. Lee, 1999, Phys. Rev. Lett. **82**, 2915.

Brinckmann, J., and P. A. Lee, 2002, Phys. Rev. B **65**, 014502.

Broun, D. M., P. J. Turner, W. Huttema, S. Ozcan, B. Morgan, R. Liang, W. N. Hardy, and D. A. Bonn, 2005, e-print cond-mat/0509223.

Bulut, N., and D. Scalapino, 1996, Phys. Rev. B **53**, 5149.

Campuzano, J. C., M. Norman, and M. Randeria, 2003, in *Physics of Conventional and Unconventional Superconductors*, edited by K. H. Bennemann and J. B. Ketterson (Springer, Berlin).

Campuzano, J. C., *et al.*, 1999, Phys. Rev. Lett. **83**, 3709.

Carlson, E. W., V. Emery, S. Kivelson, and D. Orgad, 2003, in *Physics of Conventional and Unconventional Superconductors*, edited by K. H. Bennemann and J. B. Ketterson (Springer, Berlin).

Carlson, E. W., S. Kivelson, V. Emery, and E. Manousakis, 1999, Phys. Rev. Lett. **83**, 612.

Castellani, C., C. D. Castro, and M. Grilli, 1997, Z. Phys. B: Condens. Matter **103**, 137.

Chakraborty, B., N. Read, C. Kane, and P. A. Lee, 1990, Phys. Rev. B **42**, 4819.

Chakravarty, S., H. Kee, and C. Nayak, 2002, Int. J. Mod. Phys. B **16**, 3140.

Chakravarty, S., R. B. Laughlin, D. K. Morr, and C. Nayak, 2002, Phys. Rev. B **64**, 094503.

Chen, H.-D., S. Caponi, F. Alet, and S.-C. Zhang, 2004, Phys. Rev. B **70**, 024516.

Cheong, S.-W., G. Aeppli, T. E. Mason, H. Mook, S. M. Hayden, P. C. Canfield, Z. Fisk, K. N. Clausen, and J. L. Martinez, 1991, Phys. Rev. Lett. **67**, 1791.

Chiao, M., R. Hill, C. Lupien, L. Taillefer, P. Lambert, R. Gagnon, and P. Fournier, 2000, Phys. Rev. B **62**, 3554.

Chien, T. R., Z. Wang, and N. Ong, 1991, Phys. Rev. Lett. **67**, 2088.

Christensen, N. B., D. McMorrow, H. Ronnow, B. Lake, S. Hayden, G. Aeppli, T. Perring, M. Mangkorntong, M. Nohara, and H. Tagaki, 2004, Phys. Rev. Lett. **93**, 147002.

Coldea, R., S. Hayden, G. Aeppli, T. Perrig, C. Frost, T. Mason, S. Cheong, and Z. Fisk, 2001, Phys. Rev. Lett. **86**, 5377.

Coleman, P., 1984, Phys. Rev. B **29**, 3035.

Cooper, S. L., D. Reznik, A. Kotz, M. A. Karlow, R. Liu, M. V. Klein, W. C. Lee, J. Giapintzakis, D. M. Ginsberg, B. W. Veal, and A. P. Paulikas, 1993, Phys. Rev. B **47**, 8233.

Corson, J., R. Mallozzi, J. Orenstein, J. Eckstein, and I. Bozovic, 1999, Nature (London) **398**, 221.

Corson, J., J. Orenstein, S. Oh, J. O'Donnell, and J. Eckstein, 2000, Phys. Rev. Lett. **85**, 2569.

Curro, N. J., T. Imai, C. Slichter, and B. Dabrowski, 1997, Phys. Rev. B **56**, 877.

Curro, N. J., C. Milling, J. Haase, and C. Slichter, 2000, Phys. Rev. B **62**, 3473.

D'Adda, A., P. D. Vecchia, and M. Lüscher, 1978, Nucl. Phys. B **146**, 63.

Dagotto, E., 1994, Rev. Mod. Phys. **66**, 763.

Dagotto, E., E. Fradkin, and A. Moreo, 1988, Phys. Rev. B **38**, 2926.

Dagotto, E., A. Moreo, K. Ortolani, D. Poilblanc, and J. Riera, 1992, Phys. Rev. B **45**, 10741.

Damascelli, A., Z. Hussin, and Z.-X. Shen, 2003, Rev. Mod.

Phys. **75**, 473.

Demler, E., S. Sachdev, and Y. Zhang, 2001, Phys. Rev. Lett. **87**, 067202.

Demler, E., and S.-C. Zhang, 1995, Phys. Rev. Lett. **75**, 4126.

Ding, H., T. Yokoya, J. Campuzano, T. T. Takahashi, M. Randeria, M. Norman, T. Mochiku, and J. Giapintzakis, 1996, Nature (London) **382**, 51.

Ding, H. O., and M. Makivic, 1991, Phys. Rev. B **43**, 3562.

Durst, A. C., and P. A. Lee, 2000, Phys. Rev. B **62**, 1270.

Emery, V. J., 1983, J. Phys. (Paris), Colloq. **44**, 1115.

Emery, V. J., 1986, Synth. Met. **13**, 21.

Emery, V. J., 1987, Phys. Rev. Lett. **58**, 3759.

Emery, V. J., and S. Kivelson, 1995, Nature (London) **374**, 434.

Fazekas, P., and P. Anderson, 1974, Philos. Mag. **30**, 432.

Feng, D. L., *et al.*, 2000, Science **289**, 277.

Foerster, D., 1979, Phys. Lett. **87B**, 87.

Fong, H. F., B. Keiman, P. Anderson, D. Reznik, F. Dogan, and I. Aksay, 1995, Phys. Rev. Lett. **75**, 316.

Fradkin, E., 1991, *Field Theories of Condensed Matter Systems* (Addison-Wesley, Reading, MA).

Fradkin, E., and S. H. Shenker, 1979, Phys. Rev. D **19**, 3682.

Franz, M., T. Pereg-Barnea, D. E. Sheehy, and Z. Tesanovic, 2003, Phys. Rev. B **68**, 024508.

Franz, M., and Z. Tesanovic, 2001, Phys. Rev. Lett. **87**, 257003.

Franz, M., Z. Tesanovic, and O. Vafek, 2002, Phys. Rev. B **66**, 054535.

Fujita, M., H. Goka, K. Yamada, J. Tranquada, and L. Regnault, 2004, Phys. Rev. B **70**, 104517.

Fukuyama, H., 1992, Prog. Theor. Phys. Suppl. **108**, 287.

Ginzberg, D. M., 1989, *Physical Properties of High Temperature Superconductors* (World Scientific, Singapore).

Gliozzi, F., T. Regge, and M. A. Virasoro, 1979, Phys. Lett. **81B**, 178.

Greiter, M., 1997, Phys. Rev. Lett. **79**, 4898.

Gros, C., 1988, Phys. Rev. B **38**, 931.

Gros, C., 1989, Ann. Phys. (N.Y.) **189**, 53.

Gweon, G.-H., T. Sasagawa, S. Y. Zhou, J. Graf, H. Takagi, D.-H. Lee, and A. Lanzara, 2004, Nature (London) **430**, 187.

Hanaguri, T., C. Lupien, Y. Kohsaka, D.-H. Lee, M. Azuma, M. Takano, H. Takagi, and J. Davis, 2004, Nature (London) **430**, 1001.

Hayden, S. M., H. Mook, P. Dau, T. Perrig, and F. Dogan, 2004, Nature (London) **429**, 531.

Heeb, E. S., and T. M. Rice, 1993, Z. Phys. B: Condens. Matter **90**, 73.

Herbut, I. F., and B. Seradjah, 2003, Phys. Rev. Lett. **91**, 171601.

Herbut, I. F., B. Seradjah, S. Sachdev, and G. Murthy, 2003, Phys. Rev. B **68**, 195110.

Hermele, M., T. Senthil, and M. P. A. Fisher, 2005, Phys. Rev. B **72**, 104404.

Hermele, M., T. Senthil, M. P. A. Fisher, P. A. Lee, N. Nagaosa, and X.-G. Wen, 2004, Phys. Rev. B **70**, 214437.

Hlubina, R., W. O. Putikka, T. M. Rice, and D.-V. Khveshchenko, 1992, Phys. Rev. B **46**, 11224.

Hoffman, J. E., E. Hudson, K. Lang, V. Madhaven, H. Eisaki, S. Uchida, and J. Davis, 2002, Science **195**, 466.

Holstein, T., R. Norton, and P. Pincus, 1973, Phys. Rev. B **8**, 2649.

Homes, C. C., T. Timusk, R. Liang, D. Bonn, and W. Hardy, 1993, Phys. Rev. Lett. **71**, 4210.

Honerkamp, C., and P. A. Lee, 2004, Phys. Rev. Lett. **39**, 1201.

Honerkamp, C., M. Salmhofer, N. Furukawa, and T. M. Rice,

2001, Phys. Rev. B **63**, 035109.

Hoogenboom, C., K. Kadowaki, B. Revaz, M. Li, C. Renner, and O. Fischer, 2001, Phys. Rev. Lett. **87**, 267001.

Horvatic, M., C. Berthier, Y. Berthier, P. Segramsan, P. Butaud, W. Clark, J. Gillet, and J. Henry, 1993, Phys. Rev. B **48**, 13848.

Howland, C., H. Eisaki, N. Kaneko, M. Greven, and A. Kapitulnik, 2003, Phys. Rev. B **67**, 014533.

Hsu, T., J. B. Marston, and I. Affleck, 1991, Phys. Rev. B **43**, 2866.

Hsu, T. C., 1990, Phys. Rev. B **41**, 11379.

Huse, D. A., and U. Elser, 1988, Phys. Rev. Lett. **60**, 2531.

Hybertson, M. S., E. Stechel, M. Schuter, and D. Jennison, 1990, Phys. Rev. B **41**, 11068.

Ichinose, I., and T. Matsui, 2001, Phys. Rev. Lett. **86**, 942.

Ichinose, I., T. Matsui, and M. Onoda, 2001, Phys. Rev. B **64**, 104516.

Imada, M., A. Fujimori, and Y. Tokura, 1998, Rev. Mod. Phys. **70**, 1039.

Ioffe, L. B., M. V. Feigel'man, A. Ioselevich, D. Ivanov, M. Troyer, and G. Blatter, 2002, Nature (London) **415**, 503.

Ioffe, L. B., and G. Kotliar, 1990, Phys. Rev. B **42**, 10348.

Ioffe, L. B., and A. Larkin, 1989, Phys. Rev. B **39**, 8988.

Ioffe, L. B., and A. Millis, 2002a, J. Phys. Chem. Solids **63**, 2259.

Ioffe, L. B., and A. Millis, 2002b, Phys. Rev. B **66**, 094513.

Ishida, K., Y. Kitaoka, G. Zhang, and K. Asayama, 1991, J. Phys. Soc. Jpn. **60**, 3516.

Ivanov, D. A., 2000, Ph.D. thesis (MIT, Cambridge, MA).

Ivanov, D. A., 2004, Phys. Rev. B **70**, 104503.

Ivanov, D. A., and P. A. Lee, 2003, Phys. Rev. B **68**, 132501.

Ivanov, D. A., P. A. Lee, and X.-G. Wen, 2000, Phys. Rev. Lett. **84**, 3958.

Kakuyanagi, K., K. Kumagai, and Y. Matsuda, 2002, Phys. Rev. B **65**, 060503.

Kalmeyer, V., and R. B. Laughlin, 1987, Phys. Rev. Lett. **59**, 2095.

Kane, C., P. Lee, and N. Read, 1989, Phys. Rev. B **39**, 6880.

Kao, Y.-J., Q. Si, and K. Levin, 2000, Phys. Rev. B **61**, R11898.

Kastner, M. A., R. Birgeneau, G. Shirane, and Y. Endoh, 1998, Rev. Mod. Phys. **70**, 897.

Kawamoto, A., Y. Honma, and K. Kumagai, 2004, Phys. Rev. B **70**, 060510.

Khasanov, R., A. Shengelaya, K. Conder, E. Morenzoni, I. M. Savic, and H. Keller, 2003, J. Phys.: Condens. Matter **15**, L17.

Khasanov, R., *et al.*, 2004, Phys. Rev. Lett. **92**, 057602.

Khaykovich, B., Y. S. Lee, R. Erwin, S.-H. Lee, S. Wakimoto, K. Thomas, M. Kastner, and R. Birgeneau, 2002, Phys. Rev. B **66**, 014528.

Khveshchenko, D. V., 2002, Nucl. Phys. B **642**, 515.

Khveshchenko, D. V., and P. Wiegmann, 1989, Mod. Phys. Lett. B **3**, 1383.

Kim, D. H., and P. A. Lee, 1999, Ann. Phys. (N.Y.) **272**, 130.

Kim, D. H., P. A. Lee, and X.-G. Wen, 1997, Phys. Rev. Lett. **79**, 2109.

Kimura, H., H. Hiroki, K. Yamada, Y. Endoh, S.-H. Lee, C. Majkrzak, R. Erwin, G. Shirane, M. Greven, Y. S. Lee, M. Kastner, and R. Birgeneau, 1999, Phys. Rev. B **59**, 6517.

Kishine, J., P. A. Lee, and X.-G. Wen, 2002, Phys. Rev. B **65**, 064526.

Kitaev, A. Y., 2003, Ann. Phys. (N.Y.) **303**, 2.

Kitano, S. M., K. Yamada, T. Suzuki, and T. Fukase, 2000, Phys. Rev. B **62**, R14677.

Kivelson, S. A., I. Bindloss, E. Fradkin, V. Oganesyan, J. Tranquada, A. Kapitulnik, and C. Howard, 2003, Rev. Mod. Phys. **75**, 1201.

Kivelson, S. A., D. S. Rokhsar, and J. P. Sethna, 1987, Phys. Rev. B **35**, 8865.

Kogut, J., and L. Susskind, 1975, Phys. Rev. D **11**, 395.

Kosterlitz, J. M., and D. J. Thouless, 1973, J. Phys. C **6**, 1181.

Kotliar, G., and J. Liu, 1988, Phys. Rev. B **38**, 5142.

Kugler, M., O. Fischer, C. Renner, S. Ono, and Y. Ando, 2001, Phys. Rev. Lett. **86**, 4911.

Kurosaki, Y., Y. Shimizu, K. Miyagawa, K. Kanoda, and G. Saito, 2005, Phys. Rev. Lett. **95**, 177001.

Kuzmenko, A. B., H. J. A. Molegraaf, F. Carbone, and D. van der Marel, 2005, Phys. Rev. B **72**, 144503.

Kuzmenko, A. B., N. Tombros, H. Molegraaf, M. Grueninger, D. van der Marel, and S. Uchida, 2003, Phys. Rev. Lett. **91**, 037004.

Lake, B., G. Aeppli, K. Clausen, D. McMorrow, K. Lefmann, N. Hussey, N. Mangkorntong, M. Nohara, H. Takagi, T. Mason, and A. Schroder, 2001, Science **291**, 1759.

Lake, B., *et al.*, 2002, Nature (London) **415**, 299.

Laughlin, R. B., 1995, J. Phys. Chem. Solids **56**, 1627.

Laughlin, R. B., 1997, Phys. Rev. Lett. **79**, 1726.

Lee, D.-H., 2000, Phys. Rev. Lett. **84**, 2694.

Lee, D. K. K., D. Kim, and P. A. Lee, 1996, Phys. Rev. Lett. **76**, 4801.

Lee, P. A., 1993, Phys. Rev. Lett. **71**, 1887.

Lee, P. A., 2002, J. Phys. Chem. Solids **63**, 2149.

Lee, P. A., and N. Nagaosa, 1992, Phys. Rev. B **46**, 5621.

Lee, P. A., and N. Nagaosa, 2003, Phys. Rev. B **68**, 024516.

Lee, P. A., N. Nagaosa, T.-K. Ng, and X.-G. Wen, 1998, Phys. Rev. B **57**, 6003.

Lee, P. A., and G. B. Sha, 2003, Solid State Commun. **126**, 71.

Lee, P. A., and X.-G. Wen, 1997, Phys. Rev. Lett. **78**, 4111.

Lee, P. A., and X.-G. Wen, 2001, Phys. Rev. B **63**, 224517.

Lee, S.-S., and P. A. Lee, 2005, Phys. Rev. Lett. **95**, 036403.

Lee, S.-S., and P. A. Lee, 2005b, e-print cond-mat/0507191, Phys. Rev. B (to be published).

Lee, S.-S., and S.-H. Salk, 2001, Phys. Rev. B **64**, 052501.

Lee, T.-K., and S. Feng, 1988, Phys. Rev. B **38**, 11809.

Lee, T. K., C.-M. Ho, and N. Nagaosa, 2003, Phys. Rev. Lett. **90**, 067001.

Lee, W.-C., T. K. Lee, C.-M. Ho, and P. W. Leung, 2003, Phys. Rev. Lett. **91**, 057001.

Lee, Y. S., R. Birgeneau, M. Kastner, Y. Endoh, S. Wakimoto, K. Yamada, R. Erwin, S.-H. Lee, and G. Shirane, 1999, Phys. Rev. B **60**, 3643.

Leung, P. W., 2000, Phys. Rev. B **62**, R6112.

Levin, M., and X.-G. Wen, 2003, Phys. Rev. B **67**, 245316.

Li, J.-X., and C.-D. Gong, 2002, Phys. Rev. B **66**, 014506.

Liang, R., D. A. Bonn, W. N. Hardy, and D. Broun, 2005, Phys. Rev. Lett. **94**, 117001.

LiMing, W., G. Misguich, P. Sindzingre, and C. Lhuillier, 2000, Phys. Rev. B **62**, 6372.

Littlewood, P. B., J. Zaanen, G. Aeppli, and H. Monien, 1993, Phys. Rev. B **48**, 487.

Liu, D. Z., Y. Zha, and K. Levin, 1995, Phys. Rev. Lett. **75**, 4130.

Liu, Z., and E. Manousakis, 1992, Phys. Rev. B **45**, 2425.

Loeser, A. C., Z.-X. Shen, D. Desau, D. Marshall, C. Park, P. Fournier, and A. Kapitulnik, 1996, Science **273**, 325.

Loram, J. W., J. Luo, J. Cooper, W. Liang, and J. Tallon, 2001, J. Phys. Chem. Solids **62**, 59.

Loram, J. W., K. Mirza, J. Cooper, and W. Liang, 1993, Phys. Rev. Lett. **71**, 1740.

Maggio-Aprile, I., C. Renner, A. Erb, E. Walker, and O. Fischer, 1995, Phys. Rev. Lett. **75**, 2754.

Mandelstam, S., 1979, Phys. Rev. D **19**, 2391.

Marshall, D. S., D. S. Dessau, A. G. Loeser, C.-H. Park, A. Y. Matsuura, J. N. Eckstein, I. Bozovic, P. Fournier, A. Kapitulnik, W. E. Spicer, and Z.-X. Shen, 1996, Phys. Rev. Lett. **76**, 4841.

Marsiglio, F., A. E. Ruckenstein, S. Schmitt-Rink, and C. M. Varma, 1991, Phys. Rev. B **43**, 10882.

Martinez, G., and P. Horsch, 1991, Phys. Rev. B **44**, 317.

Masutomo, R., Y. Karaki, and H. Ishimoto, 2004, Phys. Rev. Lett. **92**, 025301.

Matsuda, M., M. Fujita, K. Yamada, R. J. Birgeneau, M. A. Kastner, H. Hiraka, Y. Endoh, S. Wakimoto, and G. Shirane, 2000, Phys. Rev. B **62**, 9148.

Mattheiss, L. F., 1987, Phys. Rev. Lett. **58**, 1028.

McElroy, K., D.-H. Lee, J. Hoffman, K. Lang, J. Lee, E. Hudson, H. Eisaki, S. Uchida, and J. Davis, 2005, Phys. Rev. Lett. **94**, 197005.

Miller, R. I., R. F. Kiefl, J. H. Brewer, J. E. Sonier, J. Chakhalian, S. Dunsiger, G. D. Morris, A. N. Price, D. A. Bonn, W. H. Hardy, and R. Liang, 2002, Phys. Rev. Lett. **88**, 137002.

Millis, A. J., S. Girvin, L. Ioffe, and A. Larkin, 1998, J. Phys. Chem. Solids **59**, 1742.

Millis, A. J., and H. Monien, 1993, Phys. Rev. Lett. **70**, 2810.

Misguich, G., and C. Lhuillier, 2004, in *Frustrated Spin Systems*, edited by H. T. Diep (World Scientific, New Jersey).

Misguich, G., C. Lhuillier, B. Bernu, and C. Waldtmann, 1999, Phys. Rev. B **60**, 1064.

Mishchenko, A. S., and N. Nagaosa, 2004, Phys. Rev. Lett. **93**, 036402.

Mitrovic, V. F., E. Sigmund, H. Bachman, M. Eschrig, W. Halperin, A. Reyes, P. Kuhns, and W. Moulton, 2001, Nature (London) **413**, 505.

Mitrovic, V. F., E. Sigmund, W. Halperin, A. Reyes, P. Kuhns, and W. Moulton, 2003, Phys. Rev. B **67**, 220503.

Miyake, K., S. Schmitt-Rink, and C. M. Varma, 1986, Phys. Rev. B **34**, 6554.

Moessner, R., and S. L. Sondhi, 2001, Phys. Rev. Lett. **86**, 1881.

Molegraaf, H. J. A., C. Pressura, D. van der Marel, P. H. Kes, and M. Li, 2002, Science **295**, 2239.

Moler, K. A., D. Baar, J. Urbach, R. Liang, W. Hardy, and A. Kapitulnik, 1994, Phys. Rev. Lett. **73**, 2744.

Monthonx, P., and D. Pines, 1993, Phys. Rev. B **47**, 6069.

Mook, H. A., P. Dai, F. Dogan, and R. Hunt, 2000, Phys. Rev. Lett. **88**, 097004.

Mook, H. A., M. Yethraj, G. Aeppli, T. Mason, and T. Armstrong, 1993, Phys. Rev. Lett. **70**, 3490.

Morita, H., S. Watanabe, and M. Imada, 2002, J. Phys. Soc. Jpn. **71**, 2109.

Motrunich, O. I., 2003, Phys. Rev. B **67**, 115108.

Motrunich, O. I., 2005, Phys. Rev. B **72**, 045105.

Motrunich, O. I., and T. Senthil, 2002, Phys. Rev. Lett. **89**, 277004.

Mott, N. F., 1949, Proc. Phys. Soc., London, Sect. A **62**, 416.

Mudry, C., and E. Fradkin, 1994, Phys. Rev. B **49**, 5200.

Nagaosa, N., 1993, Phys. Rev. Lett. **71**, 4210.

Nagaosa, N., 1995, *Quantum Field Theory in Condensed Matter Physics* (Springer, New York), p. 78.

Nagaosa, N., and P. A. Lee, 1990, Phys. Rev. Lett. **64**, 2450.

Nagaosa, N., and P. A. Lee, 1991, Phys. Rev. B **43**, 1233.

Nagaosa, N., and P. A. Lee, 1992, Phys. Rev. B **45**, 966.

Nagaosa, N., and P. A. Lee, 2000, Phys. Rev. B **61**, 9166.

Nakano, T., M. Oda, C. Manabe, N. Momono, Y. Miura, and M. Ido, 1994, Phys. Rev. B **49**, 16000.

Nave, C. P., P. A. Lee, and D. Ivanov, 2005, e-print cond-mat/0510001.

Nayak, C., 2000, Phys. Rev. Lett. **85**, 178.

Nayak, C., 2001, Phys. Rev. Lett. **86**, 943.

Negele, J. W., and H. Orland, 1987, *Quantum Many-Particle Systems* (Addison-Wesley, New York).

Nelson, D. R., and J. Kosterlitz, 1977, Phys. Rev. Lett. **39**, 1201.

Ng, T. K., 2005, Phys. Rev. B **71**, 172509.

Norman, M. R., 2000, Phys. Rev. B **61**, 14751.

Norman, M. R., 2001, Phys. Rev. B **63**, 092509.

Norman, M. R., H. Ding, M. Randeria, J. Campuzano, T. Yokoya, T. Takeuchi, T. Takahashi, T. Michiku, K. Kadowaki, P. Guptasarma, and D. Hinks, 1998, Nature (London) **392**, 157.

Norman, M. R., and C. Pepin, 2003, Rep. Prog. Phys. **66**, 1547.

Onufrieva, F., and P. Pfeuty, 2002, Phys. Rev. B **65**, 054515.

Orenstein, J., and A. Millis, 2000, Science **288**, 468.

Orenstein, J., G. Thomas, A. Millis, S. Cooper, D. Rapkine, T. Timusk, L. Schneemeyer, and J. Waszczak, 1990, Phys. Rev. B **42**, 6342.

Oshikawa, M., 2003, Phys. Rev. Lett. **91**, 109901.

Padilla, W. J., Y. S. Lee, M. Dumm, G. Blumberg, S. Ono, K. Segawa, S. Komiya, Y. Ando, and D. Basov, 2005, Phys. Rev. B **72**, 060511.

Pailhes, A., Y. Sidis, P. Bourges, V. Hinkov, A. Ivanov, C. Ulrich, L. Regnault, and B. Keimer, 2004, Phys. Rev. Lett. **93**, 167001.

Pan, S.-H., E. Hudson, A. Gupta, K.-W. Ng, H. Eisaki, S. Uchida, and J. David, 2000, Phys. Rev. Lett. **85**, 1536.

Paramekanti, A., 2002, Phys. Rev. B **65**, 104521.

Paramekanti, A., M. Randeria, T. V. Ramakrishnan, and S. S. Mandal, 2000, Phys. Rev. B **62**, 6786.

Paramekanti, A., M. Randeria, and N. Trivedi, 2001, Phys. Rev. Lett. **87**, 217002.

Paramekanti, A., M. Randeria, and N. Trivedi, 2004, Phys. Rev. B **70**, 054504.

Paramekanti, A., M. Randeria, and N. Trivedi, 2005, Phys. Rev. B **71**, 094421.

Pavarini, E., I. Dasgupta, T. Saha-Dasgupta, O. Jasperson, and O. Andersen, 2001, Phys. Rev. Lett. **87**, 047003.

Polyakov, A. M., 1975, Phys. Lett. **59B**, 82.

Polyakov, A. M., 1977, Nucl. Phys. B **120**, 429.

Polyakov, A. M., 1978, Phys. Lett. **72B**, 477.

Polyakov, A. M., 1979, Phys. Lett. **82B**, 247.

Polyakov, A. M., 1987, *Gauge Fields and Strings* (Harwood Academic, London).

Proust, C., E. Boaknin, R. Hill, L. Taillefer, and A. MacKenzie, 2002, Phys. Rev. Lett. **89**, 147003.

Rantner, W., and X.-G. Wen, 2001, Phys. Rev. Lett. **86**, 3871.

Rantner, W., and X.-G. Wen, 2001, e-print cond-mat/0105540.

Rantner, W., and X.-G. Wen, 2002, Phys. Rev. B **66**, 144501.

Read, N., and B. Chakraborty, 1989, Phys. Rev. B **40**, 7133.

Read, N., and S. Sachdev, 1990, Phys. Rev. B **42**, 4568.

Read, N., and S. Sachdev, 1991, Phys. Rev. Lett. **66**, 1773.

Reizer, M., 1989, Phys. Rev. B **39**, 1602.

Ribeiro, T. C., and X.-G. Wen, 2005, Phys. Rev. Lett. **95**, 057001.

Rokhsar, D. S., and S. A. Kivelson, 1988, Phys. Rev. Lett. **61**, 2376.

Ronning, F., et al., 1998, Science **282**, 2067.

Ronning, F., et al., 2003, Phys. Rev. B **67**, 165101.

Rossat-Mignod, J., L. Regnault, C. Vettier, P. Bourges, P. Burlet, J. Bossy, J. Henry, and G. Lapertot, 1991, Physica C **185**, 86.

Runge, K. J., 1992, Phys. Rev. B **45**, 12292.

Sachdev, S., 1992, Phys. Rev. B **45**, 389.

Sachdev, S., 2003, Rev. Mod. Phys. **75**, 913.

Sandvik, A. W., E. Dagotto, and D. J. Scalapino, 1997, Phys. Rev. B **56**, 11701.

Santander-Syro, A. F., and N. Bontemps, 2005, e-print cond-mat/0503768.

Santander-Syro, A. F., R. P. S. M. Lobo, N. Bontemps, Z. Konstantinovic, Z. Li, and H. Raffy, 2002, Phys. Rev. Lett. **88**, 097005.

Savici, A. T., Y. Fudamoto, I. M. Gat, T. Ito, M. I. Larkin, Y. J. Uemura, G. M. Luke, K. M. Kojima, Y. S. Lee, M. A. Kastner, R. J. Birgeneau, and K. Yamada, 2002, Phys. Rev. B **66**, 014524.

Savit, R., 1980, Rev. Mod. Phys. **52**, 453.

Scalapino, D. J., E. Loh, and J. E. Hirsch, 1986, Phys. Rev. B **34**, 8190.

Scalapino, D. J., E. Loh, and J. E. Hirsch, 1987, Phys. Rev. B **35**, 6694.

Schmitt-Rink, S., A. E. Ruckenstein, and C. M. Varma, 1988, Phys. Rev. Lett. **60**, 2793.

Senthil, T., and M. P. A. Fisher, 1999, Phys. Rev. B **60**, 6893.

Senthil, T., and M. P. A. Fisher, 2000, Phys. Rev. B **62**, 7850.

Senthil, T., and M. P. A. Fisher, 2001a, J. Phys. A **34**, L119.

Senthil, T., and M. P. A. Fisher, 2001b, Phys. Rev. Lett. **86**, 292.

Senthil, T., and P. A. Lee, 2005, Phys. Rev. B **71**, 174515.

Senthil, T., and O. Motrunich, 2002, Phys. Rev. B **66**, 205104.

Senthil, T., A. Vishwanath, L. Balents, S. Sachdev, and M. P. A. Fisher, 2004, Science **303**, 1490.

Shen, K. M., et al., 2004, Phys. Rev. Lett. **93**, 267002.

Shih, C. T., Y. C. Chen, H. Q. Lin, and T.-K. Lee, 1998, Phys. Rev. Lett. **81**, 1294.

Shih, C. T., T.-K. Lee, R. Eder, C.-Y. Mou, and Y. Chen, 2004, Phys. Rev. Lett. **92**, 227002.

Shimizu, Y., K. Miyagawa, K. Kanoda, M. Maesato, and G. Saito, 2003, Phys. Rev. Lett. **91**, 107001.

Shraiman, B. I., and E. D. Siggia, 1988, Phys. Rev. Lett. **61**, 467.

Si, Q., Y. Zha, K. Levin, and J. Lu, 1993, Phys. Rev. B **47**, 9055.

Singh, A., and H. Ghosh, 2002, Phys. Rev. B **65**, 134414.

Sorella, S., G. B. Martins, F. Bocca, C. Gazza, L. Capriotti, A. Parola, and E. Dagotto, 2002, Phys. Rev. Lett. **88**, 117002.

Stajis, J., A. Iyengar, K. Levin, B. Boyce, and T. Lemberger, 2003, Phys. Rev. B **68**, 024520.

Stock, C., W. J. L. Buyers, R. A. Cowley, P. S. Clegg, R. Coldea, C. D. Frost, R. Liang, D. Peets, D. Bonn, W. N. Hardy, and R. J. Birgeneau, 2005, Phys. Rev. B **71**, 024522.

Stock, C., W. J. L. Buyers, R. Liang, D. Peets, Z. Tun, D. Bonn, W. N. Hardy, and R. J. Birgeneau, 2004, Phys. Rev. B **69**, 014502.

Stock, C., et al., 2005a, e-print cond-mat/0505083.

Sulewsky, P. E., P. Fleury, K. Lyons, S. Cheong, and Z. Fisk, 1990, Phys. Rev. B **41**, 225.

Susskind, L., 1979, Phys. Rev. D **20**, 2610.

Sutherland, M., et al., 2003, Phys. Rev. B **67**, 174520.

Sutherland, M., et al., 2005, Phys. Rev. Lett. **94**, 147004.

Suzumura, Y., Y. Hasegawa, and H. Fukuyama, 1988, J. Phys. Soc. Jpn. **57**, 2768.

Svetitsky, B., 1986, Phys. Rep. **132**, 1.

Taguchi, Y., Y. Oohara, H. Yoshizawa, N. Nagaosa, and Y. Tokura, 2001, Science **291**, 2573.

Taillefer, L., B. Lussier, R. Gagnon, K. Behnia, and H. Aubin, 1997, Phys. Rev. Lett. **79**, 483.

Takigawa, M., W. Hults, and J. Smith, 1993, Phys. Rev. Lett. **71**, 2650.

Takigawa, M., A. P. Reyes, P. C. Hammel, J. D. Thompson, R. H. Heffner, Z. Fisk, and K. C. Ott, 1991, Phys. Rev. B **43**, 247.

Tallon, J. L., and J. W. Loram, 2000, Physica C **349**, 53.

Tanamoto, T., H. Konno, and H. Fukuyama, 1993, J. Phys. Soc. Jpn. **62**, 1455.

Tchernyshyov, O., M. Norman, and A. Chubukov, 2001, Phys. Rev. B **63**, 144507.

Timusk, T., and B. Statt, 1999, Rep. Prog. Phys. **62**, 61.

Tohyama, T., *et al.*, 2000, J. Phys. Soc. Jpn. **69**, 9.

Tokura, Y., *et al.*, 1989, Nature (London) **337**, 345.

Tranquada, J. M., B. J. Sternlieb, J. D. Aye, Y. Nakamura, and S. Uchida, 1995, Nature (London) **375**, 561.

Tranquada, J. M., H. Wou, T. Perring, H. Goka, C. Gu, G. Xu, M. Fujita, and K. Yamada, 2004, Nature (London) **429**, 534.

Tranquada, J. M., *et al.*, 1988, Phys. Rev. B **38**, 2477.

Trivedi, N., and D. Ceperley, 1989, Phys. Rev. B **40**, 2737.

Tsuchiura, H., M. Ogata, Y. Tanaka, and S. Kashiwaya, 2003, Phys. Rev. B **68**, 012509.

Tsuchiura, H., Y. Tanaka, M. Ogata, and S. Kashiwaya, 2000, Phys. Rev. Lett. **84**, 3105.

Ubbens, M., and P. A. Lee, 1992, Phys. Rev. B **46**, 8434.

Ubbens, M. U., and P. A. Lee, 1994, Phys. Rev. B **49**, 6853.

Uchida, S., 1997, Physica C **282**, 12.

Uchida, S., T. Ido, H. Takagi, T. Arima, Y. Tokura, and S. Tajima, 1991, Phys. Rev. B **43**, 7942.

Uemura, Y. J., *et al.*, 1989, Phys. Rev. Lett. **62**, 2317.

Ussishkin, I., S. Sondhi, and D. Huse, 2002, Phys. Rev. Lett. **89**, 287001.

Valla, T., A. Fedorov, P. Johnson, B. Wells, S. Hulbert, Q. Li, G. Gu, and N. Koshizuka, 1999, Science **285**, 2110.

Varma, C. M., 1997, Phys. Rev. B **55**, 14554.

Varma, C. M., S. Schmitt-Rink, and E. Abrahams, 1987, Solid State Commun. **62**, 681.

Vershinin, M., M. Shashank, S. Ono, Y. Abe, Y. Ando, and A. Yazdani, 2004, Science **303**, 1995.

Vojta, M., and S. Sachdev, 1999, Phys. Rev. Lett. **83**, 3916.

Vollhardt, D., 1984, Rev. Mod. Phys. **56**, 99.

Volovik, G., 1993, JETP Lett. **58**, 469.

Wakimoto, S., G. Shirane, Y. Endoh, K. Hirota, S. Ueki, K. Yamada, R. Birgeneau, M. Kastner, Y. S. Lee, P. Gehring, and S.-H. Lee, 1999, Phys. Rev. B **60**, R769.

Wang, Y., L. Li, M. Naughton, G. Gu, S. Uchida, and N. P. Ong, 2005, cond-mat/0503190, Phys Rev. Lett. (to be published).

Wang, Y., and A. MacDonald, 1995, Phys. Rev. B **52**, R3876.

Wang, Y., N. P. Ong, Z. Xu, T. Kakeshita, S. Uchida, D. Bonn, R. Liang, and W. Hardy, 2002, Phys. Rev. Lett. **88**, 257003.

Wang, Y., S. Ono, Y. Onose, G. Gu, Y. Ando, Y. Tokura, S. Uchida, and N. P. Ong, 2003, Science **299**, 86.

Wang, Y., Z. Yu, T. Kakeshita, S. Uchida, S. Ono, Y. Ando, and N. P. Ong, 2001, Phys. Rev. B **64**, 224519.

Warren, W. W., R. Walstedt, G. Brennert, R. Cava, R. Tycko, R. Bell, and G. Dabbaph, 1989, Phys. Rev. Lett. **62**, 1193.

Wegner, F., 1971, J. Math. Phys. **12**, 2259.

Wells, B. O., Z.-X. Shen, A. Matsura, D. M. King, M. A. Kastner, M. Greven, and R. J. Birgeneau, 1995, Phys. Rev. Lett. **74**, 964.

Wen, H.-H., L. Shan, X.-G. Wen, Y. Wang, H. Gao, Z.-Y. Liu, F. Zhou, J. Xiong, and W. Ti, 2005, e-print cond-mat/0502377.

Wen, X.-G., 1991, Phys. Rev. B **44**, 2664.

Wen, X.-G., 1995, Adv. Phys. **44**, 405.

Wen, X.-G., 2002a, Phys. Rev. Lett. **88**, 011602.

Wen, X.-G., 2002b, Phys. Rev. B **65**, 165113.

Wen, X.-G., 2003a, Phys. Rev. B **68**, 115413.

Wen, X.-G., 2003b, Phys. Rev. D **68**, 065003.

Wen, X.-G., 2003c, Phys. Rev. Lett. **90**, 016803.

Wen, X.-G., 2004, *Quantum Field Theory of Many-Body Systems—From the Origin of Sound to an Origin of Light and Electrons* (Oxford University Press, Oxford).

Wen, X.-G., and P. A. Lee, 1996, Phys. Rev. Lett. **76**, 503.

Wen, X.-G., and P. A. Lee, 1998, Phys. Rev. Lett. **80**, 2193.

Wen, X.-G., F. Wilczek, and A. Zee, 1989, Phys. Rev. B **39**, 11413.

Wen, X.-G., and A. Zee, 2002, Phys. Rev. B **66**, 235110.

Weng, Z.-Y., 2003, e-print cond-mat/0304261.

Weng, Z. Y., D. N. Sheng, and C. S. Ting, 2000, Physica C **341-348**, 67.

White, S. R., and D. J. Scalapino, 1999, Phys. Rev. B **60**, R753.

Wilson, K. G., 1974, Phys. Rev. D **10**, 2445.

Witten, E., 1979, Nucl. Phys. B **149**, 285.

Wu, C.-L., C.-Y. Mou, X.-G. Wen, and D. Chang, 1998, e-print cond-mat/9811146.

Wu, M. K., J. Ashburn, C. Torng, P. Hor, R. Meng, L. Gao, Z. Huang, Y. Wang, and C. Chu, 1987, Phys. Rev. Lett. **58**, 908.

Wynn, J., D. Bonn, B. Gardner, Y.-J. Lin, R. Liang, W. Hardy, J. Kirtley, and K. Moler, 2001, Phys. Rev. Lett. **87**, 197002.

Yamada, K., *et al.*, 1998, Phys. Rev. B **57**, 6165.

Yasuoka, H., T. Imai, and T. Shimizu, 1989, in *Strong Correlation and Superconductivity*, edited by H. Fukuyama, S. Maekawa, and A. P. Malozemoff (Springer, Berlin), p. 254.

Ye, J., 2003, Phys. Rev. B **67**, 115104.

Ye, J., Y. Kim, A. J. Millis, B. Shraiman, P. Majumda, and Z. Tesanovic, 1999, Phys. Rev. Lett. **83**, 3737.

Yokoyama, H., and M. Ogata, 1996, J. Phys. Soc. Jpn. **65**, 3615.

Yoshida, T., *et al.*, 2003, Phys. Rev. Lett. **91**, 027001.

Yoshioka, D., 1989, J. Phys. Soc. Jpn. **58**, 1516.

Yu, J., A. Freeman, and J.-H. Xu, 1987, Phys. Rev. Lett. **58**, 1035.

Zaanen, J., G. Sauatzky, and J. Allen, 1985, Phys. Rev. Lett. **55**, 418.

Zhang, F. C., C. Gros, T. M. Rice, and H. Shiba, 1988, Supercond. Sci. Technol. **1**, 36.

Zhang, F. C., and T. Rice, 1988, Phys. Rev. B **37**, 3759.

Zhang, S.-C., 1997, Science **275**, 1089.

Zheng, G.-Q., T. Odaguchi, T. Mito, Y. Kitaoka, K. Asayama, and Y. Kodama, 2003, J. Phys. Soc. Jpn. **62**, 2591.

Zhou, X.-J., *et al.*, 2004, Phys. Rev. Lett. **92**, 187001.